U.S.NRC
United States Nuclear Regulatory Commission
Protecting People and the Environment

RECLAMATION
Managing Water in the West

EROSION TESTING OF ZONED ROCKFILL EMBANKMENTS

Date Published: September 2021

Prepared by:
T. Wahl

U.S. Department of the Interior
Bureau of Reclamation
Technical Service Center
Hydraulic Investigations and Laboratory Services Group
Denver Colorado

Jake Philip, Joseph Kanney NRC Project Managers

Research Information Letter
Office of Nuclear Regulatory Research

This report was published as U.S. Bureau of Reclamation (USBR) Hydraulic Laboratory Report HL-2019-01 to document of a series of experiments funded by the U.S. Nuclear Regulatory Commission's Office of Regulatory Research. The report has been re-published as an NRC Research Information Letter (RIL).

Disclaimer

ABSTRACT

Two 3-ft high, zoned rockfill embankment dam models were tested in the Bureau of Reclamation hydraulics laboratory to gain a better understanding of erosion and dam breach processes associated with overtopping flow and internal erosion. A preceding internal erosion test of a homogeneous embankment comprised of materials similar to the core section of the zoned embankments is also described. Erosion rates of the model embankments were evaluated from visual records, and erodibility parameters of the soils were compared to small-scale submerged jet erosion tests performed on the test embankments and other compacted soil samples. The experiments were also modeled using the WinDAM C and DL Breach computational simulation models, and comparisons were made to previous dam breach experiments carried out on zoned embankments and embankments comprised of broadly-graded earthen materials.

FOREWORD

Mission of the U. S. Department of the Interior: To protect and manage the Nation's natural resources and cultural heritage; provide scientific and other information about those resources; and honor its trust responsibilities or special commitments to American Indians, Alaska Natives, and affiliated island communities.

Mission of the Bureau of Reclamation: To manage, develop, and protect water and related resources in an environmentally and economically sound manner in the interest of the American public.

Disclaimer: The information provided in this report is believed to be appropriate and accurate for the specific purposes described herein, but users bear all responsibility for exercising sound engineering judgment in its application, especially to situations different from those studied. References to commercial products do not imply endorsement by the Bureau of Reclamation and may not be used for advertising or promotional purposes.

Peer Review: This report was reviewed and approved for publication in accordance with the Technical Service Center's standard peer review processes.

TABLE OF CONTENTS

LIST OF FIGURES

LIST OF TABLES

EXECUTIVE SUMMARY

Two 3-ft high, zoned rockfill embankment dam models were tested in the Bureau of Reclamation hydraulics laboratory to gain a better understanding of erosion and dam breach processes associated with overtopping flow and internal erosion. A preceding internal erosion test was also performed on a homogeneous embankment composed of materials similar to the core of the two zoned embankments. The zoned embankments had a silty clay core with upstream and downstream shells of well-graded gravel with clay and sand. (*Well-graded* soils contain a mix of particles of all sizes from the maximum size of a particular gradation down to the No. 200 sieve and meet a mathematical requirement for a gradually decreasing percentage of each particle size, so that the finer particles effectively fill but do not overfill the voids between the larger particles. Soils described in this report as *broadly-graded* contain a similar range of soil sizes, but do not meet the mathematical requirements of a well-graded soil.) The homogeneous embankment and one of the zoned embankments were constructed with internal flaws designed to produce internal erosion failures, while the other zoned embankment was subjected to overtopping flow. The construction of the test facility and testing of the homogeneous embankment were funded by the Bureau of Reclamation's Dam Safety Office Technology Development program. The tests of the zoned embankments were funded by the U.S. Nuclear Regulatory Commission (NRC), Office of Nuclear Regulatory Research.

The homogeneous silty clay embankment test served as a useful predecessor to the zoned embankment tests, since the soil used for it was also used in the core of the zoned embankments. Prior to this test, the soil was characterized through standard soil property tests (gradation analysis, compaction testing, specific gravity, etc.). Submerged jet erosion tests (Hanson and Cook 2004) were also performed on compacted soil specimens and on the actual test embankments. In its compacted state this soil was characterized as very erodible, the most erodible designation available in a five-tier system suggested by Hanson and Simon (2001). The detachment rate coefficient of the soil, k_d, determined from jet tests was about 5.5 ft/hr/(lb/ft^2). This coefficient expresses the rate at which erosion increases per unit of additional shear stress applied to the soil.

The internal erosion test of the homogeneous embankment started with the withdrawal of a #4 rebar (½-inch = 12.7-mm diameter) which had been embedded at mid-height in the embankment during its construction. Erosion of this conduit took place rapidly over the course of about 48 minutes. Erosion progress was monitored visually through an acrylic sidewall of the model, and extensive digital photo imagery was collected for documentation and analysis, along with reservoir water level and breach outflow discharge data. Following the test, the WinDAM C (USDA 2016) computational model was used to simulate the internal erosion process and resulting breach outflow hydrograph. This simulation was used to work back toward an estimate of the effective value of k_d for the soil, and a value of about 2 ft/hr/(lb/ft^2) was obtained. Considering that k_d for typical cohesive soils can easily vary by up to 3 orders of magnitude (1000:1 ratio), this value is very close to the value obtained from the jet tests.

The first zoned embankment was constructed with a small pilot channel in the crest and was tested in an overtopping flow condition. The general erosion pattern was characterized by gradual surface erosion of the downstream slope (the well-graded gravel soil) and a relatively uniform lowering of the crest of the core zone (the silty clay soil). The breach channel exhibited vertical side slopes typical of cohesive soils, and while small headcuts formed briefly in the bed of the breach channel at the start of the test, they surprisingly did not develop into larger

headcuts. This may have been due to a low tailwater condition that prevented significant recirculation of the flow against the toe of the embankment. Photo imagery and flow records were used to estimate erosion rates and applied stresses, and these data were used to estimate the effective k_d parameter of the gravel zone, which was in the range of 0.5 to 2 ft/hr/(lb/ft^2). This indicated that the gravel zone was less erodible than the core, but not dramatically so. It is not known whether this is typical of real dams since the k_d values of most real dams—and especially of specific zones within most dams—are unknown.

The jet erosion test was originally developed for use with cohesive soils and is typically not performed with gravel soils, since the gravel particles can armor the finer soil during the test. However, following the overtopping test of the zoned embankment, a series of jet erosion tests was performed on several compacted soil specimens created from the gravel soil. These included the full gradation original soil and several specimens created by screening with U.S. No. 4 and U.S. 3/8-inch sieves to remove coarser material. Comparison of these results to the estimates of k_d obtained from the photo records of the overtopping test gave encouraging indications that the erodibility of the broadly-graded gravel soil could be estimated from jet tests performed on specimens screened through either of these sieves. There was also some indication that the presence of gravel particles in these soil mixes may have contributed a small amount of additional erosion resistance, but the data set was very limited, so this should be studied further.

It was not possible to effectively apply the WinDAM C dam breach model to the overtopping test of the zoned embankment, since a headcut pattern of breach development did not occur. The DL Breach model (Wu 2016a, 2016b) was applied to the test using several different alternative methods for defining the embankment and modeling the erosion processes. These included zoned and homogeneous cross sections, surface erosion and headcut erosion breach development patterns for the downstream slope, and the use of soil erosion equations designed for cohesive and noncohesive soils. One successful run was made with a homogeneous embankment definition in which headcut erosion was enabled, but the breach development occurred mostly due to surface erosion of the dam crest. Another simulation that approximately matched the experimental results was made with a zoned configuration modeling surface erosion of cohesive soil. However, to obtain a good result in this simulation, a reduction of the k_d value for the gravel zone (the downstream slope) was needed, compared to the estimates of k_d obtained from analysis of the photographs of the breach development. This adjustment was needed because DL Breach applies the excess stress equation (which is used by both WinDAM C and DL Breach to calculate erosion rates of cohesive soils) using total shear stress against the channel boundary instead of just the effective stress applied to the erodible soil grains. (The effective stress approach considers the stress applied to bedforms of the boundary to be ineffective for causing soil detachment.) This is an important difference that must be understood by modelers.

The second zoned embankment test, similar to the homogeneous embankment test, considered an internal erosion failure triggered by withdrawal of an embedded piece of rebar passing through the embankment. This test was conducted over a four-day period, with a total of about 48 hours of flow. Initially, the gravel zones acted as a filter and successfully healed the flaw created by withdrawal of the rebar from the embankment. In a second phase of the test, the rebar was reinserted into the embankment, which enlarged and intensified the flaw and the rebar was then withdrawn again to restart the test. After the restart, the gravel zones were no longer able to fully heal the flaw, but they still significantly limited the flow and the erosion rates. A stope began to slowly develop within the core zone, with the internal erosion conduit slowly migrating vertically toward the crest, but barely enlarging. Eventually, this stope could have

reached the crest of the embankment, possibly leading to a sinkhole that would allow overtopping flow, but the test was stopped before the failure mode could fully develop.

The internal erosion test of the zoned embankment was not amenable to numerical simulation with any available computational models because of the limiting effects of the gravel zones and the complex erosion processes that occurred. The best tool that could be identified for analyzing a stoping failure (a vertically migrating internal collapse) such as this was the joint Bureau of Reclamation and U.S. Army Corps of Engineers document, "*Best Practices in Dam and Levee Safety Risk Analysis, Chapter IV-4, Internal Erosion Risks for Embankments and Foundations*" (USBR and USACE 2015). This publication provides a conceptual framework for analyzing internal erosion failure processes through the use of an event tree considering each of the sequential processes needed to produce a failure. The analysis provides estimates of the likelihood of failure and the possible range of failure times, and it suggested that this embankment might complete the process of stoping and dam breach in a period of about 1 to 7 days.

The final section of this report compares and contrasts these physical model tests with prior experimental investigations of zoned embankments and embankments comprised of uniform and broadly-graded gravel materials. No other tests could be found of internal erosion of zoned embankments containing such materials, but several overtopping flow tests are discussed. These previous tests show that uniform, clean gravels (i.e., less than 5% of particles passing the U.S. No. 200 sieve) generally have little or no erosion resistance, but broadly-graded gravels often have significant erosion resistance. This is consistent with the observed behavior of the well-graded gravel soils used in these tests.

ABBREVIATIONS AND ACRONYMS

ASTM	American Society for Testing And Materials
DL Breach	Dam and Levee Breach computer program
DSLR	Digital Single Lens Reflex camera
EMBREA	Embankment BREAch computer program
FEMA	Federal Emergency Management Agency
JET	Submerged Jet Erosion Test
LL, PL, PI	Liquid Limit, Plastic Limit, Plasticity Index
NRC	Nuclear Regulatory Commission
USBR	United States Bureau of Reclamation
USACE	United States Army Corps of Engineers
USCS	Unified Soil Classification System
WinDAM C	"C" version of the Windows Dam Analysis Modules computer program

GLOSSARY OF SYMBOLS

c_u	undrained shear strength of soil, lb/ft^2
C_u	coefficient of uniformity, $C_u = D_{60}/D_{10}$
C_c	coefficient of curvature, $C_c = D_{30}^2/(D_{60}D_{10})$
C_2	headcut rate coefficient for DL Breach, $s^{-2/3}$
D_{xx}	diameter for which xx percent of soil particles are finer
g	acceleration due to gravity, $32.2\ ft/s^2 = 9.81\ m/s^2$
k_d	soil detachment rate coefficient, $ft/hr/(lb/ft^2)$
n	Manning's roughness coefficient for the total flow
n_s	Manning's roughness coefficient due to soil grain roughness
n_f	Manning's roughness coefficient due to channel bedforms
R	hydraulic radius (area divided by wetted perimeter), ft
S	channel bed slope
γ	unit weight of water, $62.4\ lb/ft^3 = 1000\ kg/m^3$
γ_d	dry density of soil, lb/ft^3
ε_r	soil erosion rate ft/hr
τ	total hydraulic shear stress on channel bed lb/ft^2
τ_c	critical shear stress needed to initiate erosion, lb/ft^2
τ_e	total effective stress applied to soil grains, lb/ft^2

1 BACKGROUND AND PURPOSE

Erosion processes that lead to the breaching and failure of embankment dams are critically important to both the Bureau of Reclamation (Reclamation) and the U.S. Nuclear Regulatory Commission (NRC). Reclamation has constructed over 240 embankment dams in the western U.S. and provides dam safety program assistance to other Department of the Interior agencies. NRC regulates several nuclear power plants that are located downstream from embankment dams, for which the potential failure of the upstream dam produces the design flooding condition that must be considered when locating and protecting critical infrastructure. Following the damage that occurred to the Fukushima nuclear facility in Japan after a 2011 earthquake and tsunami flood, all U.S. nuclear plants underwent reviews of their design-basis flood estimates. For some plants, this required modeling potential dam-break floods.

Currently, most dam breach analyses employ regression equations to predict gross parameters that describe the dam breaching process: width, depth and shape (side slope angle) of final breach, and the time for breach formation. One review of such methods is given by Wahl (1998). Most regression equations are simplistic, considering only a handful of basic dam and reservoir characteristics, typically the dam height, some measure of the volume of stored water, and sometimes the failure mode. Occasionally, additional parameters such as shape factors for the reservoir storage function or parameters describing the bulk erodibility of the embankment materials have been included. After regression analysis is used to estimate breach parameters, the results are used to describe the opening of the breach parametrically, typically assuming a linear increase of the breach size from a starting condition to the predicted final size, and outflows through the breach are estimated using basic hydraulic equations for weir or orifice flow. This approach to breach modeling does not directly account for the physical erosion of dam materials through erosion or sediment transport processes.

Since the 1990s, work has been underway by several organizations to develop physically based computational dam breach simulation models. These models simulate time-dependent erosion and geotechnical mass wasting processes and incorporate idealized representations of the mechanics of embankment breach, as observed in laboratory physical model tests and a few well-documented real-world failure events. Most of the laboratory testing supporting the development of these models has been performed on homogenous embankments constructed from a single material. Some of the developed models (e.g., WinDAM C) are restricted to modeling homogeneous embankments, while others (e.g., HR BREACH and DL Breach) can be applied to zoned embankments. Although the latter models are configured to simulate behavior of zoned embankments, there has been very little laboratory testing to validate them for these applications.

Several dams located upstream from nuclear power plants in the U.S. are zoned rockfill embankments. Since most laboratory testing has focused on homogeneous embankments, even dam breach models capable of considering zoned embankments have rarely been tested in a meaningful way for this application. As a result, NRC commissioned Reclamation to perform two erosion tests of zoned rockfill dams in the Denver hydraulics laboratory to fill this knowledge gap. The embankments were of similar design, with breach triggered by overtopping flow in one case and by internal erosion through a constructed flaw in the other case. This report documents the two zoned embankment tests as well as a preceding test of a homogeneous embankment containing materials similar to the core of the zoned embankments. The report describes the observed erosion processes, rates, etc., and makes comparisons to laboratory measurements of soil erodibility parameters and computational results from present-

day dam breach models. Recommendations for model use and additional research are provided.

1.1 Overview of Testing

Three embankment dam breach tests were conducted at the Bureau of Reclamation from 2015 through 2017. The first test of a homogeneous silty clay embankment failed by internal erosion was funded by Reclamation's Dam Safety Technology Development Program. Two subsequent tests of zoned rockfill dams (with silty clay cores) subjected to overtopping flow and internal erosion were funded by the Nuclear Regulatory Commission. Results of all three tests are reported here due to similarity of materials and interesting comparisons and contrasts that can be made between the tests and the observed embankment behaviors. In addition to providing the test data, this report also discusses the tests in comparison to other similar research documented in the dam safety literature, and makes comparisons to results from computational models and a joint Reclamation / U.S. Army Corps of Engineers procedure for evaluating internal erosion risks at embankment dams (USBR and USACE 2015).

1.2 Literature Review

Dam breach modeling with computational tools began to develop during the 1980s, following significant dam failure events and passage of dam safety legislation in the U.S. and other countries in the late 1970s. The parametric approach already outlined in the introduction has prevailed since that time, and common practices for breach parameter estimation and computational modeling have been summarized by several researchers, including Wahl (1998), Washington State Department of Ecology (2007), State of Colorado (2010), and others.

As dam breach modeling technology has begun to advance beyond simple breach parameter estimation to more physically-based erosion simulation models, physical model testing has been important for gaining an understanding of erosion and breach process mechanics and for obtaining validation data that can be used to test different computational approaches. Case study investigations of real dam failures have also been useful, although the quality of data is often poor because of a lack of reliable eyewitnesses, since the focus of witnesses is often on other emergency issues during the times of greatest interest for modeling purposes. Wahl (2007) reviewed laboratory testing programs and Courivaud (2007) assembled case study data for a dam breach research effort coordinated by CEATI International. Wu (2013) provided a more recent review of laboratory tests and available numerical models. These reviews showed that most physical model testing has been conducted on homogeneous embankments composed of either cohesive soils or relatively uniform, clean (i.e., less than 5% of particles passing the U.S. No. 200 sieve), granular soils. Previous breach tests of zoned embankments and dams composed of broadly-graded gravels (i.e., rockfill-type soils) have been quite limited. A few such tests are summarized below.

- Franca and Almeida (2002) conducted 22 tests of 0.5-m high homogeneous rockfill dams. These embankments were constructed with a coarse rockfill material having a minimum grain size of 9.5 mm and a median grain size of D_{50}=19 mm. The embankments were equipped with an intentionally fragile plastic/paper water retaining barrier on the upstream face that only served to ensure that failure would occur strictly due to overtopping flow, rather than by a combination of through-flow and overtopping. The embankments were reported to be rather sturdy in comparison to earthfill dams, enduring unit discharges of 0.16±0.015 ft²/s (0.015±0.0014 m²/s) before first movement of material on the downstream slope. General sliding of the downstream slope occurred

at about 0.21±0.014 ft^2/s (0.020±0.0013 m^2/s), and breach development was initiated at about 0.32 ft^2/s (0.030 m^2/s). These tests led to the subsequent development of a numerical model, RoDaB (Franca and Almeida 2004).

- Simmler and Sametz (1982) also performed 22 tests on homogeneous embankments and embankments provided with thin, impervious central core zones (core walls) or upstream impervious layers. These embankments ranged from 0.15 to 0.6-m high. Materials in most of these dams were either relatively uniform sands or broadly-graded sands. The coarsest of the broadly-graded materials had a median grain size of about 5 mm.

- IMPACT tests (2002-2004) – The European IMPACT project performed large-scale field tests of several dams, including four 6-m high embankment dams composed of homogeneous or zoned rockfill. An overtopping test was performed on a homogeneous well-graded gravel dam, followed by an overtopping test of a zoned embankment with a broadly-graded (but not well-graded[1]) downstream rockfill zone (0.3- to 600-mm diameter), a moraine core (10% fines [$d \leq 0.074$ mm] and material up to 200-mm diameter), and an upstream zone of uniform rockfill (300- to 500-mm riprap). An internal erosion test was performed on a similar zoned embankment, and a second internal erosion test was performed on an embankment with a homogeneous section constructed from the moraine material. Additional information about these tests will be provided later in this report in a discussion that compares them to the tests performed in the present study.

- Pugh (1985) and Tinney and Hsu (1961) tested zoned embankments designed to breach in a controlled manner for use in fuse plug spillways. These embankments had thin clay cores that were inclined downstream over a relatively clean granular zone with D_{10} of about 0.3 to 0.4 mm (U.S. No. 50 to No. 40 sieve) and no material smaller than the No. 75 sieve. This configuration caused overtopping erosion to quickly scour out the downstream zones, leaving the cores to fail as unsupported cantilevered beams. The use of dirtier soil mixes with particles finer than the No. 75 sieve often led to slower and more variable erosion rates and prolonged breaching times.

---

[1] Well-graded soils contain all particle sizes between the maximum size and the No. 200 sieve, and meet a mathematical requirement for a gradually decreasing percentage of each smaller particle size, so that the finer particles effectively fill but do not overfill the voids between the larger particles. The coefficient of uniformity, $C_u = D_{60}/D_{10}$ must be greater than or equal to 4 for gravel soils and greater than or equal to 6 for sands, where D_{10} and D_{60} are the particle sizes at which 10% and 60% of the particles are finer, respectively. In addition, all well-graded soils must have a coefficient of curvature, $C_c = (D_{30})^2/(D_{60}D_{10})$ that is in the range of 1 to 3. Soils described in this report as broadly-graded contain a similar range of soil sizes, but do not meet the mathematical requirements of a well-graded soil.

2   MODEL DESIGN AND CONSTRUCTION

2.1   Test Facility

The facility utilized for the present tests was constructed in 2014 to conduct embankment breach-related research for Reclamation's Dam Safety Office. One test was performed prior to the NRC-funded project, an internal erosion failure through a homogeneous silty clay (CL-ML) embankment. This test and the details of the facility are described by Wahl et al. (2016). An overview description of the facility is provided here.

The dam breach test facility consisted of a 12.44-ft-base-width (3.79-m), 3-ft-high (0.91-m) embankment test section in a 27-ft-long (8.23 m) headbox that was elevated 2 ft (0.61 m) above a large tailbox (approx. 42 ft long by 22 ft wide, 12.8 m by 6.7 m) intended to capture the flow released during a breach test (Figure 2-1). Capturing the full flow volume allowed sediment to be retained and settled out in the tailbox before water was returned to the lab sump, minimizing the effect on other laboratory operations. However, the finite volume of the tailbox limited the total testing time once a breach had enlarged significantly; for the initial test of the homogeneous silty clay dam the test time was only about 48 minutes. For the tests of the zoned rockfill dams, the decision was made to extend the testing time and allow turbid water to return to the lab sump through a spillway section provided in the tailbox.

Figure 2-1   Embankment breach test facility viewed from the upstream end of the headbox, overlooking the homogeneous CL-ML embankment (Dam Safety-funded first test).

The test section of the headbox was provided with a 3/4-inch-thick (19 mm), clear acrylic wall on the left side (looking downstream) to allow viewing of erosion progress during a test. Both the acrylic wall and the opaque right wall were constructed with a 1:10 (h:v) slope to enable good compaction and soil contact against the abutments.

Flow into the headbox was provided from the laboratory's fixed pumps and was measured with venturi flow meters that are calibrated periodically against a weighing tank. Accuracy of flow measurement for this system is generally ±0.5% or better.

The headbox was provided with an adjustable-crest spillway section so that excess flow (exceeding that passing through the breach) could be provided into the model, avoiding the need to constantly adjust or rapidly increase the inflow as a breach was developing. Stoplogs in the spillway opening were used by an operator to regulate the headbox water level within a narrow range during each test. As the breach enlarged, spillway flows were reduced to keep the reservoir level constant, simulating the behavior of a reservoir with a very large water surface area. The flow passing over the spillway section was measured with a broad-crested weir before it returned to the lab sump so that the net flow through the breach could be computed. Ultrasonic level sensors were installed in stilling wells connected to the flume approach channel, headbox and tailbox to record changes in water levels during a test. Data from those sensors was recorded using a DASYLab data acquisition system.

It was anticipated that the accuracy of flows calculated through the embankment breach during the early stages of the two internal erosion tests would be poor, because the net flow would be a very small fraction of the total flow provided into the model and the flow spilled over the adjustable weir, and thus the difference (i.e., flow through the breach) would be lost in the uncertainty of the flow measurements. To overcome this, the test facility was fitted with a small supercritical flume (Figure 2-2) adapted from the concept described by Smith et al. (1981) for measuring sediment laden runoff from natural watersheds. The flume consisted of a triangular trough with a 2h:1v side slope and a 3% slope in the flow direction, attached to the sidewall of the model box just downstream from the toe of the embankment at the left abutment. In addition, prior to the internal erosion test of the zoned embankment, a small triangular notch was cut in a 2x6-inch wood stoplog added just downstream from the toe of the dam to provide a small amount of tailwater and ensure that initial flows were directed to the flume. This flume was calibrated in place with clear water prior to construction of any of the embankments, so that the flow depth and visually observed width of the water surface could be related to the flow rate. It was anticipated that this flume might be useful up to flow rates approaching 100 gallons per minute (gpm), or 6.3 L/s.

The width of the embankment test section was about 13 ft (4 m), which was much greater than the width of any expected breach opening. The extra width enabled the model to adequately simulate the three-dimensional flow conditions approaching the breach and erosion processes within the breach. The additional width was also provided so that during the Dam Safety Office-funded work, geophysical instrumentation used to detect internal erosion failures in progress could be deployed on the embankment at a reasonable distance away from the initial site of erosion and the boundaries of the embankment. It should be emphasized that with the erosion initiated at the abutment, erosion is one-sided in these tests. When erosion is initiated at the middle of the embankment, erosion would progress on both sides simultaneously, leading to a doubling of the breach widening rate.

Figure 2-2 **Supercritical flume downstream from left edge of embankment. The bottom photo is taken from directly overhead and shows the scales used to indicate the depth and width of flow, which were correlated to flow rate through in-place calibration.**

2.2   Model Size and Scale

The size of the test facility was maximized within laboratory space and flow-capacity constraints, with the objective of performing tests at a scale that was sufficiently large to create a test environment that could represent the dominant physical processes of a prototype embankment erosion and breach event, while not being so small that it might cause irrelevant processes at prototype scale to become dominant at model scale (e.g., surface tension). The dominant processes in embankment breach are believed to be gravity-driven open-channel flow, pressure-driven closed conduit flow, erosion of granular soils, erosion of cohesive soils, and slope stability and structural collapse of masses of granular and cohesive soils. Obviously, the desire to model each of these processes carries with it a requirement to ensure similarity of the ratios of important forces in the model and prototype, such as gravitational and inertial forces associated with open-channel flow (the Froude number), viscous and inertial forces for pressurized conduit flow (the Reynolds number), etc. Satisfying all of these competing requirements simultaneously is always impossible when simulating phenomena that involve multiple dominant physical processes, so scale effects are always present to some degree.

Assessing the magnitude of such scale effects generally requires validation testing of models at different scales, but this was beyond the scope of the present project. The chosen model size is large enough that each of the important physical processes listed can occur, and the relative importance of each is believed to be similar in a 3-ft embankment, a 30-ft embankment, or perhaps even a 300-ft embankment.

An important consideration with respect to model scaling is also the choice of materials, in this case the embankment soils. True geometric scaling of soil particle sizes would likely cause some of the granular materials in a prototype embankment to behave in a cohesive manner in a model, which obviously changes the dominant physical processes. Thus, no attempt was made to actually scale the soils used in the models. Rather, the engineering properties of the soils were evaluated as they were used in the models, using methods such as submerged jet erosion testing. In this sense, the models were not truly "scaled" representations of a prototype, but were simply prototypes of a small size.

2.3   Photogrammetry

Two arrays of still photo cameras were used to record images of the erosion taking place at the left abutment of the embankment test section and on the upstream and downstream surfaces of the embankments (Figure 2-3). Eight digital single lens reflex (DSLR) cameras were set up to take overlapping photos through the acrylic abutment wall, and 6 GoPro video/still cameras were positioned overhead to obtain overlapping photos of the surface of the left end of the embankment. Each camera's field of view included photogrammetry targets to enable subsequent image analysis. Picture rates were adjusted as needed during the various tests, with intervals varying from 10 seconds up to 5 minutes. Following the completion of the tests, images were processed to create time-lapse imagery and models of the erosion progress.

Figure 2-3   Camera equipment used during the test included six GoPro cameras deployed above the embankment and eight DSLR cameras viewing the left abutment through the acrylic wall.

Additional still cameras were set up at various viewing positions during the construction of the test facility and during the tests to record time-lapse progress of construction and other activities. Video cameras also recorded the testing from several locations and live streaming video was provided during the NRC-funded tests to allow interested parties to watch from remote locations.

2.4   Embankment Configuration

There is not a strict definition for the term *zoned rockfill dam*. The embankments tested in this study were not meant to specifically model any particular structure, since the interest is in a range of structures with some commonalities and significant individual differences. The tested embankments are meant to be representative of typical zoned embankment dams, especially those having relatively coarse shell (exterior) zones that might be described as rockfills, but might also be described with terms such as "selected sand, gravel, and cobbles", "quarry run", "plus 4-inch", "minus 4-inch", etc. For many dams, accurate and detailed as-built gradation information for shell zones is not readily available, or the variability of actual materials used is large.

After reviewing characteristics of several typical dams in the categories of interest, the configuration chosen for this study was a zoned embankment containing a relatively thick core zone comprised of a low permeability cohesive soil, specifically a CL-ML silty clay (Figure 2-4). Other soil types that are commonly used in such a configuration include clay (CL), sandy clay (SC), silt (ML), or silty sand (SM) (USCS Soil Classification symbols; see Appendix C for details regarding USCS soil classifications). The interior slope of the core zone was arbitrarily set at ¼:1 (h:v). The exterior (upstream and downstream) embankment zones were comprised of coarser materials, representative of rockfill. Due to the size of the headbox, the exterior (upstream and downstream) embankment slopes were set at 2:1, although typical embankment slopes on large zoned and rockfill dams are generally in the range of 2:1 to 3:1, or sometimes even flatter. For this testing, a relatively simple zoning was adopted without filter and drain components, which is representative of embankments commonly constructed in the U.S. during the early to mid-1900s. More recent designs often incorporate seepage management and seepage protection features such as filter zones, toe drains, and chimney drains. These features make internal erosion failures less likely, and can affect breach mechanisms and progression to failure for events triggered by either overtopping or internal erosion.
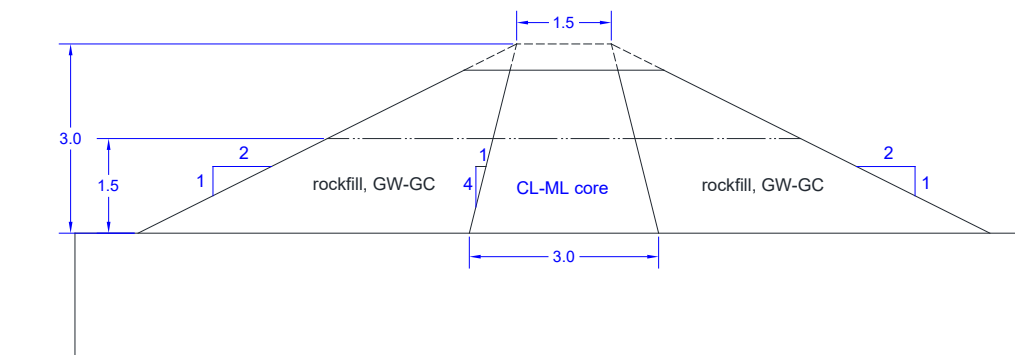
Figure 2-4   Cross-section view of 3-ft-high (0.91-m) embankment test section for overtopping test, with flow from right to left. The pilot channel was approximately 5 inches (13 cm) deep. The internal erosion initiation point was at mid-height.

Discussions with NRC, Reclamation embankment dam designers, and staff of the U.S. Army Corps of Engineers did not reveal any firm definition or quantitative criteria for the gradation of typical rockfill zones. The consensus among those consulted was that the characteristics of rockfills vary widely, but when examined in the field, most prove to be "dirtier" than might be expected from specifications, drawings, or what the term "rockfill" might imply. Considering all of the factors discussed above, the decision was made to construct the zoned test embankment shells from a broadly-graded Class 6 road base material available from a local aggregate supplier. Under the Unified Soil Classification System the material was classified as Well-Graded Gravel with Clay and Sand (GW-GC). The coefficients of uniformity and curvature for this material were $C_u=D_{60}/D_{10}=180$ and $C_c=D_{30}^2/(D_{60}D_{10})=1.09$ ($C_u \geq 4$ and $1 \leq C_c \leq 3$ needed for a well-graded gravel). Further details of the embankment soils are provided in the next section.

2.5   Materials

2.5.1   Embankment Core

The core of the zoned embankments and the entire section of the preliminary homogeneous embankment were constructed from a silty clay (CL-ML) soil obtained from a borrow area established during the construction of Reclamation's Bonny Dam (1948-1951) in northeastern Colorado. This material has also been used in other ongoing Reclamation research studies relating to internal erosion through cracks in embankment dams. The material was delivered to the laboratory in early 2015 in 4 truckloads, with samples pulled for laboratory analysis from each load and a composite sample representing a mix of the loads. Gradation analysis and Atterberg limit tests were performed by a contracted laboratory (detailed results provided in Appendix A). The composite sample results inexplicably differed from the average results of the individual load samples for the gradation of the fines; an average of the properties of the individual samples is believed to best represent the material. Atterberg limits were similar for all 5 samples. Average values of pertinent properties include:

- Liquid Limit, LL = 27
- Plastic Limit, PL = 21
- Plasticity Index, PI = 6
- clay fraction (≤ 0.002 mm) = 3.5%
- 89% fines (passing U.S. No. 200 sieve) and 11% sand.

A Standard Proctor compaction test was also performed by the contracted laboratory, which indicated a maximum density of 105.2 lb/ft³ (1.69 g/cm³) at 17% water content.

Prior to the preliminary homogeneous embankment test, Reclamation also compacted a series of cylinders at a range of water contents and performed submerged jet erosion tests (JET) on each specimen (ASTM D5852; Hanson and Cook 2004). This test measures soil erodibility by directing a submerged ¼-in-diameter (6.35-mm) jet at the soil surface to create a scour hole, as shown in Figure 2-5. The observed scour depth versus time data are used to determine the parameters k_d and τ_c of the linear excess stress equation used to model soil erosion in many dam breach models (e.g., WinDAM C, DL Breach, and HR BREACH):

$$\varepsilon_r = k_d(\tau_e - \tau_c) \tag{1}$$

where ε_r is the soil erosion rate (ft/hr), k_d is the detachment rate coefficient [ft/hr/(lb/ft²)], τ_e is the effective shear stress applied to the soil grains (lb/ft²), and τ_c is the critical shear stress (lb/ft²) needed to initiate erosion. In addition to the testing of the compaction cylinders, JETs were also

performed as each of the embankments were constructed. Figure 2-6 summarizes density and erodibility testing performed on all of the compaction cylinders and embankments. In situ embankment density and water content values were obtained from sand cone tests performed during construction. For the preliminary test of the homogeneous embankment, sand cone tests were performed at the mid-height of the embankment and prior to placing the last lift on the crest, and a JET was conducted at mid-height. For the zoned embankments, sand cone tests and JETs were conducted only at the intermediate height, since working space was limited as the embankments were topped out. On the second zoned embankment (internal erosion test) a JET could not be successfully performed during construction because the silty clay zone had become contaminated with gravel particles from the adjacent zones (probably tracked in on the boots of the workers building the embankment), and this prevented obtaining a good water seal at the bottom of the JET submergence tank. The small quantity of gravel (9% by weight, based on material excavated during the sand cone test) is not believed to have been sufficient to affect the erosion resistance of the core zone during the second test, but it was enough to prevent successful JET testing.
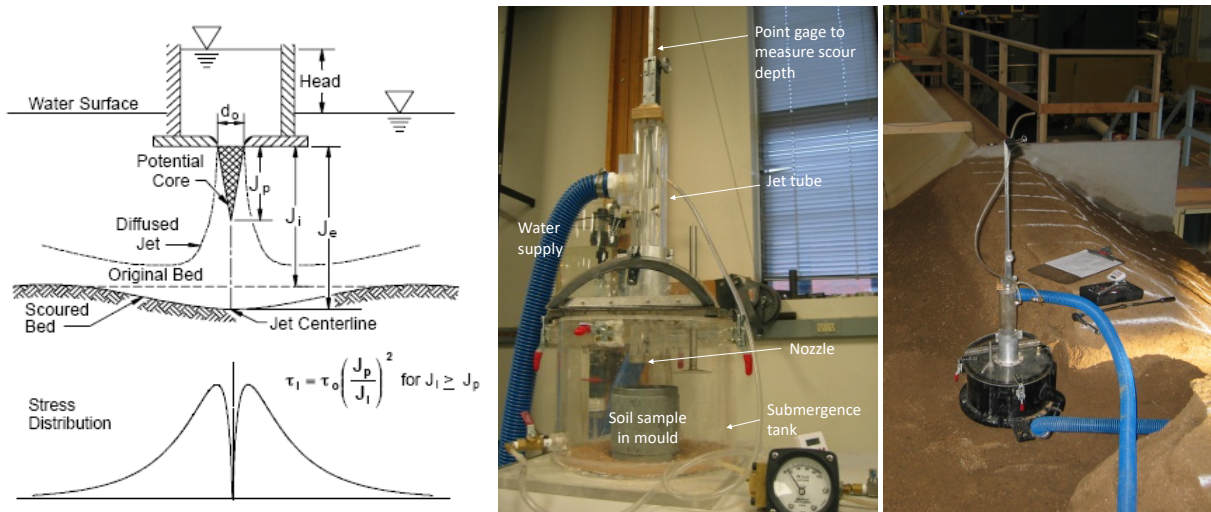
Figure 2-5   Schematic diagram of submerged jet erosion test, laboratory configuration with labeled components, and a typical *in situ* test setup.

Figure 2-6 shows that the densities and erodibility parameters achieved for the embankment soils were comparable to those obtained at optimum water content in the compaction tests. This is a good indication that the placement methods used for the embankment were imparting approximately Standard Proctor compaction energy (12,375 ft-lb/ft^3 = 593 kN-m/m^3) during the construction of each of the embankments. The one exception is the density test result obtained near the crest of the first homogeneous embankment, which showed lighter compaction, due either to drier soil conditions or less effective compaction within the limited area of the narrow crest. For the second zoned embankment in which gravel contamination of the core zone occurred, the total dry unit weight was about 4% higher than that measured for the first zoned embankment; with a correction applied for the oversize material, the unit weight of the silty clay material was computed to be only 0.6% higher than in the first zoned embankment.
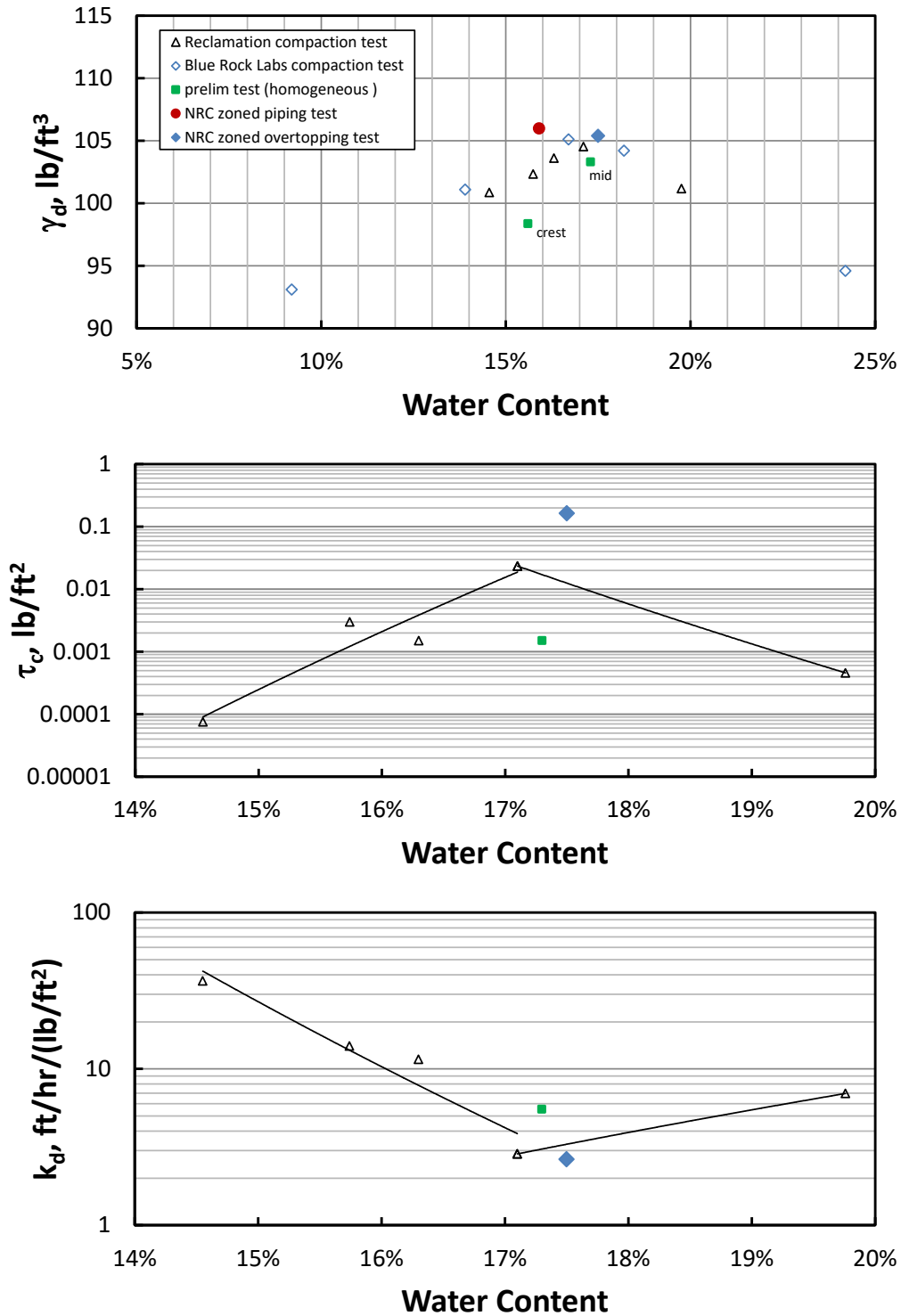
Figure 2-6 Compaction and erodibility characteristics determined from compaction testing and from JET and sand cone tests. Lines on the k_d and τ_c charts illustrate linear regression trends through dry-of-optimum and wet-of-optimum data points.

2.5.2   Upstream and Downstream Rockfill Zones

The upstream and downstream portions of the zoned embankments were constructed from a Class 6 road base soil obtained from a Denver-area aggregate supplier. For use as a road base material, this soil was required to meet the following specifications:

- LL ≤ 30
- 100% passing 1-inch (25.4 mm) sieve
- 95-100% passing ¾-inch (19 mm) sieve
- 30-65% passing #4 sieve (4.75 mm)
- 25-55% passing #8 sieve (2.4 mm)
- 3-12% fines, passing U.S. No. 200 sieve (0.074 mm)

The material was delivered to Reclamation in April 2017 and a sample was tested by a contracted lab to determine the gradation and plasticity properties and USCS soil classification. Full results are provided in Appendix A. The soil did meet the road base specification, with the maximum allowable amount of fines. A summary of other relevant information from the lab tests is given below:

- USCS Soil Description and Classification: **Well-Graded Gravel with Clay and Sand (GW-GC)**
- Angular coarse aggregate, maximum size ¾-inch (19 mm)
- 54% gravel, 34% sand, 12% fines including 3% clay (≤ 0.002 mm)
- Coefficient of uniformity, $C_u = D_{60}/D_{10}$ = 180 (≥ 4 required for well-graded gravel, ≥ 6 required for well-graded sand)
- Coefficient of curvature, $C_c = (D_{30})^2/(D_{60}D_{10})$ = 1.1 (1 ≤ C_c ≤ 3 required for well-graded)
- LL = 25, PL=19, PI = 6
- Fraction passing the No. 40 sieve is classified as Silty Clay, CL-ML.

This soil has an interesting dual-symbol classification, GW-GC. Soils with 5 to 12% fines content are known to be variable and less predictable in their engineering behavior, sometimes performing like coarse grained soils, and at other times performing like fine-grained soils (Howard and Howard 2015). This is reflected by assigning them a symbol representing each type of behavior. Interestingly, one additional percent of fines content would have pushed this soil into another dual-symbol classification, Silty, Clayey Gravel with Sand (GC-GM). The reason for dual symbols in that case would be the CL-ML classification of the fines; the soil may behave as a silty material or a clayey material, but with a little more or less plasticity, the soil would behave definitely as one or the other, becoming either Clayey Gravel with Sand (GC) or Silty Gravel with Sand (GM). The "with Sand" suffix would be added in either case because the sand percentage is ≥15%. In soils with 13% or more fines, the fines tend to dominate the behavior of the soil more than the gradation characteristics (well-graded vs. poorly graded) of the coarse component (the gravel in this case), so the gradation characteristic is dropped from the soil name.

The contracted laboratory that evaluated the road base soil also performed a standard compaction test, using ASTM D698 Method C procedures (Appendix A). This compaction test applies Standard Proctor energy, but utilizes a larger mold (2.12 L = 0.075 ft^3) due to the presence of the coarse materials. The compaction test indicated that maximum dry density was 140.0 lb/ft^3 at 7.5% water content. Following the construction of the first zoned embankment, a sand cone test indicated a placed material dry density of 127.3 lb/ft^3 at 5.6% water content (91%

of the standard Proctor maximum density). This result was surprising because moisture checks carried out during soil placement had indicated that the soil was probably being placed near or wet of the optimum water content of 7.5%, and the compaction curve suggested that a dry density of about 138 lb/ft^3 should have been achieved even if the drier 5.6% water content was accurate. A visual examination of the material in place and subjective evaluation of its density during the digging of the hole for the sand cone test suggested that very good compaction had been achieved, so it seemed doubtful that the density could be almost 10% less than expected from the compaction test curve.

During the construction of the second zoned embankment (internal erosion test), similar compaction procedures were used, and another sand cone test was performed at the midpoint of embankment construction. This sand cone test used a larger diameter 12-inch (30.5 cm) cone instead of the 8-inch (20.3 cm) cone that had been used for the test of the first zoned embankment. The result was much more consistent with expectations, yielding a dry density of 140.1 lb/ft^3 and a placed water content of 6.9%. Visual examination of this material suggested that its compaction was very similar to that achieved on the first embankment. The sand cone result for the first embankment was thus considered to be an unreliable indicator of the condition of the road base zone in that embankment. No jet testing was performed during initial embankment construction to evaluate the erodibility of the gravel zone, since the high gravel content would have prevented establishing the seal against the ground surface needed to submerge the test site. However, subsequent jet testing was performed on samples of the gravel soil that were screened to remove the coarsest particles (Table 4-2). Results of those tests are discussed in section 4.3.

2.6   Embankment Construction

The embankments for each of the tests were constructed in about one to two weeks, and were tested within a few days after completion of construction. (The reservoirs were kept empty until immediately before each test.) The first zoned embankment for the NRC-funded tests was constructed in mid-June 2017 and the overtopping test was conducted on June 19-20, 2017. This embankment filled the full width of the test section, approximately 13.5 ft (4.1 m) wide at the crest of the embankment. Erosion during the overtopping test only affected a 2-ft-wide (0.6 m) section of the embankment immediately adjacent to the acrylic wall at the left end. Following the test, about 4 ft (1.2 m) of the embankment adjacent to the left wall was excavated and this portion was then reconstructed in mid-August for the internal erosion test. Identical zoning of the embankment was used so that the reconstructed and remnant embankments matched one another. Erosion during the internal erosion test did not progress into the interface between the two zones, so this "partial" reconstruction of the embankment did not affect the second test.

Prior to starting embankment construction, the necessary soils were brought into the indoor laboratory and moisturized or spread for drying, depending on their initial moisture state. Soils that needed additional moisture were stirred (usually by repeatedly lifting with forklift tongs) after moisture was added, then covered and left to condition overnight. The placement objective for all zones was optimum water content. Moisture levels were periodically checked during construction using rapid microwave oven moisture tests and overnight convection oven-based tests.

The embankments were constructed by placing soil in loose lift layers that were about 6 inches (15 cm) thick. Compaction of each layer was provided with two initial passes of a vibratory compactor, and the soil layer was then covered with a conveyor belt "blanket" and compacted

through the cover by a pneumatic "pogo stick" with a smooth, disk-shaped foot approximately 6 inches (15 cm) in diameter. All zones of the embankment received similar compaction treatment. The gravel zones were slightly overbuilt and then trimmed back with a shovel, although this was made difficult by the presence of the ¾-inch (19-mm) gravel, so the embankment was built as close to finished dimensions as possible. When the placement reached a height of about 15 to 18 inches (38 to 46 cm), construction was paused and sand cone tests and submerged jet erosion tests were performed. Following the completion of these tests, the areas affected by the testing were overexcavated, backfilled, and recompacted before the next lift was added. The surface of each lift was scarified lightly before the next lift was added.

For the overtopping test, a pilot channel was cut at the left abutment after the embankment was finished (Figure 2-7). The pilot channel was excavated to a depth of 5 inches (13 cm) and a base width of 15 inches (38 cm) with a 1:1 side slope on the embankment side. The invert of the pilot channel had segments of the core zone and the gravel zones exposed within it.

Figure 2-7   Pilot channel in zoned embankment prior to overtopping test.

For the internal erosion tests (both the preliminary homogeneous embankment and NRC Test 2), a #4 rebar (1/2-inch = 12.7-mm diameter) was embedded in the embankment adjacent to the acrylic left wall of the test section, about 18 inches (46 cm) above the base of the embankment. During the test of the homogeneous embankment, an attempt was made to measure the flow through the internal erosion conduit at the start of the test by forcing the exiting flow into the supercritical flume described earlier, which had been calibrated in advance to establish a relation between the observed top width of flow vs. discharge. This was done to overcome the fact that breach discharge determination by subtracting the spillway flow from the measured inflow is unable to resolve small changes in flow at the beginning of the test when breach flow rates are still small. This attempt was mostly unsuccessful because a cleat accidentally left in place at the toe of the embankment caused the flow to be deflected away from the measuring flume as the flow rate increased. For the internal erosion test of the NRC zoned embankment, a

different approach was taken. A short weir wall (about 5 inches = 13 cm high) was constructed at the downstream edge of the headbox, with a small V-notch weir opening provided to discharge the flow into the supercritical flume and allow its measurement. This weir wall also provided some small tailwater depth against the toe of the embankment. While this flow measurement scheme worked better, the flow rates through the internal erosion failure site during this test did not vary significantly during the test, so the ability to quantitatively measure the flow was of limited value.

2.7   General Test Protocol

All embankments were tested by filling the headbox rapidly and establishing the desired depth in the reservoir by regulating the spillway stop logs. The inflow to the model was set at a constant level throughout each test, and spillway stop logs were added as needed to maintain the desired reservoir head as the breach developed. The preliminary homogeneous embankment test was performed with a constant inflow of 16 ft^3/s (0.45 m^3/s). This proved to be more flow than was necessary and caused waves in the reservoir that were damaging to the upstream face of the embankment, although it did not materially affect the erosion processes in the breach. For subsequent tests the inflows were greatly reduced; a flow of 5 ft^3/s (0.14 m^3/s) was provided for the overtopping test, and 2 ft^3/s (0.057 m^3/s) was provided for the internal erosion test. These flow rates were selected based on pre-test numerical modeling used to estimate the expected increase in flow rate through the breach.

3   PRELIMINARY TEST – HOMOGENEOUS EMBANKMENT

3.1   Conduct of Test and General Observations

A condensed description of the internal erosion test of the homogenous silty clay embankment is given here; for more details, see Wahl et al. (2016). The test was initiated by pulling the embedded rebar from the embankment, which created a continuous hole or "pipe" with a diameter of about 0.5 inch (1.25 cm) through the embankment. Discharge of water from the pipe was immediately muddy and visibly increasing with time. Although the rebar was not in direct contact with the acrylic left abutment of the test section, erosion progressed quickly and the hole enlarged enough within about 3-4 minutes to become visible through the acrylic. Figure 3-1 shows the progression of breach conduit development at 6 min intervals.
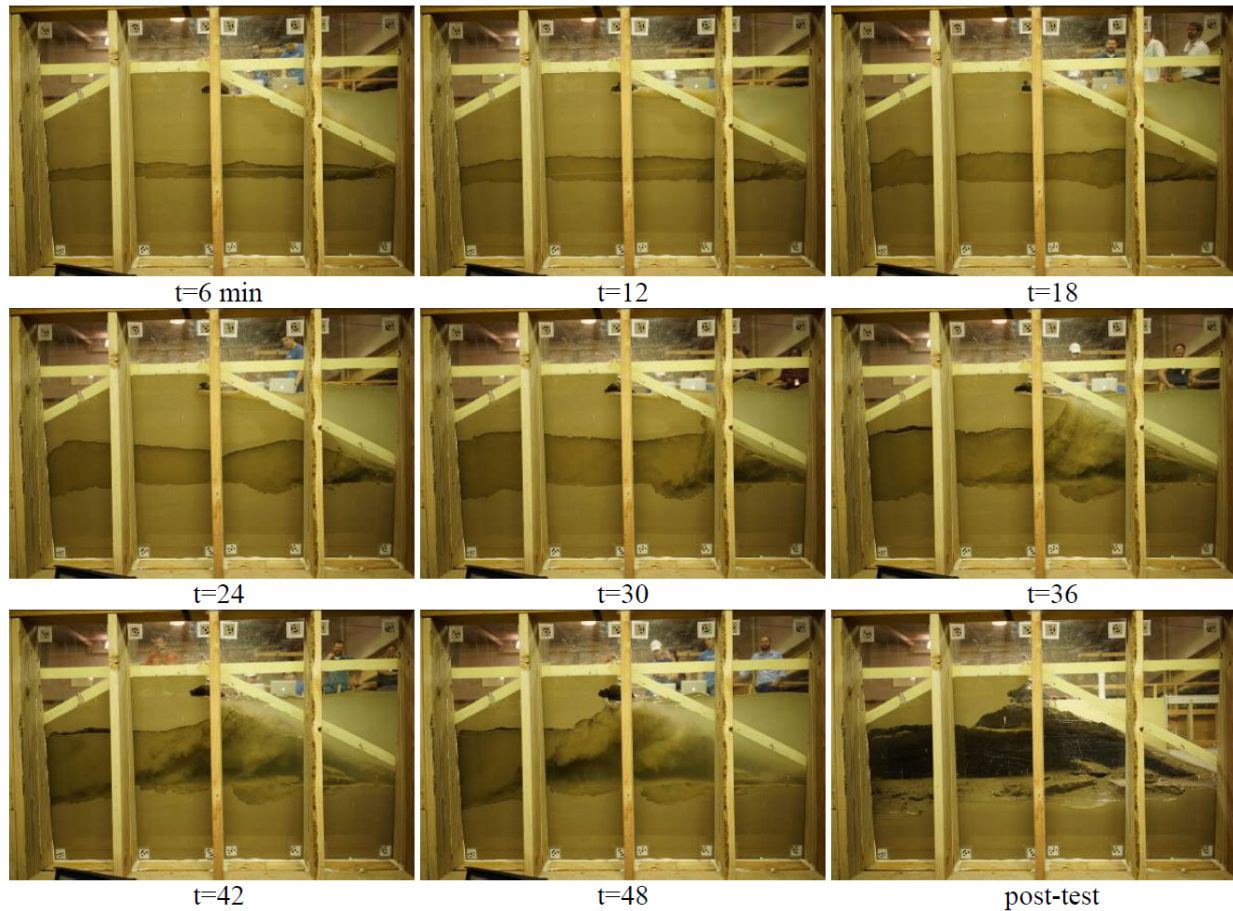
Figure 3-1   Incremental erosion during internal erosion test of homogeneous silty clay embankment.

Initially, the pipe enlarged in a relatively uniform manner along its length and on all sides of the initial centerline, but as the diameter of the pipe began to approach the depth of submergence of the intake ($t = 15$ min), the flow entering the pipe from the reservoir began to separate from the roof of the pipe, producing a strong jet along the floor of the pipe and a recirculating eddy at the roof of the conduit. Head loss in the entrance appeared to be large enough that a free

3-1

surface nearly developed inside of the entrance and by t = 24 min the floor jet began to produce a flow structure similar to a submerged hydraulic jump in the upstream end of the pipe. This led to increased scour and the development of an oversized chamber in the upstream end of the pipe (Figure 3-2). This chamber also expanded laterally, again seemingly due to separation of flow at the entrance followed by recirculation in a strong eddy just inside the pipe. Flow downstream from the chamber seemed to bounce from the bottom to the top of the pipe for several minutes, but the pipe eventually straightened again as it continued to enlarge.
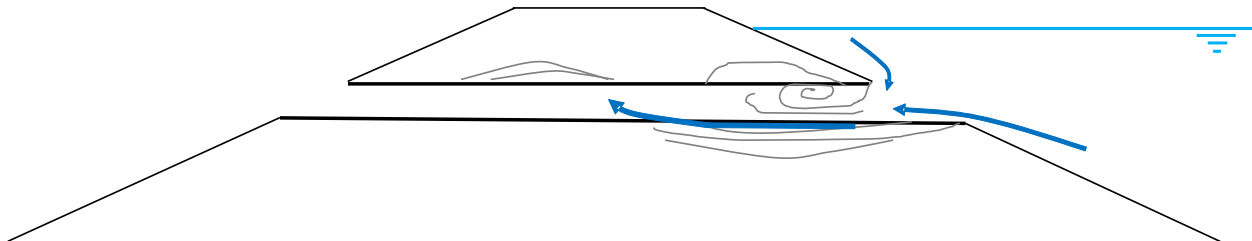
Figure 3-2   Sketch showing flow structure and related erosion patterns observed during internal erosion test (Wahl et al. 2016).

One flow feature that was unexpectedly absent from the test was significant headcut[2] erosion where the flow exited the internal erosion channel onto the downstream slope of the embankment. This has been a feature of some previous erosion tests involving piping of relatively weak soils (Hanson et al. 2010). However, in this test, there was very little downward erosion of the downstream slope. This is believed to be due, at least in part, to the fact that the lower half of the embankment seemed to be better compacted than the upper half, based on the sand cone density test results. This may have been due to a combination of lower water content in the upper portion of the embankment, some natural difficulty of compacting the lifts as the embankment grew taller and narrower, and overcompaction of the lower layers as upper lifts were added. Headcut development may have also been inhibited by the fact that there was an abrupt overfall immediately downstream from the embankment and thus there was no significant tailwater pool against the embankment toe for most of the test. A tailwater pool provides the opportunity for flow recirculation that may contribute to development of a vertical face (Frenette and Pestov 2005). Robinson and Hanson (1996) reported that stresses applied to a headcut wall and rates of headcut advance were greatest with a tailwater depth to headcut height ratio of 0.8; as low tailwater inhibits headcut advance, it may also retard headcut formation.

3.2   WinDAM C Modeling

The WinDAM C embankment breach model (USDA 2016) was applied to the homogeneous embankment test and its results were compared to the observed erosion. The embankment geometry was entered into the model and the following input parameters were initially provided, based on the pre-test JET measurements of erodibility and compacted soil density:

- k_d = 5.5 ft/hr/(lb/ft^2) = 9.73 cm^3/(N-s) (result from JET test at mid-height)

---

[2] Headcut erosion is characterized by the formation of a vertical or near-vertical drop or overfall in the channel bed and a plunge pool at the base of the drop. Flow over the drop leads to scour in the plunge pool that undermines the base of the overfall until the face collapses. Repetition of this cycle causes upstream migration of the headcut.

- c_u = 835 lb/ft² = 40 kPa (undrained shear strength, estimated for soft-to-firm soil consistency, from guidance in Hanson et al. [2011])
- Total unit weight of soil = 122 lb/ft³ = 1.95 g/cm³ (moist unit weight from compaction tests; water content = 17.3%)
- τ_c = 0.1 lb/ft² = 4.79 Pa (median of JET results near optimum water content of 17%)
- Initial conduit height and width = ½ inch = 13 mm (size of rebar)

Most of these input parameters have been previously introduced, with the exception of the undrained shear strength, c_u. This parameter is one component of WinDAM C's stress-based model for determining the rate of soil-block failures at the face of an advancing headcut, as illustrated in Figure 3-3. (The stress-based headcut model was used, rather than the optional energy-based model.) The undrained shear strength determines the shearing resistance that can be developed along the failure plane, line L. Values of c_u can be obtained from laboratory tests, such as the unconfined compression test, or estimated in the field on the basis of hand tests of soil consistency. Guidance for estimating a value of c_u is provided by Hanson et al. (2011).
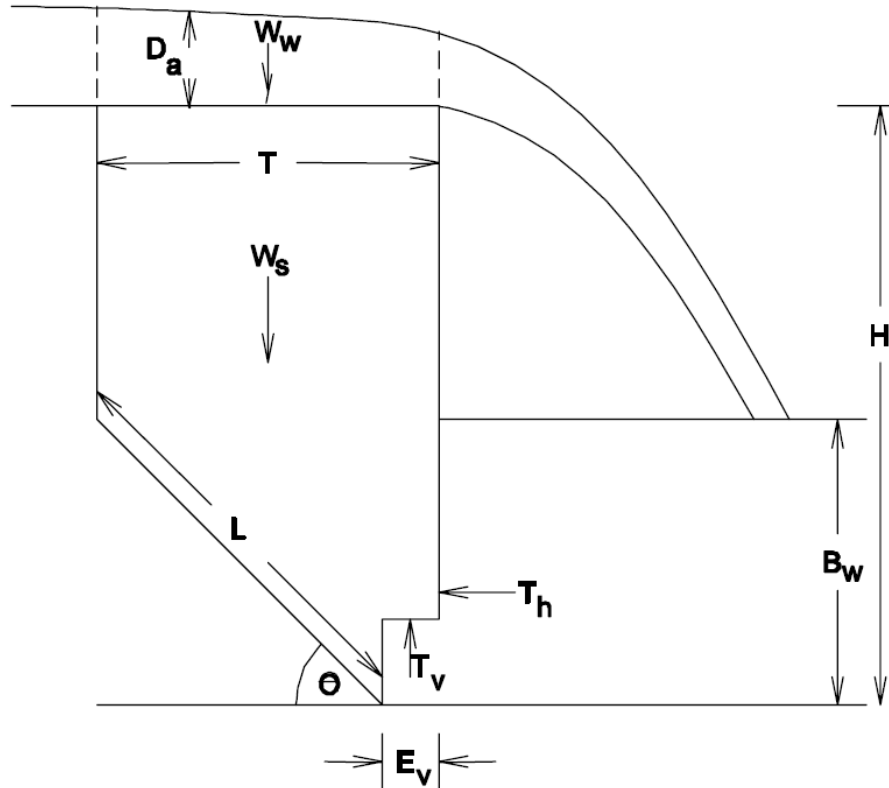
Figure 3-3 **Schematic diagram of the geometry and forces applied to a soil block at the face of an advancing headcut (from Robinson and Hanson 1994). Block failure occurs when the extent of erosion at the toe of the block, E_v, shortens the distance L so that shearing resistance along line L is insufficient to keep the block from sliding. T_h and T_v are the net forces caused by the tailwater, B_w. H is the headcut height, D_a is the approach flow depth, and W_w and W_s are the weights of water and soil, respectively. T gives the location of the tension crack and θ is the angle of the slip-failure plane.**

With the input parameters listed above, the model predicted growth of the breach conduit and discharge that were more rapid than actually observed. The model also predicted headcut development and advancement at the exit of the conduit, but this had little effect on the outflow rate during the period of comparison (Figure 3-4). (The model simulated conduit growth well past the time at which the experiment was stopped, continuing into the phase in which the top of the conduit collapses and the breach becomes an open channel flow.) Testing different values of the input parameters led to the conclusion that the k_d value and initial conduit dimensions had the most influence on the outputs. A final run with k_d reduced to 2 ft/hr/(lb/ft^2) [3.54 cm^3/(N-s)] and an initial conduit size of 1 inch by 1 inch (2.5 cm square) produced output that compared well with the observed data (Figure 3-5). This value of k_d seems reasonable, since k_d varied from about 2.5 to 5.5 ft/hr/(lb/ft^2) [4.4 to 9.7 cm^3/(N-s)] in the JET tests of this embankment and the other embankments constructed from the same soil, and it is possible that the lower portions of the embankment received additional compaction as upper lifts were added. The initial size of the conduit also seems reasonable. WinDAM C defines the erosion pipe as a rectangular conduit and tracks the height and width independently. Since the pipe was located adjacent to the abutment, the growth of the height is greater than the growth of the width, and the height corresponds to what was observed visually through the acrylic abutment, even though the actual conduit was not truly rectangular in section. Although the rebar embedded in the embankment was a #4 bar (nominally 0.5-inch = 13 mm diameter), the area disturbed when it was withdrawn was probably greater, so a starting dimension of 1 inch (25 mm) is reasonable.
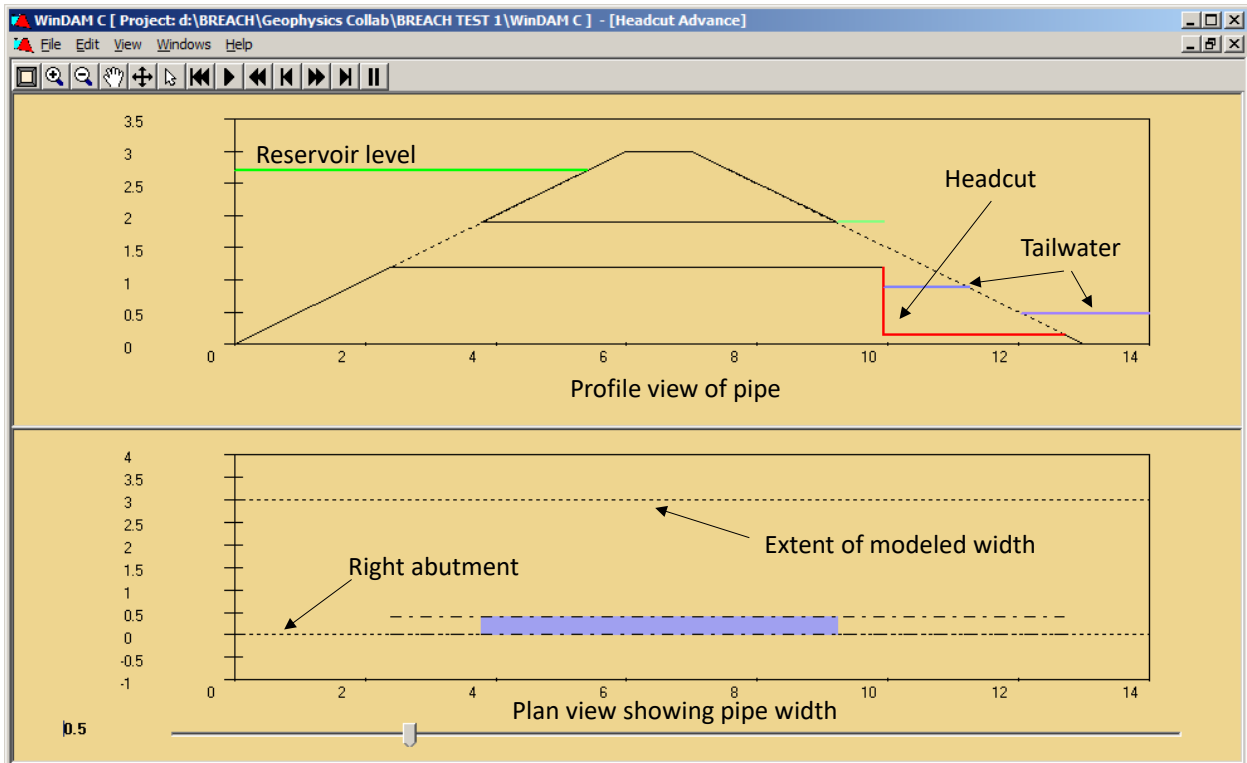
Figure 3-4 Cross-sectional elevation view (top) and plan view of internal erosion breach conduit development during WinDAM C simulation of the homogeneous embankment test at t=0.5 hr. Headcut erosion is depicted at the outlet of the conduit, but this did not occur in the physical model test.
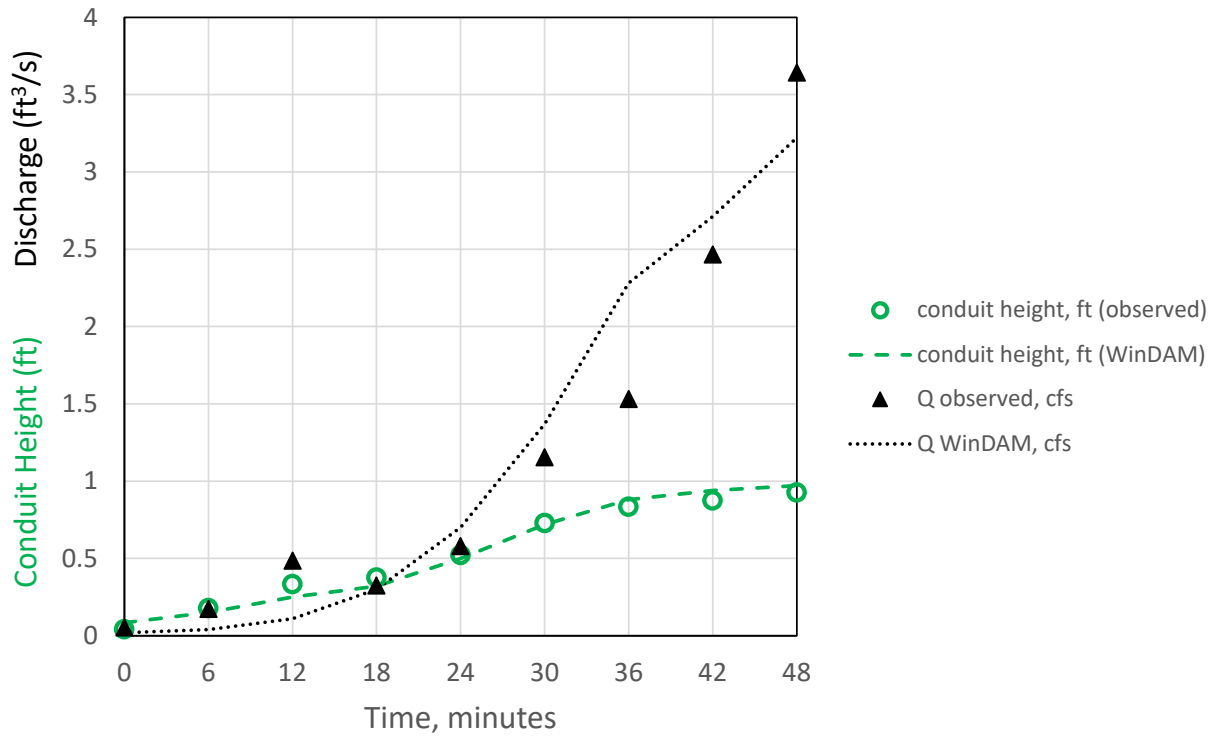
Figure 3-5 WinDAM C model comparison to homogeneous embankment internal erosion test.

4   ZONED EMBANKMENT TEST 1 – OVERTOPPING FLOW

4.1   Conduct of Test and General Observations

The first zoned embankment test took place over the course of two days, June 19-20, 2017. On the first day, flow was established with an overtopping head of about 4 inches (10 cm) through the 5 inch (13 cm) deep pilot channel (flow rate approximately 0.6 ft^3/s = 0.017 m^3/s). This maintained enough freeboard to eliminate any chance for the remainder of the embankment to be overtopped. Erosion was initially observed on both the downstream slope of the gravel zone and the top surface (crest) of the core zone where it was exposed within the pilot channel. Rates of downward erosion of the core were clearly equal to or more than the rates of surface erosion of the downstream slope. Since stresses applied to the downstream slope were significantly greater than the stresses applied by the flow across the crest, this suggested immediately that the critical shear stress needed to erode the silty clay was much lower than that needed to erode the gravel, and/or that the detachment rate coefficient of the silty clay was much larger than that of the gravel. The downstream slope of the gravel zone initially appeared to develop small overfalls (steps with vertical or near-vertical faces) with concentrated erosion of locally weak areas leading to deep erosion in the lee of more resistant areas. In fine-grained materials these small overfalls typically grow in height and steepen toward vertical, then begin advancing upstream as small headcuts, combining over time to form larger headcuts. However, during this test the crests of these overfalls tended to be eroded off before significant overfall height could develop, and the overall process was one of surface erosion.

The first day of testing lasted only 33 minutes, with the test stopped when the downstream tailbox was completely filled. Discharge through the breach reached a maximum of about 1.9 ft^3/s (0.054 m^3/s) at the end of the first day. Post-test analysis of the photographic and video records showed that although a classical vertical headcut did not develop, the downstream slope was gradually steepening toward vertical, rotating about 5° from the initial slope of 26.6° (2:1, h:v) to a final slope of about 32° (1.6:1).

On the second day, testing was resumed with the same inflow (5 ft^3/s = 0.14 m^3/s) and the same fixed reservoir level. Testing was continued for about 4 hrs, and during this time the breach discharge gradually increased to nearly 5 ft^3/s (0.14 m^3/s). For the last 42 minutes of the test, the inflow was increased repeatedly so that the reservoir water surface could be held steady, and the breach continued to enlarge. The maximum breach outflow was about 10.7 ft^3/s (0.30 m^3/s). During this second day of testing, the tendency for the downstream slope to steepen gradually reversed, and the channel ultimately flattened back to a slope of about 18° (3:1).

The erosion mechanism observed throughout the test was a combination of surface erosion of both the downstream slope and the crest of the core zone. At times the crest of the core actually eroded to levels significantly below the upstream edge of the gravel zone, especially at the start of the second day when there was rapid downward erosion of the top of the core, which had become saturated overnight by water standing in small depressions on the surface (see Figure 4-1). Although the core seemed less erosion resistant than the gravel zones, it was protected from more rapid erosion by the presence of the downstream gravel zone that prevented direct hydraulic attack against the downstream edge of the core.

The initial pilot channel widened as downward erosion was taking place. Significant widening occurred below the water surface but was not visible until the flow was stopped or when the channel would erode down enough that eroded areas became visible above the water surface.

The widening of the pilot channel appeared to some degree to be driven by flow contraction taking place at the entrance of the pilot channel and then the creation of horizontal recirculation zones immediately downstream from the pilot channel entrance. These horizontal eddies worked on the soil at the edges of the pilot channel, causing the pilot channel to widen, often at a rate that exceeded the deepening of the pilot channel. As the test progressed, an overhang began to form, with soil above the water surface hanging over areas that had eroded and widened. Eventually this overhanging soil broke off like a cantilevered beam and fell into the channel. Widening of the channel downstream from the crest was significant in the first 33 minutes of flow on the first day of testing, with the channel growing from about 15 to 24 inches wide (38 to 61 cm). Widening of the pilot channel during the first day was restricted somewhat by a wood stake that was embedded in the downstream edge of the embankment crest during construction (to hold a board separating zones as soil was initially placed) and accidentally left in place (Figure 4-2). This stake was removed before flow was resumed on the second day. As a result, the pilot channel width grew more rapidly for a short time during the second day of testing, but overall the width of the downstream channel grew slowly during the second day. Figure 4-3 shows the flow conditions just before the test was ended.

Figure 4-1   Erosion of top surface of core zone after about 6 minutes of flow on the second day of testing.

Figure 4-2   Breach pilot channel at the end of the first day of testing. Note the embedded wood stake that appeared to restrict lateral erosion.

Figure 4-3   Flow conditions through the breach channel near the end of the zoned embankment overtopping test (t=2 hr 56 min).

The breach channel developed during the first test in a much different manner from that predicted in WinDAM C model simulations.   In WinDAM C a headcut is assumed to develop initially at the top of the downstream slope. This headcut deepens and begins to advance upstream, often deepening all the way to the base of the embankment. The headcut advances upstream through the core zone, maintaining a vertical overfall within the core. Only when this headcut has advanced through the upstream edge of the original crest of the pilot channel does the flow through the breach significantly increase. There is no erosion and enlargement of the section controlling the flow until headcut advance moves the control section into the reservoir.

In the physical model test, downward erosion of the crest that contributed to an enlargement of the control section began immediately at the start of the test. As previously noted, the downstream gravel zone seemed to exhibit more erosion resistance than the core zone. This prevented a headcut from developing in the core zone because it never allowed an overfall to form in which toe scour could exceed the rate of downward erosion of the crest. The gravel zone eroded in a surficial manner with the 2:1 slope varying gradually during the test between 18° to 32° (S = 0.32 to 0.62). At times the slope would steepen, and at times small headcuts would even develop in the gravel, but those headcuts never grew to a height of more than about 2 to 3 inches (5 to 8 cm) before the protruding high points would be eroded away, restoring a relatively smooth overall slope. As the gravel zone eroded downward, the crest of the core zone would also erode downward with it, but the core zone remained approximately horizontal across the top throughout most of the test. At times the bed of the breach channel through the core zone would develop a slight slope, but it was typically horizontal. The upstream gravel zone also did not exhibit headcutting. At times a slight overfall would develop at the interface between the upstream gravel zone and the upstream edge of the core, but as this interface eroded, it tended to return back to an inclined slope rather than progress to a vertical slope.

The tendency of soils to erode surficially and not adopt a headcutting form is often attributed to an inability of the soil to stand as an unsupported vertical face. However, in this test, the sides of the breach opening were vertical and the gravel soil demonstrated a definite ability to stand vertically, even while subjected to significant hydraulic stress. This is discussed further in the Erosion Morphology section below. The failure to develop a headcut in the streamwise profile does not seem in this case to be caused by soil factors, but by another property of the flow situation. Regardless of the reason, this pattern of breach development makes it difficult to use WinDAM to model the breach development process, since it assumes headcutting with no surface erosion of the top of the dam crest.

4.2   Erosion Morphology

The observed mode of erosion in this test was surface erosion of the downstream face of the gravel zone and on the crest of the core zone. Headcut erosion did not take place in either zone, which was somewhat surprising because both soils had a cohesive nature.

During the first few minutes of the test, headcut erosion seemed likely to develop along the downstream slope, as a series of small overfalls developed. Two factors may have been responsible for the lack of further development of these headcuts. First, there was no significant tailwater pool immediately downstream from the embankment in the early stages of the test, which prevents a recirculating eddy from developing at the toe of the dam. Recirculation of flow could have accelerated erosion of the toe and led to steepening of the downstream slope toward a headcut configuration. Second, the low erosion resistance of the core zone led to rapid surface erosion of the top of the core, and this quickly increased the flow through the breach to a point that may have significantly exceeded the critical shear stress of the gravel soil.

This allowed the high points of any developing overfalls to be eroded, rather than persisting long enough to produce large vertical drops. One factor often cited for the lack of headcut development in noncohesive soils is an inability of the soil to stand unsupported at nearly vertical slopes, but Figure 4-4 clearly shows that the gravel zone was capable of standing at such slopes. These slopes developed while flow was primarily attacking the toe of the slope (Figure 4-4a).

(a)   (b)
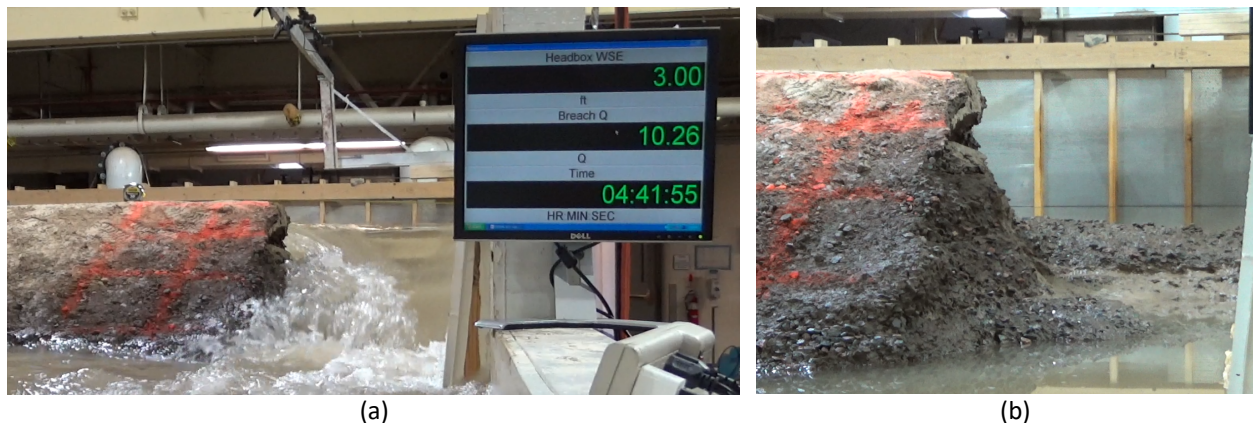
Figure 4-4   Views from downstream show that the sides of the breach were clearly able to stand at nearly vertical slopes. View (a) on the left shows flow through the opening, and (b) on the right shows the breach after the flow was stopped.

Headcut erosion did not develop in the core zone due to the comparatively high erosion resistance of the downstream gravel zone. Because the gravel zone seemed to have more erosion resistance than the core, an overfall at the downstream edge of the core was never created and the gravel zone protected the downstream face of the core from backward erosion. If the erosion resistance characteristics had been reversed, with a highly erodible granular material downstream and a more resistant cohesive core zone, it is likely that the downstream zone would have eroded quickly and completely, leaving the core standing free and subject to headcut erosion from an overfall with a height equal to the dam height. This vertical face would have advanced upstream as the toe was eroded, causing failure of undercut soil blocks.

4.3   Analysis of Imagery to Estimate Stresses, Erosion Rates, and Soil Erodibility Parameters

This test provides a potentially valuable opportunity to estimate the erodibility parameters of the embankment soils by determining observed erosion rates as they are subjected to overtopping flow stresses. In particular, the downstream gravel zone seemed to regulate the overall rate of erosion development during this test, but the erodibility of this material is typically difficult to evaluate in small-scale erosion test devices.

To estimate erodibility parameters of the downstream gravel zone, videotape records of the test were reviewed to identify test segments that contained steadily progressing erosion that could be analyzed to estimate applied stresses and erosion rates. The first 3 hours of the test were analyzed in this manner; the end of the test was not considered because erosion rates varied rapidly as the inflow to the model was increased at the end. Still photos recorded from the third most downstream camera viewing the left abutment (which had the best view of the downstream slope for most of the test) were collected and processed to estimate flow depths,

the slope of the eroding breach channel, and the rate of streambed erosion perpendicular to the slope. With these data, applied shear stresses were estimated from (Temple 1980; Hanson 1989)

$$\tau_e = \gamma RS \left(\frac{n_s}{n}\right)^2 \tag{2}$$

where τ_e is the effective stress applied to the soil grains, γ is the unit weight of water, R is the hydraulic radius (area divided by wetted perimeter), S is the bed slope (presumed to approximate the energy slope of the flow), n_s is the Manning's roughness coefficient for the soil grain roughness, and n is the Manning's roughness coefficient for the total flow. The ratio $(n_s/n)^2$ represents the fraction of the total channel shear stress ($\tau = \gamma RS$) that is applied to the soil grains to functionally cause soil detachment. The Manning's n value of the total flow is given by $n^2=n_s^2+n_f^2$, where n_f is the Manning's roughness factor of the bedforms, which carry a portion of the stress, making it unavailable for causing soil detachment. This effective stress approach has been successfully applied in the past to problems in which shear stress was partitioned among components due to soil grain roughness, vegetation, and bedforms (e.g., Einstein 1950, Temple 1980, Temple et al. 1987, Hanson 1989). To apply this method, n is determined with the Manning equation and the bulk flow characteristics, and n_s must be estimated based on the soil properties. Numerous relations for computing n_s are available, most being so-called *Strickler-type equations* (USGS 2012) that relate the roughness coefficient to the sixth root of a reference soil diameter; for soils with D_{75} greater than 0.05 inches (1.27 mm), Temple et al. (1987) suggest $n_s=(D_{75})^{1/6}/39$, with D_{75} given in inches, and that equation was used here. For the gravel zone, D_{75} was estimated from the gradation curve as 0.49 inches (12.4 mm), yielding $n_s=0.023$. For comparison, $n_s = 0.0156$ has been used in many studies of the erodibility of fine-grained soils (e.g., Hanson 1989, 1990). During the embankment overtopping test, values of Manning's n for the total flow ranged from 0.09 to 0.19 (back-calculated from Manning's equation), yielding values of $(n_s/n)^2$ ranging from 0.014 to 0.070. These values of Manning's n for the total flow are large in comparison to typical values for lined channels, and even exceed the range of values commonly recommended for most natural channels. The most likely reason for such large n values is the presence of large bedforms while the channel was actively eroding, although bedforms observed at the end of the test did not seem extraordinary (see Section 4.2). In the compilation of roughness coefficients by Chow (1959), values approaching or exceeding 0.2 are only associated with channels having large or dense vegetation or very large boundary roughness elements.

Once the applied effective stress was estimated, values of the detachment rate coefficient, k_d, were determined by applying the linear excess stress equation (Eq. 1), assuming that the critical shear stress was about $\tau_c = 0.02$ lb/ft^2 (an estimate based on subsequent jet erosion test results given in the next section). Because applied stresses are much larger than this critical shear stress, the resulting values of k_d are insensitive to the assumed value of τ_c.

Table 4-1 provides a summary of the data obtained from the photos shown in Figure 4-5 and Figure 4-6 from the first 3 hours of testing and the resulting k_d values. The k_d value at the end of each incremental time period was computed using the observed erosion during the preceding time interval and the average shear stress during that interval. Figure 4-7 shows the results graphically. The rate of erosion was rapid during the first 5 minutes of the test, but slowed dramatically thereafter. This was likely due to difficulty obtaining good compaction at the edge of the placement where there was no way to confine the soil. The highly erodible layer was about 6 inches (15 cm) thick. After the first few minutes, the flow depth was more difficult to determine from the photos due to turbulence, splashing, and aeration of the surface of the flow.

However, it appeared that the depth of solid water near the boundary was relatively steady, even as discharge through the breach approximately tripled in the first 33 minutes. Photos and video from the downstream side of the embankment showed that the channel width approximately doubled during the first day of testing (Figure 4-8 and Figure 4-9). The slope of the eroding channel gradually steepened during this first phase, starting at about 27° and steepening to about 32°.

Table 4-1   Flow and breach channel properties used to estimate value of k_d for gravel zone.

Elapsed time, hh:mm:ss	Channel width, ft	Flow depth, ft	Discharge, ft^3/s	Velocity, ft/s	Channel slope, S ft/ft	Manning's n	Shear stress[1], $\tau_e = \gamma RS'(n_s/n)^2$ lb/ft^2	Bed position normal to slope, ft	k_d ft/hr/(lb/ft^2)
0:03:20	1.10	0.23	0.61	2.42	0.51	0.123	0.158	0.34	---
0:05:20	1.16	0.23	0.73	2.69	0.53	0.114	0.193	0.45	22.54
0:07:20	1.22	0.24	0.84	2.92	0.57	0.110	0.225	0.47	2.98
0:14:20	1.42	0.24	1.17	3.43	0.58	0.097	0.305	0.51	1.43
0:19:20	1.57	0.24	1.50	3.94	0.60	0.088	0.398	0.54	1.18
0:26:20	1.77	0.25	1.81	4.13	0.60	0.086	0.432	0.59	1.13
0:34:28	2.07	0.25	2.01	3.88	0.62	0.096	0.376	0.64	1.19
0:37:00	2.08	0.26	2.01	3.79	0.58	0.096	0.357	0.67	1.31
0:47:00	2.10	0.29	2.21	3.61	0.53	0.105	0.313	0.71	0.73
1:17:00	2.16	0.38	2.5	3.02	0.49	0.140	0.204	0.82	1.18
2:00:00	2.25	0.61	3.63	2.66	0.45	0.192	0.141	0.88	0.70
3:00:00	2.38	0.64	4.55	3.00	0.32	0.153	0.177	0.95	0.36

[1]For steep slopes, channel slope used in Manning's equation and in the shear stress equation is S' = sin[tan^{-1}(S)]
Conversions: 1 ft = 0.3048 m; 1 ft^3/s = 0.0283 m^3/s; 1 ft/s = 0.3048 m/s; 1 lb/ft^2 = 47.88 Pa;
        1 ft/hr/(lb/ft^2) = 1.768 cm^3/(N-s)

On the second day, the channel continued to widen, but at a much slower rate. The slope stabilized and began to flatten again as the exposed top of the core zone continued to erode down, allowing the discharge to increase substantially. The analysis of erosion rates showed that the erosion resistance of the gravel zone tended to increase toward the interior of the embankment, perhaps indicating more effective compaction in the bottom layers, which received additional compaction energy as successive lifts were added. With the exception of the high erodibility estimated during the first few minutes of the test, the k_d values were in a similar range or slightly lower than those of the CL-ML soil used in the core zone of the embankment [about 2 to 5 ft/hr/(lb/ft^2) = 3.5 to 8.8 cm^3/(N-s)]. This range of k_d values is relatively narrow, considering that k_d of natural and compacted cohesive soils has been observed to vary by 5 to 6 orders of magnitude, from 0.001 to nearly 1000 ft/hr/(lb/ft^2) [0.0018 to 1800 cm^3/(N-s)] (Hanson and Simon 2001; Hanson and Hunt 2007; Wahl et al. 2008).

Figure 4-5 Photos of breach channel downward erosion progress on the first day of the zoned embankment overtopping test. Elapsed times (mm:ss) in the photos from left-to-right, top-to-bottom are: 3:20, 5:20, 7:20, 14:20, 19:20, 26:20, 33:20, and 33:20 (after flow was stopped).

Figure 4-6 Photos of breach channel downward erosion progress on the second day of the zoned embankment overtopping test. Total elapsed times in minutes in the photos from left-to-right, top-to-bottom are: 34.5, 37, 47, 77, 120, 180.
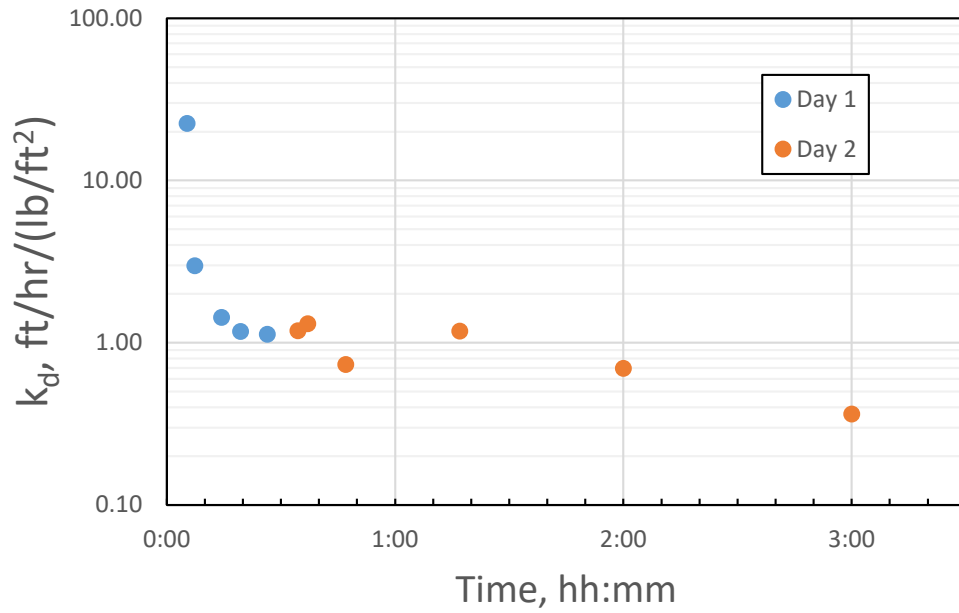
Figure 4-7   Variation of estimated k_d values for downstream gravel zone during zoned embankment overtopping test.
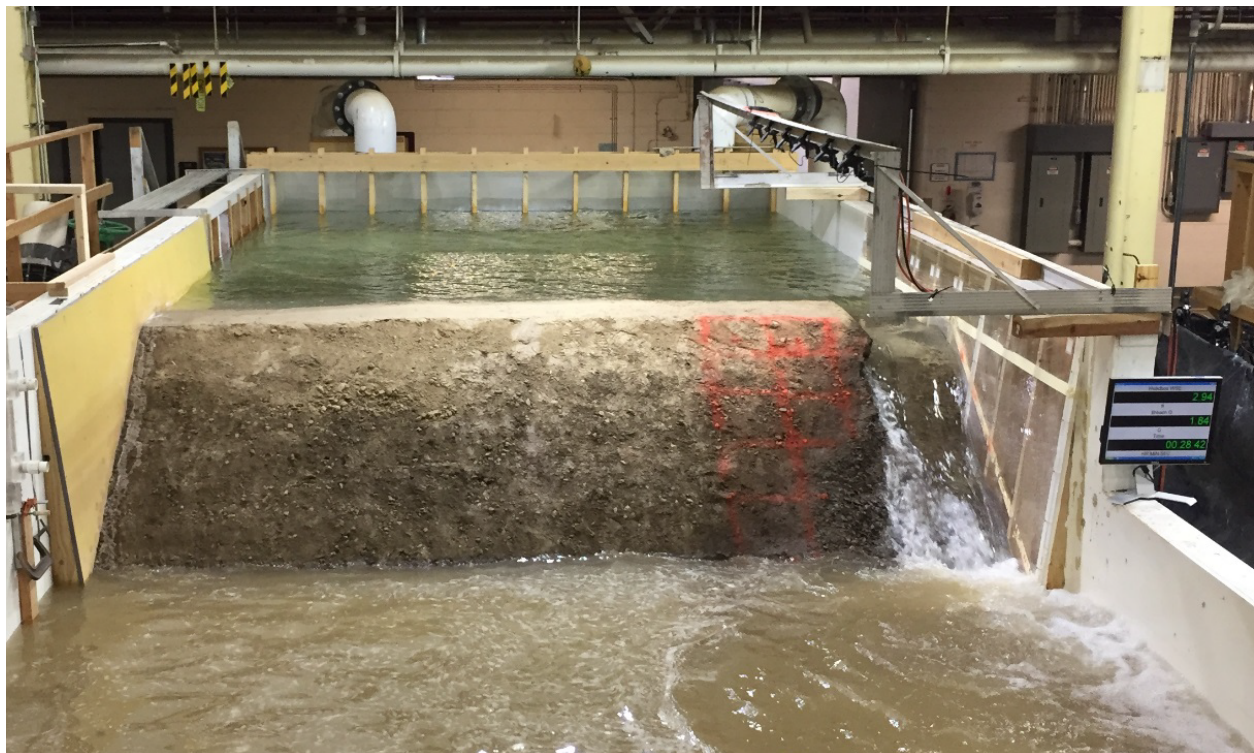
Figure 4-8   Downstream view of the breach channel 28 minutes after the start of overtopping flow. Vertical lines on the embankment face are at 1 ft (30.5 cm) intervals. Horizontal lines are at 0.5 ft (15.3 cm) elevation intervals.
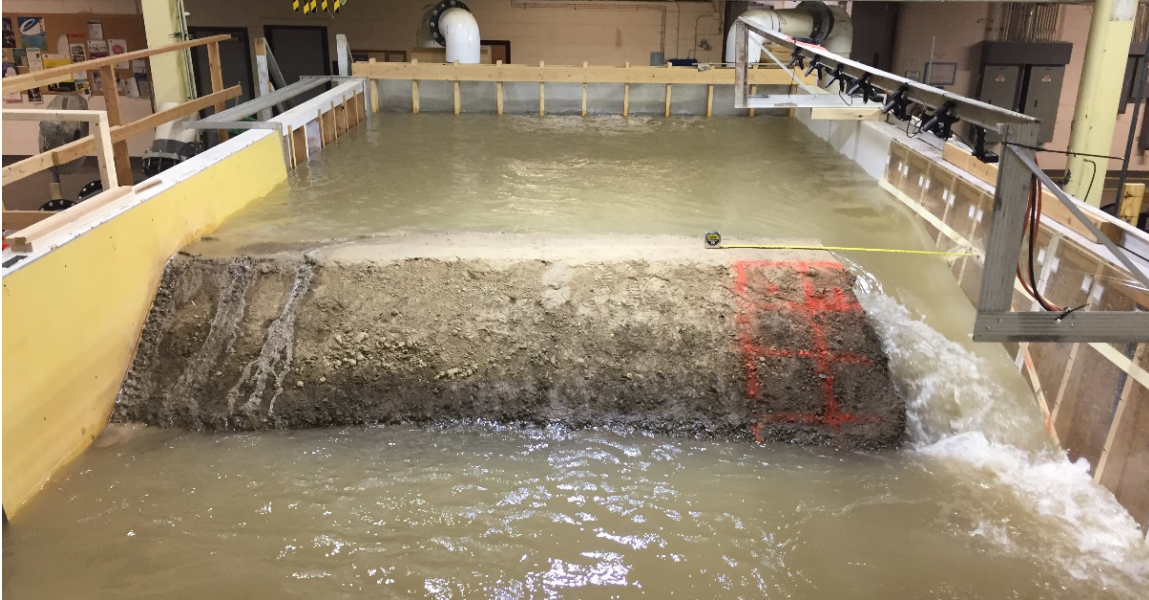
Figure 4-9   Downstream view of embankment near the end of the second day of testing, after a total elapsed test time of 5 hours, 8 minutes.

4.4   Jet Testing to Evaluate Erodibility of Rockfill Zone

The large-scale embankment test indicated that the gravel zones of this embankment had significant erosion resistance when subjected to overtopping flow. It would be valuable to have methods for evaluating this erosion resistance through readily applied lab or field test procedures. The submerged jet erosion test provides this capability for cohesive soils, but cannot be applied in situ to a gravelly soil because the bottom edge of the submergence tank cannot be easily driven into the soil to create the water-retaining seal needed to submerge the soil surface. There are also questions about the applicability of the test result when the scale of gravel particle size (D_{75}=12.4 mm) approaches or exceeds the diameter of the nozzle (¼ inch = 6.35 mm).

Wahl (2014) hypothesized that the erosion resistance of a gravelly soil might be comparable to the erosion resistance of a finer fraction of the soil, such as that obtained by removing the material larger than either the No. 4 (4.75 mm) or No. 40 (0.42 mm) sieve. If gravel particles are a small enough fraction of the soil, they might contribute minimally to the overall erosion resistance. This concept was tested by performing JETs on specimens of an SC Clayey Sand soil containing 14 percent fine gravel (up to ¾-inch or 19-mm diameter) and specimens of the minus No. 4 and minus No. 40 fractions of that soil. JETs on the full soil were performed with the specimen tilted up so that gravity could assist the removal of gravel particles from the scour hole once the surrounding finer-grained soil was eroded. The gravel content of the test soil was low enough that the finer-grained soil specimens could be compacted with the water content and final dry density adjusted through an oversize correction procedure (ASTM D4718, *Standard Practice for Correction of Unit Weight and Water Content for Soils Containing Oversize Particles)* so that the compacted condition of the finer fraction soil was similar to that component in the full soil. Although there was significant scatter of the individual JET results, mean values suggested that the hypothesis might be valid. No preference for screening at the No. 4 or No. 40 sieve was evident.

The gravel soil used in this embankment dam breach experiment had a much higher percentage of gravel (54%) than that used in the study by Wahl (2014), and is in fact a well-graded soil. If the gravel particles are numerous enough to armor the finer grained fraction of the soil against erosion, this could add erosion resistance. To test this concept, a series of JETs were performed in an attempt to evaluate the effect of the gravel on k_d and τ_c. The quantity of gravel in this soil exceeds the recommended level for application of the ASTM D4718 oversize correction (not more than 40% gravel), but because the soil is well-graded, contact between gravel particles is probably minimal, so ASTM D4718 procedures were still used to compute estimates of the water content and dry density of the finer fractions of the compacted gravel soil. Table 4-2 shows the specimens that were created and summarizes the JET results. In contrast to Wahl (2014), all JETs were performed with the surface of the test specimens in a normal, horizontal orientation. The distance of the jet nozzle from the soil surface was set as large as possible to maximize the extent of the jet impingement zone. The jet pressure was adjusted in each test to produce an estimated initial shear stress of approximately 1.5 lb/ft^2. Estimated applied stresses during the overtopping embankment test ranged from about 5 to 10 lb/ft^2 and it would be desirable to run JETs in a similar stress range, but it was also necessary to keep erosion rates low enough in the JET apparatus that reliable measurements could be made. Erosion rates that are too rapid (faster than 1 inch/min or 2.5 cm/min) make it difficult to collect usable information from the test.

The first row of Table 4-2 (specimen ID 0) shows a reference condition for the full soil, the optimum standard Proctor compaction condition from the compaction curve shown in Appendix A (7.5% percent water content and γ_d = 140 lb/ft^3). This was thought to be representative of the conditions of the compacted full soil during both zoned embankment tests, although there was some variability and uncertainty as discussed earlier. Columns 5 and 6 show the effective dry density and water content of the minus No. 4 fraction of the hypothetical specimen 0. The next two rows of Table 4-2 show two specimens (ID 1 and 2) that were created by using hand compaction in 5 layers to achieve a similar water content and target density as hypothetical specimen 0. This compaction effort was also expected to produce compaction that was similar to standard Proctor procedures. The next two specimens (3 and 4) were compacted with modified Proctor effort to see the effect of increased dry density. Specimen 3 was compacted at a similar water content as specimens 1 and 2, which is probably wetter than optimum for the modified (greater) compaction effort. Specimen 4 was compacted in a somewhat drier condition, but without a full modified Proctor compaction test curve, it is not known whether this specimen was compacted, dry, wet, or at optimum. The fact that a higher density was achieved suggests that it was closer to optimum than specimen 3. Specimen 5 was compacted with standard Proctor effort for comparison to specimens 1 and 2, and specimen 6 was compacted with modified Proctor effort for comparison with specimen 3 and specimen 4. Specimen 7 was a full gradation sample of the original gravel, compacted with standard Proctor procedures at near-optimum water content. The target water contents of specimens 5 and 6 were adjusted using ASTM D4718 so that they would be comparable to the water contents of specimens 1, 2, 3, and 7, but in reality they were compacted a little wetter than planned. It should be noted that each of the samples meets criteria for a well-graded material, although this is not reflected in the soil classification names for the minus No. 4 and minus 3/8-inch (9.5-mm) specimens, which would both be classified as SC-SM (Silty, Clayey Sand). In the Unified Soil Classification System, the relatively large fraction of fines in both of these soils causes their behavior for engineering purposes to be determined more by the properties of the fines than the gradation of the coarse fraction, so the fact that they are well graded is not reflected in their classification symbols or descriptions.

Table 4-2 Laboratory JET results on specimens derived from road base gravel.

ID (1)	Specimen (2)	Measured water content of tested specimen, w, % (3)	Measured dry density of tested specimen, γ_d, lb/ft^3 (4)	Water content of minus No. 4, computed using ASTM D4718 w_{-4}, % (5)	Dry density of minus No. 4, computed using ASTM D4718 γ_{d-4}, lb/ft^3 (6)	Compaction method (7)	Detachment rate coefficient, k_d, ft/hr/(lb/ft^2) (8)	Critical shear stress, τ_c, lb/ft^2 (9)
0	Reference, full sample at optimum compaction	7.0	140.0	12.4	114.3	Standard Proctor	–	–
1	Minus No. 4 fraction	12.4	113.2	12.4	113.2	5-layers, targeting Standard Proctor density $\gamma_d =$ 114 lb/ft^3 w = 12.5%	5.1	0.00024
2	Minus No. 4 fraction	12.8	112.9	12.8	112.9	5-layers, targeting Standard Proctor density $\gamma_d =$ 114 lb/ft^3 w = 12.5%	4.9	0.00029
3	Minus No. 4 fraction	13.0	124.8	13.0	124.8	modified Proctor, 56,250 ft-lb/ft^3 2,700 kN-m/m^3	0.63	0.025
4	Minus No. 4 fraction	11.4	130.3	11.4	130.3	modified Proctor	0.45	0.046
5	Minus 3/8-inch fraction	11.0	132.3	14.2	121.7	standard Proctor, 12,375 ft-lb/ft^3 593 kN-m/m^3	1.01	0.0056
6	Minus 3/8-inch fraction	10.3	133.7	13.2	123.3	modified Proctor	0.31	0.044
7	Full sample	8.4	140.3	15.5	114.8	standard Proctor	3.1	0.07

Conversions: 1 lb/ft^3 = 0.01602 g/cm^3; 1 ft/hr/(lb/ft^2) = 1.768 cm^3/(N-s); 1 lb/ft^2 = 47.88 N/m^2 = 47.88 Pa

The fifth and sixth columns of Table 4-2 compare the effective water content and dry density of the material passing the No. 4 screen in each of these specimens. Ideally, specimens 1, 2, 5, and 7 should be similar, and they are, with the exception of specimen 5 which compacted more effectively than expected and specimen 7 which was wetter than planned, but achieved a similar dry density as specimens 1 and 2. Specimens 3, 4, and 6 compacted about as expected, showing greater density due to the modified compaction effort. Specimen 4 compacted most effectively, as expected, since it was probably compacted at conditions that were close to optimum for the greater compaction effort.

Examining the JET results in the last two columns of Table 4-2 shows some expected trends, and good comparisons with the estimated k_d values from the overtopping zoned embankment test [around 0.5 to 2 ft/hr/(lb/ft^2) = 0.9 to 3.5 cm^3/(N-s) for most of the duration of test, see Table 4-1]. Tests on specimens 1 and 2 were very consistent with one another, as were tests on specimens 3 and 4, demonstrating an order of magnitude increase in erosion resistance when compaction effort was increased (one order of decrease of k_d and two orders of magnitude increase in τ_c). Specimen 5 was intended to investigate the effect of additional gravel content and did show increased erosion resistance compared to tests 1 and 2, but the result may well be due to the increased effectiveness of compaction, which was unexpected since the compaction effort was thought to be similar and the water content was greater than the target

value and greater than optimum. Specimen 6 provides a good comparison to specimen 3, with the water content and density values for the minus No. 4 material matching closely. The JET results show the k_d value to be lower by a factor of two (greater erosion resistance), but the critical shear stress values are similar, so the effect of the greater gravel content and larger maximum particle size appears to be minor. (It must be kept in mind that these are single tests and erodibility is inherently variable.) Finally, specimen 7 showed less erosion resistance when the specimen had the full gravel content. The observations of this test suggest that it was difficult to achieve sample uniformity and good compaction of the coarse gravel in the small soil mold (even though a 6-inch mold was used because of the larger gravel), and that scale effects (jet nozzle diameter vs. maximum particle size) were probably invalidating the test at this point. Segregation of material and nonuniformity of the specimen seemed likely (see Figure 4-10). In contrast, the tests of the minus 3/8-inch specimens seemed to proceed well and probably gave a valid indication of soil erodibility. This may represent an approximate upper limit on gravel size for use of this size JET device.

| Specimen 4 | Specimen 6 | Specimen 7 |
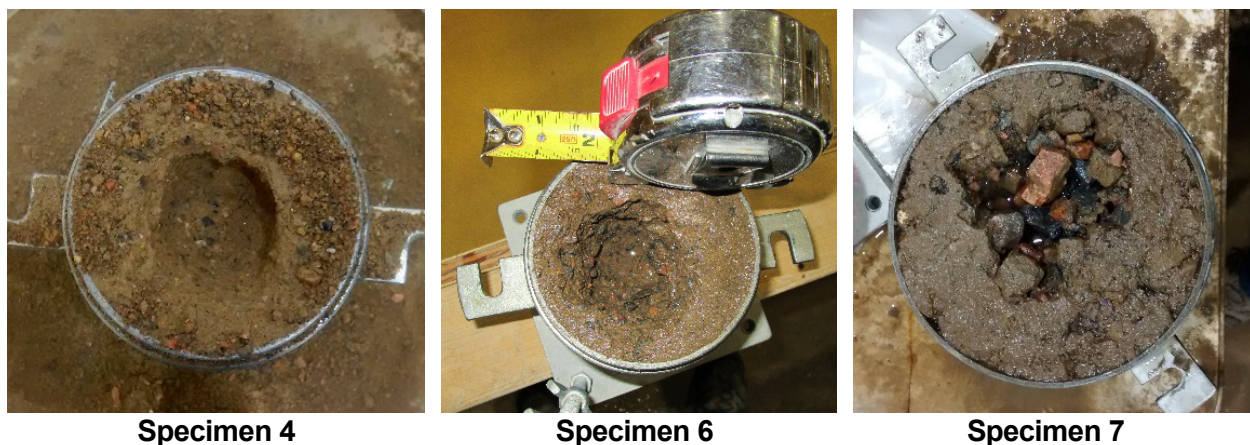
Figure 4-10 Selected JET specimens after testing.

Ultimately, this small series of jet tests was not sufficient to confirm that increased gravel content or a larger maximum particle size lead to increased erosion resistance, but increased compaction effectiveness and density did appear to consistently correlate with greater erosion resistance, as expected. There are suggestions that gravel content may increase erosion resistance, but more careful study with many more test repetitions and better control of other variables is needed to draw any firm conclusions. The JETs carried out on finer fractions of the gravelly soil did yield k_d values that are in the same order of magnitude as those estimated for the full gravel soil in the downstream zone of the overtopped embankment. The one JET performed on the full soil may have been beyond the scale limitations of the ¼-inch diameter JET device for this material, but even so, it yielded a k_d estimate that was in the same range as the value deduced from the embankment erosion observations.

4.5   Numerical Modeling – WinDAM C

The ultimate goal of the laboratory embankment breach testing program is to develop and improve the ability to model potential embankment failures numerically for risk assessment and emergency planning purposes. To evaluate the capabilities of existing numerical models, an attempt was made to simulate the overtopping test using two existing models that are often considered for overtopping-induced embankment failures, WinDAM C (USDA 2016), and DL

Breach (Wu 2016a, 2016b). Use of a third model, EMBREA (Morris 2011), was also considered but was not attempted at this time (see Section 4.7 for additional discussion).

WinDAM C allows the modeling of overtopping or internal erosion, but only for homogeneous embankments. To apply WinDAM C to a zoned embankment, one must identify the embankment zone that has the greatest erosion resistance and utilize material properties for the full embankment that will represent an average erosion rate. In this test, the gravel zones were the most resistant and should have the bulk of the influence on the overall erosion rate of the embankment.

Unfortunately, the occurrence of surface erosion instead of headcut erosion makes modeling this test with WinDAM C nearly impossible, since WinDAM C only simulates headcut erosion. A WinDAM C model was created and run for a range of soil parameters that could represent the gravel zones (k_d, τ_c, and undrained shear strength, c_u), but as expected, the model predicts development of a large headcut in the downstream slope, with no downward erosion of the dam crest (Figure 4-11). This is a fundamentally different erosion mechanism than was observed in the test and it leads to a dramatically different erosion progression. The maintenance of a constant reservoir head leads to a small, constant breach discharge in the WinDAM C model until the headcut advances through the crest, but in the physical model there is a constantly increasing discharge due to the crest lowering that starts immediately at the beginning of the test.

Figure 4-11 shows the WinDAM C simulation result when a constant discharge of 0.58 ft^3/s (0.016 m^3/s) is provided through the 15-inch (0.38-m) wide pilot channel located at the dam abutment. This corresponds to 4 inches (10 cm) of overtopping head. In this simulation, k_d is set to 2.65 ft/hr/(lb/ft^2) [4.7 cm^3/(N-s)] and 15.5 hrs of overtopping flow is needed for the headcut to advance to the threshold for entering the upstream reservoir. Increasing or decreasing k_d (or adjusting τ_c or c_u) changes the breach time (and the rate of breach enlargement after the reservoir begins to be released), but it does not change the fact that no downward erosion of the crest occurs. This is a fundamental assumption of WinDAM C. If downward erosion of the crest could occur in the model, that would lead to increasing flows and an acceleration of the erosion process.
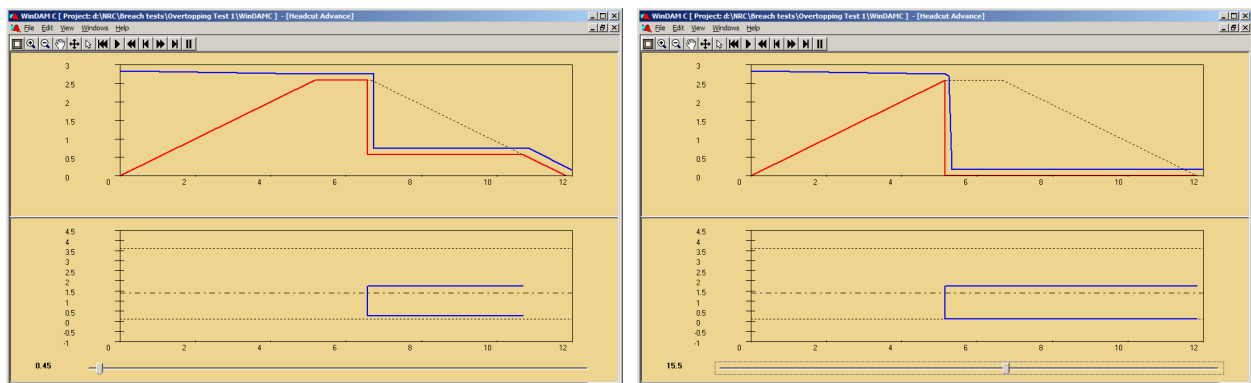
Figure 4-11 Headcut erosion simulation in WinDAM C. The left panel shows earlier progression of the headcut after 0.45 hr, and the right panel shows deepening and further advancement of the headcut after 15.5 hr. The bottom of each screenshot shows a plan view of the breach-channel growth.

4.6   Numerical Modeling – DL Breach

The DL Breach model is a relatively new dam breach simulation model developed by Wu (2013). The current version of the model (2016.4) is made freely available to the public, with user documentation (Wu 2016a, 2016b). This model is comprehensive and flexible, with capability to analyze homogeneous and zoned embankments experiencing overtopping flow or internal erosion. The model supports both surface erosion and headcut erosion processes, with three optional energy-based headcut erosion models, including the energy-based model that is available in WinDAM C. It does not provide WinDAM C's stress-based headcut model (which was used for the application of WinDAM C to the homogeneous internal erosion breach test discussed in section 3.1).

The idealized breach morphology adopted in DL Breach has significant differences from that of WinDAM C. In the surface erosion modes, simultaneous erosion of the downstream slope and crest of the embankment are possible, as illustrated in Figure 4-12. For the zoned embankment (b), the figure appears to depict a process similar to headcutting, but the process is still being modeled as surface erosion. In the illustrated case a steep slope develops on the downstream side of the core zone due to assumed greater erosion resistance of the core, but that slope does not become truly vertical as it would when headcut erosion takes place.

(a)   (b)
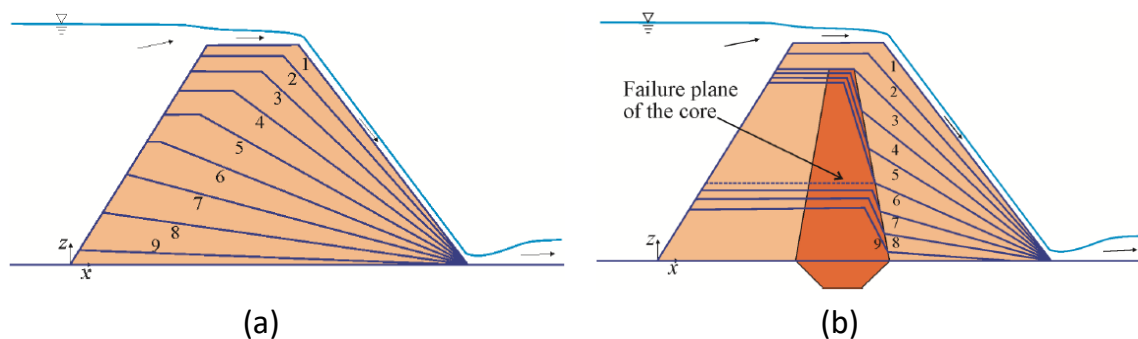
Figure 4-12 Temporal evolution of longitudinal profile for breach by surface erosion of a homogeneous embankment (a) and a zoned embankment (b). Numbers indicate incremental times. From Wu (2016a).

In the headcut erosion mode, DL Breach assumes that the headcut process initiates at the toe of the downstream slope, as shown in Figure 4-13; in contrast, WinDAM C assumes that headcutting starts at the top of the downstream slope and deepens and advances from that point (Figure 4-11), which conservatively starts the headcut as close to the crest as possible. DL Breach increases the headcut advance rate in the initial stages of headcutting based on an argument that a smaller volume of material is being eroded near the toe, so the rate should be faster. The net result may be similar predictions by WinDAM C and DL Breach of the total time needed for a headcut to advance into the crest and through the full embankment.

DL Breach only makes the headcut erosion option available for homogeneous embankments. When the headcut mode of breach formation is selected, erosion and lowering of the top surface of the crest can still take place using the same surface erosion options (cohesive or noncohesive soils) that are available for zoned embankments. Surface erosion of the downstream slope does not occur when headcutting is enabled; all erosion of the downstream

portion of the embankment must occur by headcut advance. It should also be noted that homogeneous embankments can be analyzed using either the surface erosion process described above and applied to both the crest and the downstream slope, or the headcutting process; the headcutting mode is not mandatory for homogeneous embankments.
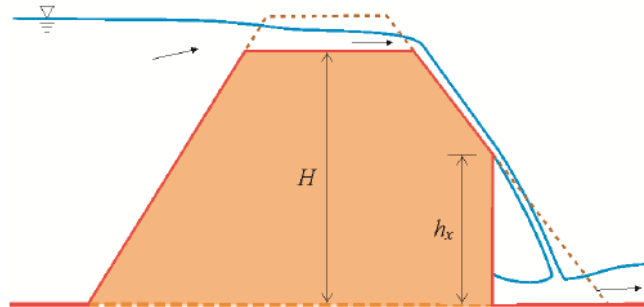
Figure 4-13 Early-stage headcut migration in the DL Breach model. From Wu (2016a).

DL Breach analyzes several mass-wasting processes deterministically through force-balance analysis of idealized failure masses. When headcut erosion is selected for a homogeneous dam, a potential sliding failure is considered for the full body of the dam upstream from the advancing headcut face. For the zoned embankment option a sliding failure through the core zone is possible. Both of these failure modes are shown in Figure 4-14 (also see Figure 4-12a), and both can lead to dramatic increases in breach outflow when sudden failures of these soil blocks occur. DL Breach also considers geotechnical stability of breach channel side slopes (Figure 4-15) using a balance-of-forces analysis. In comparison, WinDAM C analyzes headcut advance deterministically (see Figure 3-3), but it does not consider sliding failures through sections of the embankment, and side-slope failures are accounted for through an empirical relation between the headcut advance rate and the breach channel widening rate.
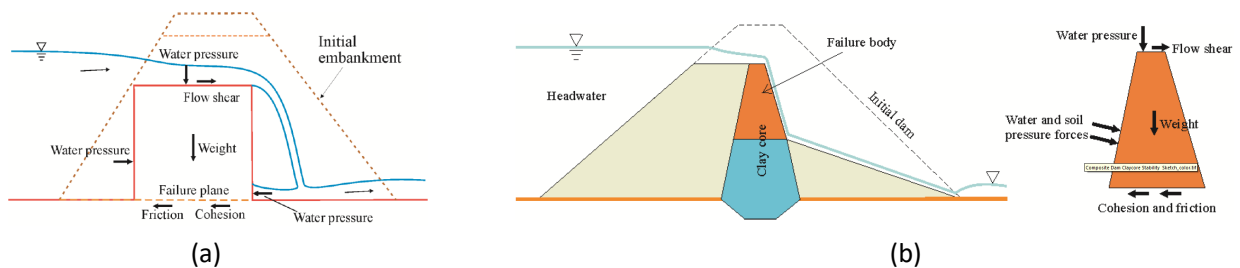
Figure 4-14 Force analysis for sliding failures during (a) homogeneous embankment headcutting and (b) zoned surface erosion. From Wu (2016a).
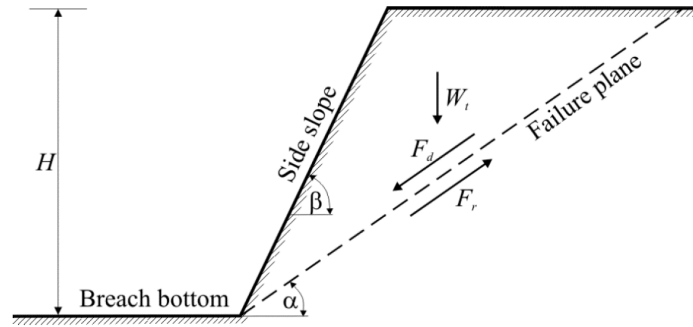
Figure 4-15 Geometry and forces used to analyze a planar sliding failure of the side slope of a breach channel in DL Breach.

After considering the modeling options offered, DL Breach was applied to the overtopping breach test with several different model configurations:

1. **Zoned embankment with surface erosion breach progression, utilizing cohesive soil erosion equations for all zones.** This configuration was chosen because it seemed to best describe the geometry and erosion mechanisms observed in the lab test.
2. **Zoned embankment with surface erosion breach progression, utilizing noncohesive soil erosion equations for some or all zones.** This configuration was tested to see the difference between cohesive and noncohesive erosion equations, and because the gravel zones contained soil with both cohesive and noncohesive characteristics.
3. **Homogeneous embankment with headcut erosion breach progression (simultaneous surface erosion of the crest to deepen and widen the pilot channel can also occur based on cohesive soil erosion equations).** This configuration was tested to see the effect in the numerical model of the headcut erosion process (even though headcutting was not observed in the lab test).
4. **Homogeneous embankment with surface erosion breach progression, using cohesive soil erosion equations.** This configuration was tested to see how it compared to the use of a zoned geometry.

The embankment model configuration that seemed at the outset to be most similar to the geometry and observed behavior of the tested embankment was option 1, the zoned embankment breached by surface erosion processes assuming cohesive soils (soils appeared to behave in a cohesive manner, even though headcutting did not develop). Based on information already presented, reasonable estimates of the k_d and τ_c parameters of each soil zone were available. Values of other necessary input parameters (representative soil particle diameter, specific gravity, porosity, clay content, cohesion, and internal friction) were estimated based on judgment and experience. (Some of these parameters were only relevant when noncohesive soil erosion equations were used in later model runs.)

- sediment diameter = 0.24 in. = 6 mm (D_{50} of gravel zone)
- specific gravity = 2.77 (from lab test)
- sediment porosity = 0.19 (estimated from compaction test result)
- clay content of main embankment (gravel zones) = 3% (from lab gradation test)

4-18

- cohesion (c_u) = 1440 lb/ft^2 = 69 kPa (handbook estimate based on soil type GW-GC)
- internal friction factor = 0.9 (42° friction angle)

Initial model runs were made using values of k_d and τ_c obtained from the submerged jet tests and from the analysis of the photos described earlier. For the core zone, k_d = 2.66 ft/hr/(lb/ft^2) and τ_c = 0.165 lb/ft^2 were used (Figure 2-6, data point for "zoned overtopping test"). For the gravel zones the averages of the values calculated in Table 4-1 for times after t = 6 minutes were used [k_d = 1.2 ft/hr/(lb/ft^2) and τ_c = 0.020 lb/ft^2]. The first runs produced an outflow hydrograph that increased very slowly at first then very rapidly (too rapidly compared to the observed outflow hydrograph) as a period of rapid crest-lowering occurred (Figure 4-16). It was difficult to infer the exact geometry of the erosion pattern because the principal output from the program was a simple text-file listing of breach bottom elevation, upstream and downstream slopes, and breach outflows. While spreadsheet templates could be used to display these data visually, no true animation or real-time view of the embankment geometry was available. A one-sided breach growth option was used for all DL Breach simulations, since the pilot channel in the model was located at the abutment.
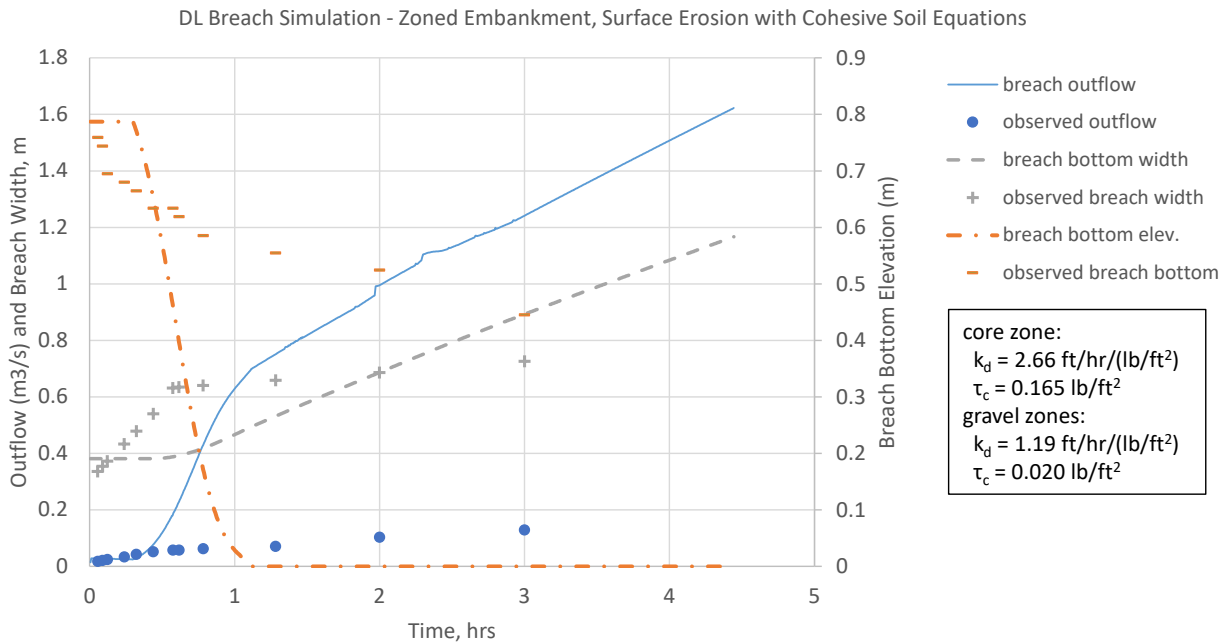
Figure 4-16 DL Breach simulation results for an initial program run with zoned embankment and cohesive soil erosion equations. Flow out of the breach becomes too large when the downstream slope is lowered enough that it begins to accelerate the lowering of the crest.

Trial-and-error adjustments were made to the k_d and τ_c values for the core and the gravel zones to obtain breach development and outflow hydrograph outputs that were more consistent with the experimental results. The value of τ_c for the core zone was reduced to 0.020 lb/ft^2 to be more consistent with the values obtained from JETs conducted on the full series of compaction test cylinders (see Figure 2-6), but the results did not seem very sensitive to this parameter. Results were more sensitive to the k_d values for the embankment body (upstream and

downstream gravel zones) and the core. A reasonable similarity of model-predicted outflows and experimental results was obtained using the following soil parameters (Figure 4-17):

- core zone: k_d = 2.0 (ft/hr)/(lb/ft²) and τ_c = 0.020 lb/ft²;
- gravel zones k_d = 0.057 (ft/hr)/(lb/ft²) and τ_c = 0.020 lb/ft².

The values of k_d are lower than those estimated for the core zone from jet tests, and for the gravel zone from analysis of the test photos (Table 4-1 and Figure 4-7).
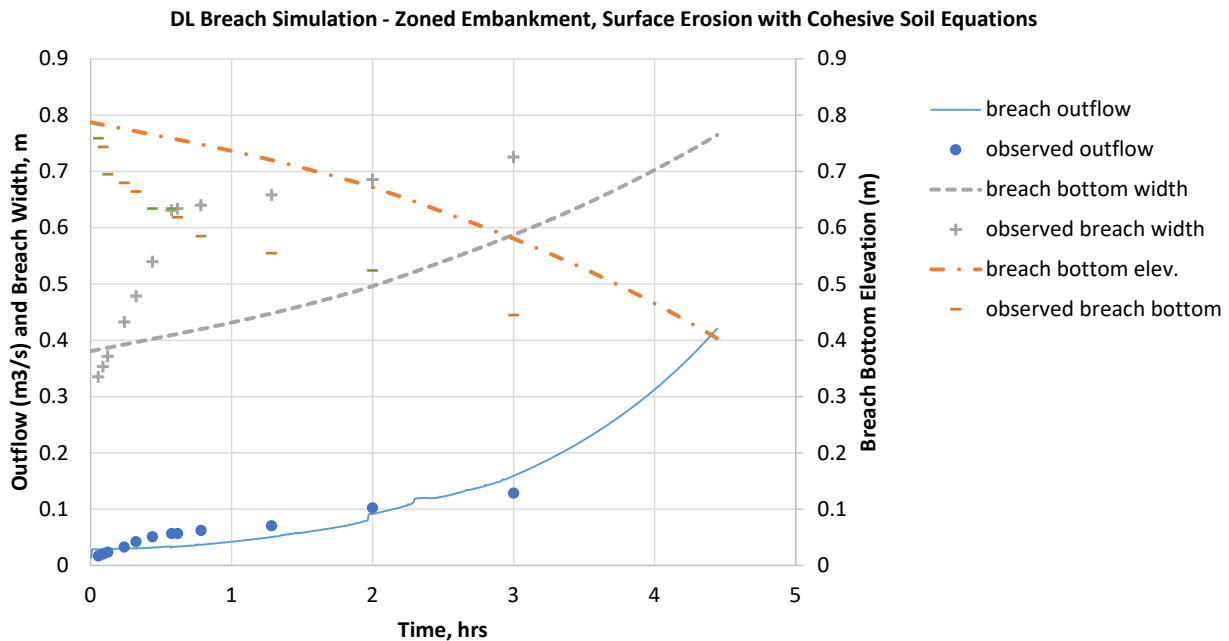
Figure 4-17 DL Breach simulation results for an improved run using zoned geometry with cohesive soil erosion equations.

In the course of making these adjustments, it was also confirmed that DL Breach does not use an effective stress approach (i.e., computing erosion rates based on the stress applied to soil grains, rather than total channel boundary stress) when calculating erosion rates of cohesive soils. This is in contrast to the WinDAM C model, and the noncohesive soil erosion equations in DL Breach. WinDAM C computes the erosionally effective stress using Eq. 2, which modifies the boundary stress with the $(n_s/n)^2$ multiplier, where n_s is the soil grain roughness and n is the Manning's roughness factor for the whole channel. For soils with D_{75} greater than 0.05 inches (1.27 mm), WinDAM C uses $n_s = (D_{75})^{1/6}/39$, with D_{75} given in inches. For finer soils, WinDAM C gives n_s the fixed value of 0.0156. For noncohesive soils the DL Breach model computes the erosionally effective stress by multiplying the boundary stress by $(n_s/n)^{1.5}$, with $n_s = (d_{50})^{1/6}/36.9$ (d_{50} being the median soil particle diameter specified in inches). However, for cohesive soils, although DL Breach, like WinDAM C, uses the excess stress equation (Eq. 1), it applies the equation differently, basing the erosion rate on the total boundary stress instead of the effective stress on the soil grains. This observation helps explain the need to reduce the k_d values to get good agreement of the model and the experimental results.

Another important consideration in this respect is the value of Manning's n used to calculate flow depths in the breach channel. A value for this parameter must be supplied by the user, and for DL Breach it is suggested (Wu 2016a) that the value be set to the larger of 0.016 (for breach channels through fine-grained soils) or $(d_{50})^{1/6}/A_n$ with A_n having a value between about 18.4 and 36.9 when d_{50} is given in inches. This is again a Strickler-type equation, and appropriate values of A_n are suggested by Wu (2016a) to be larger for laboratory settings and smaller for field cases to account for differences in sediment transport and bedform scale, but this must be a subjective decision of the model user. Yen (1991, 2002) explains that Strickler-type equations by themselves do not account for bedform resistance as a dominant factor (see also USGS 2012). Even if bedform roughness is accounted for by adjusting the value of A_n, the DL Breach approach is considering the stress applied to those bedforms to be effective for causing soil particle detachment, and this is contrary to the stress-partitioning approach adopted by previous investigators (Einstein 1950, Temple 1980, Temple et al. 1987, Hanson 1989).

Using the recommended approach for DL Breach, values of n in the range of 0.025 to 0.05 would be obtained based on d_{50} of the gravel zone, and these are much smaller than the values of 0.1 to 0.2 that were calculated from the flow data collected during the overtopping test (Table 4-1). Attempts to run the model with n values in the latter range produced very large total channel shear stresses and erosion rates, since DL Breach considers all of the shear stress applied to the channel boundary to be fully effective for causing erosion. (Changes in calculated shear stresses are being inferred, since the model does not provide output to confirm the calculated stresses; it only provides breach channel sizes through time.) Ultimately, after experimenting with some larger n values, most runs of the model were made with $n = 0.016$, and k_d values were adjusted to produce appropriate erosion rates based on total channel stresses.

Additional efforts were made to model the overtopping breach test using other DL Breach embankment configurations. Noncohesive soil erosion equations were applied to the gravel and core zones separately and together, but no suitable combination of inputs was found that produced a breach process similar to that observed during the test. Some combinations of parameters led to what was an apparent sudden failure of the entire embankment, with the breach width increasing in one time step from about 20% to 100% of the embankment width. The exact mechanism for this event (side slope failure or a sliding failure of the main body of the embankment) could not be determined from the limited output provided by DL Breach.

The headcut mode of erosion and breach was also investigated, which required defining the embankment as a homogeneous section. In this configuration k_d and τ_c values assigned to the embankment regulate the rates of surface erosion for the crest (but not the downstream slope), while headcut model parameters regulate the rate of upstream advance of a vertical headcut face. The headcut model chosen for these runs was DL Breach's headcut model 3, which is similar to the energy-based model available in WinDAM C, but with some differences in the way it is implemented during the early stages of the process when the headcut is located within the downstream slope. (This headcut model was not functional in the first version of DL Breach obtained from the program's website, but I contacted Dr. Wu directly, and he fixed the problem and placed a new executable file on the website.) The headcut advance rate, dx/dt is calculated by

$$\frac{dx}{dt} = C_2(qH)^{1/3} \tag{3}$$

where q is the discharge per unit width, H is the headcut height measured from the invert of the partially eroded crest to the base of the overfall, which is assumed to be the base of the dam. (The headcut height includes the elevation drop on the upper portion of the downstream slope when the headcut has only advanced partly into the downstream slope as shown in Figure 4-13.) C_2 is a rate coefficient that has been correlated to k_d in flume tests of headcut migration rates through cohesive soils (Hanson et al. 2011). The equation recommended from these studies is $C_2 = (0.25) k_d / 3600$, where k_d has units of $cm^3/(N\text{-}s)$, C_2 has units of $s^{-2/3}$, 0.25 is an empirical, dimensionless coefficient, and 3600 is a unit conversion factor. (In the WinDAM C implementation of this energy-based headcut model, H in Eq. 3 is the height of the headcut overfall [Hanson et al. 2011], which is less than the total embankment height until local, concentrated erosion deepens the base of the headcut to the bottom of the embankment.)

To run this headcut model in DL Breach, C_2 was set to a value of 0.000146 $s^{-2/3}$, corresponding to k_d = 1.2 ft/hr/(lb/ft^2) = 2.1 cm^3/(N-s) (an estimate for the gravel zone obtained from the earlier photo analysis), and the value of k_d for the embankment was also initially set to 1.2 ft/hr/(lb/ft^2). When this scenario was run, headcutting did not materially affect the simulation. Based on output from the program, all erosion was of the surface of the crest and headcut advance was so slow that it did not progress through the crest and thus had no effect on the outflow hydrograph. This was consistent with observations from the actual test, where no headcut development or advance occurred (even though surface erosion of the downstream slope did take place), so the value of C_2 was not adjusted further. Tuning of the model was accomplished by adjusting the k_d value of the embankment soil (which affects the rate of crest surface erosion) to a value of 1.7 ft/hr/(lb/ft^2) or 3 cm^3/(N-s), which produced an outflow hydrograph approximately matching that observed during the test (Figure 4-18). This was similar to the optimized value of k_d = 2 ft/hr/(lb/ft^2) used for the core in the zoned embankment surface erosion case (Figure 4-17). (Note that although C_2 can be related to k_d values from jet erosion tests or other sources, there is no linkage in DL Breach between the value of C_2 and the specified k_d value for the embankment.)

DL Breach Simulation - Homogeneous Embankment, Headcut Erosion and Cohesive Soil Equations
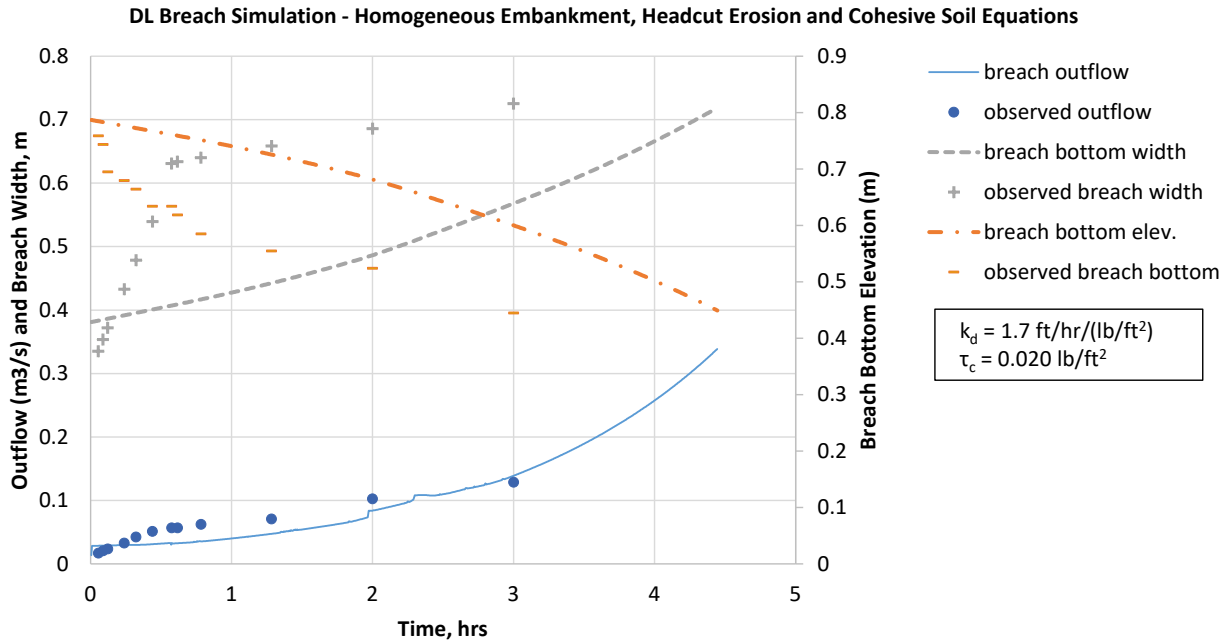
Figure 4-18 DL Breach simulation results for a homogeneous embankment with headcutting enabled. The headcut rate coefficient is so low that headcutting has no practical effect.

Following this simulation, two additional runs were made for comparison and to gain a better understanding of the internal workings of the model. One run was made with the same parameters just used for the successful headcut run shown in Figure 4-18, except that headcutting was disabled, which instead enables surface erosion of the downstream slope. This run produced the result in Figure 4-19, which appears to indicate that rapid surface erosion of the downstream slope is occurring, leading to a quick deepening of the breach that did not take place in the headcut-enabled model. This run together with the previous run confirms that in the headcut-enabled model there is no surface erosion of the downstream slope, and all erosion of the downstream portion of the embankment must occur through headcutting. This confirmation is valuable, because the DL Breach documentation states that surface erosion of the crest can occur when headcutting is enabled, but is silent about whether surface erosion of the downstream slope can still occur.
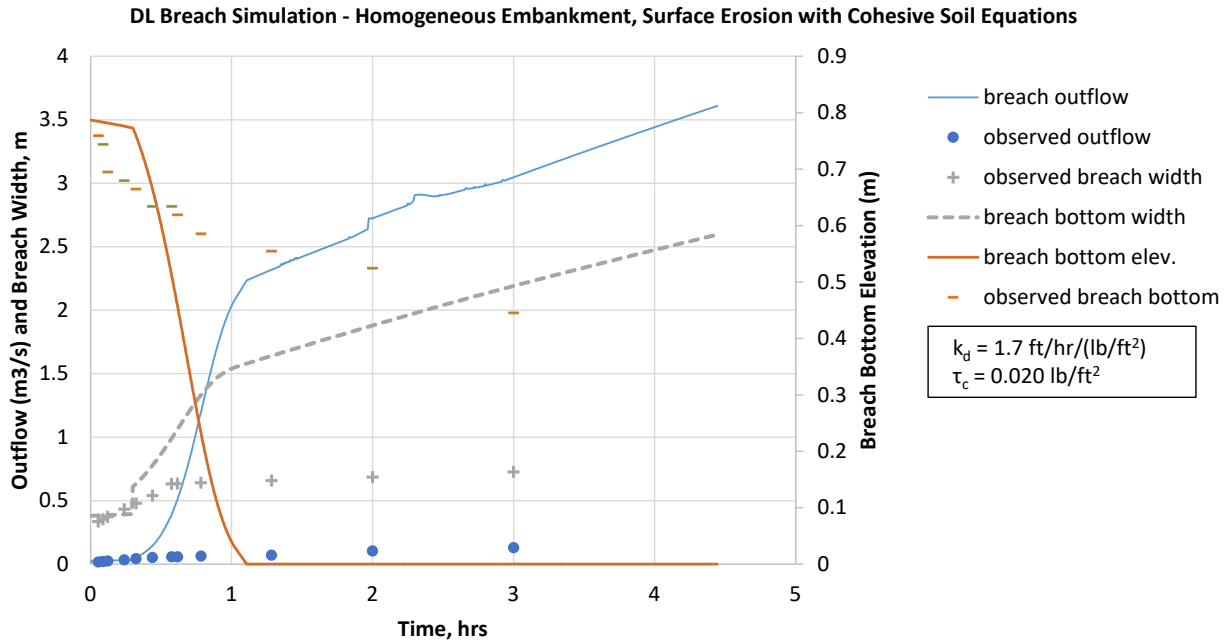
Figure 4-19 DL Breach simulation results for homogeneous embankment with surface erosion of cohesive soil. A rapid breach lowering takes place, apparently due to lowering of the downstream slope.

A final run was made with a zoned configuration, but with all soil parameters of the two zones set equal to one another, including k_d = 1.7 ft/hr/(lb/ft^2) = 3.0 cm^3/(N-s), so the embankment was defined in a zoned manner, but was quasi-homogeneous using equations for surface erosion of cohesive soils. The results, shown in Figure 4-20, were somewhat similar to the previous run, exhibiting rapid lowering of the breach bottom. However, unlike the previous run, when the breach reached the bottom of the embankment there apparently was an instantaneous sliding failure of the remainder of the embankment that caused the breach width to immediately increase to the full width of the embankment.

4-24

DL Breach Simulation - Zoned Embankment, Surface Erosion with Cohesive Soil Equations
All Zones Identical (Quasi-Homogeneous)

k_d = 1.7 ft/hr/(lb/ft^2)
τ_c = 0.020 lb/ft^2
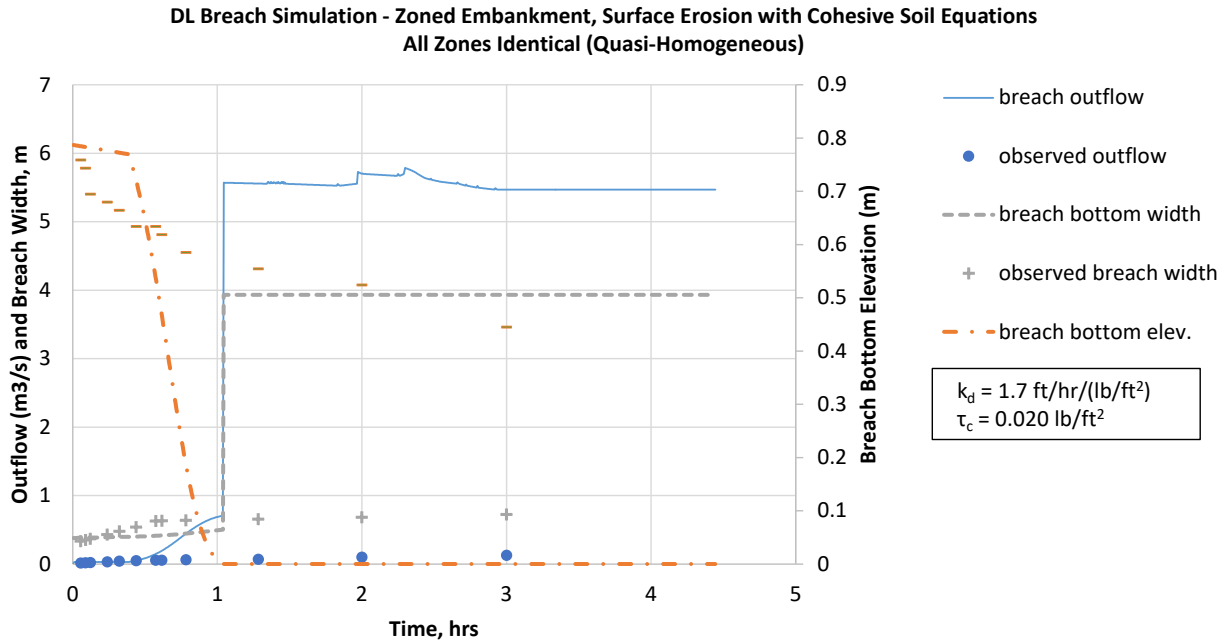
Figure 4-20 DL Breach simulation results for quasi-homogeneous zoned embankment with surface erosion. Headcutting is disabled.

The variety of behaviors and surprising results seen in some of these simulations show that there are complex interactions of the many different physical processes being simulated by DL Breach. Clearly, to successfully apply it, a modeler must have a solid understanding of the internal workings of all components.

4.7   Potential Future Comparisons – EMBREA

The EMBREA dam breach model (Morris 2011) is the successor to the HR BREACH model developed at HR Wallingford (Mohamed 2002). This model provides capability to alternately simulate surface erosion or headcut erosion processes for homogeneous and zoned embankment dams failed by overtopping flow or internal erosion. The headcut erosion model is the same energy-based option as that available in WinDAM C. Compared to the original HR BREACH model, EMBREA has increased flexibility to model a variety of zoned geometries. As a result of the author's attendance at a December 2017 dam breach modeling workshop organized by Electricité de France, preliminary plans are being made to apply EMBREA to this zoned overtopping embankment breach test. That comparison would be undertaken as part of a new international research collaboration.

4.8   Discussion - Effective Stress for Calculating Surface Erosion

The issue of using effective stress or total stress for the calculation of surface erosion rates is complex in these models, especially as discussed above for DL Breach. A brief summary of the approaches of each model is in order here.

- WinDAM C uses an effective stress approach, but only during the earliest phases of headcut development, when surface erosion is causing the concentrated erosion that will

4-25

develop into a headcut. Once surface erosion has been sufficient to create an overfall in the channel, headcut advance takes place through either an energy-based method or a stress-based deterministic method that considers all of the stress generated by the overfalling jet to be useful for causing erosion at the toe of the headcut face. During headcut advance there is no partitioning of stresses between soil grains, bed forms, vegetation, or other elements.

- DL Breach uses an effective stress method for surface erosion of noncohesive soils, but not for surface erosion of cohesive soils. When the headcut breaching mode is enabled, the effective stress approach (for noncohesive soils) is only applied to the crest of the embankment, since the downstream slope erodes by headcutting. DL Breach's headcutting equations do not use an effective stress approach, since they are all energy-based.

5   ZONED EMBANKMENT TEST 2 – INTERNAL EROSION

5.1   Conduct of Test and General Observations

The internal erosion test of the zoned rockfill embankment was initially carried out in a fashion similar to the preliminary test of the homogeneous silty clay embankment test. A summary of significant events and observations during the test is given in Table 5-1. To begin the test, the rebar embedded into the left end of the embankment during construction was withdrawn just after noon local time on Tuesday September 5, 2017. For the first few minutes, a small flow was observed from the resulting hole. At the same time, flow was observed leaking slowly near the right abutment of the embankment, but it was later determined that most of this flow was leaking through the battered false wall forming the right abutment (1:10 h:v slope), and did not represent actual embankment seepage. The total flow out of both locations was estimated from the supercritical flume to be about 34 gpm (129 L/min).

Table 5-1   Summary of events during internal erosion test.

Clock time	Total Elapsed Time (h:mm)	Notes
2017.09.05 12:06:16	0:00	Start of test
2017.09.05 13:36:16	0:90	Seepage stopped, test paused
2017.09.06 14:47:00	0:00	Test restarted with rebar reinserted and withdrawn again; turbid seepage. **Elapsed time reset to zero.**
2017.09.06 17:15:00	2:28	Seepage continuing, but mostly clear, with intermittent turbidity
2017.09.06 18:16:00	3:29	Internal erosion channel agitated with mason's line 3 times over 30 minutes
2017.09.07 07:30:00	16:43	Pipe channel within core has migrated upward to form a nearly horizontal channel about 6-7 inches below water surface
2017.09.07 08:35:00	17:48	Agitated upstream zone along pipe channel alignment using rebar rod with negligible effect
2017.09.07 10:35:00	24:18	From 8:35 to 10:35, repeatedly agitated downstream zone along pipe channel using rebar rod to widen exit of erosion conduit
2017.09.07 15:05:00	46:53	Additional agitation of upstream zone using rebar rod
2017.09.08 13:40:00	48:05	Dug large channel through upstream zone using a shovel
2017.09.08 13:52:00	50:00	Test stopped

Initially the flow from the site of the internal erosion was turbid, but within a few minutes the turbidity began to diminish and the flow rate began to decrease gradually. After about 90 minutes the flow from the left end of the embankment stopped entirely; the gravel zone had acted as a filter zone to heal the damage to the core. The total flow rate through the supercritical flume dropped to about 29 gpm, indicating that flow from the rebar induced flaw had been a minor part of the total. Although it would not be an ideally designed filter material due to excessive fines content (Foster and Fell 2001, FEMA 2011), the gravel zone meets recommended gradation criteria (Reclamation 1987) for a filter against the core zone as follows:

- D_{15} of the filter / D_{15} of base soil ≥ 5
  - 0.12 mm / 0.015 mm = 8.0
- D_{15} of the filter / D_{85} of base soil ≤ 5
  - 0.12 mm / 0.07 mm = 1.71

Although the gravel zone did meet the criteria for a filter to the core, it was still somewhat surprising that it was able to heal such a significant defect as the approximately 0.5-inch diameter hole created by removing the rebar. Typically, a filter zone placed against a perforated drain pipe would be required to have a maximum particle size at least twice as large as the diameter of the perforations; for this filter the maximum particle size was only 0.75 inches, compared to a nominal defect size of 0.5 inch. Healing took place quickly enough that the hole through the core did not enlarge enough to become visible at the acrylic abutment. Additionally, the rebar appeared to have drifted a short distance away from the boundary during embankment construction (probably 1-2 inches).

On the second day of the test the rebar was driven back through the embankment in an attempt to create a more significant defect and to put that defect closer to the acrylic wall so that erosion or healing processes could be observed. Despite best attempts, the rebar did not follow the original alignment, but instead ended up on a slope of about 7° (Figure 5-1) and still was not in close contact with the acrylic wall. This time, a piece of mason's line (nylon string) was tied to the end of the rebar before it was withdrawn to restart the test. This line was later used to periodically agitate the erosion channel.
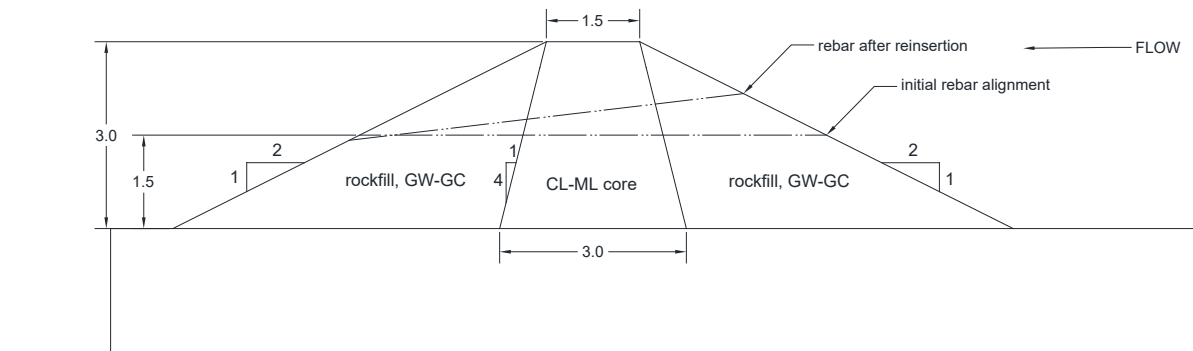
Figure 5-1   Embankment cross section showing alignment of rebar as originally installed (horizontal) and after reinsertion. Flow direction for the test is right to left.

On this second day of testing the flow from the left end of the embankment at the induced flaw was again small. Prior to withdrawing the rebar the flow was measured at 29 gpm through the supercritical flume, and after the rebar was withdrawn the flow returned again to 34 gpm and was turbid. Turbidity of the outflow gradually decreased, but the flow did not decrease as it had on the first day. Outflow from the internal erosion site was steady and slow, but was sufficient to clean out finer grained material from the downstream gravel zone where it had been disturbed by the rebar insertion and removal. This cleaning and slow enlargement of the pipe through the gravel zone gradually progressed upstream, and 19 minutes after removing the rebar, erosion became visible in the downstream edge of the core zone. In the gravel zones, flow channels that were devoid of material finer than medium sand gradually became visible, but interlocked medium to coarse sand and fine gravel prevented further enlargement. In the core zone, the pipe became visible at the upstream edge of the core zone 75 minutes after the rebar was

removed. The initial process was consistent with what is typically described as concentrated leak erosion (USBR and USACE 2015). Figure 5-2 shows the upstream progress of erosion. The photos also show that there was not a perfect delineation of the zone boundaries as each lift was placed, but the straying of materials across the zone boundaries did not seem to affect the tests.

Figure 5-2   Pipe beginning to develop through embankment after removal of rebar on second day of testing. Elapsed times since the restart on the second day are 1 min (left) and 103 minutes (right). In the first photo the pipe is only visible in the downstream gravel zone. In the right hand photo, the color variation in the portion of the pipe within the core zone indicates redeposition of soil in the bottom of the pipe as erosion occurs from the roof.

As the pipe through the core zone began to enlarge, a pattern emerged of roof collapse followed by deposition on the floor of the pipe. As the pipe enlarged, erosion from the roof seemed to become dominated more by gravity-induced collapse than shear-stress induced detachment of soil. Much of the soil coming loose from the roof seemed to do so as aggregations of particles (peds), rather than as individual silt-sized soil grains. Gradually, the alignment of the pipe migrated up, as the flow velocity through the pipe seemed insufficient to carry away the larger peds (and probably a few sand-size particles migrating in from the upstream gravel zone). This allowed aggradation of the bed at the same time that the roof was migrating upward. For much of this day, the size of the pipe through the core increased very slowly.

The test was allowed to continue overnight into a third day and during this time the pipe through the core continued to migrate upward, but also enlarged significantly as the breadth of the channel increased and the roof became more unstable. The enlargement of the channel illustrates that the capacity to transport material detached from the roof was slightly exceeding the rate of detachment. This process of repeated roof collapse and upward migration of the void is often described as *stoping*, and the void is called a *stope*.

Figure 5-3 shows that as the pipe continued to migrate upward, the erosion channel developed into a sequence of stepped pipes, with large losses of head occurring through the gravel zones and a low hydraulic gradient through most of the core of the embankment. In fact, flow through most of the void being created in the core appears to have a free surface, as evidenced by foam on the water surface. Near the downstream end of the core, there appears to be pressurized flow again in a steep portion of the pipe approximately paralleling the interface between the core and downstream gravel zones.

Figure 5-3   Development of stepped profile of erosion channel. An approximate hydraulic grade line for the flow is sketched over the photo in blue. As the roof of the channel collapsed and the bed migrated upward, most of the core zone began to experience open-channel, rather than pressurized flow.

At this point it appeared that the most probable failure mode for the embankment was a continued upward migration of the stope, leading to a collapse of the roof of the pipe in the core zone extending up to the surface of the core (a sinkhole). Such a sinkhole might be large enough to immediately allow overtopping flow, or might remove structural support for the upstream gravel zone, allowing it to fail. However, it appeared that this failure mode would be very slow to develop and was unlikely to occur before it became necessary to stop the test. (Logistical issues with instrumentation and other activities in the lab made it necessary to have the test completed on Friday.) There appeared to be two things that might accelerate the failure process.

1. If the pipe through the downstream gravel zone were to experience an erosion event that enlarged it significantly, then the hydraulic gradient through the steep portion of the pipe in the downstream side of the core would be increased, which might lead to headcutting that could progress upstream through the core.
2. If the flow through the upstream gravel zone were to increase due to further removal of fine materials from the voids between gravel pieces, that might accelerate the rates of soil detachment and sediment transport in the core zone.

After considering these possibilities, it was decided to test whether either of these processes could progress to a rapid catastrophic breach of the embankment. In an initial attempt to accelerate removal of fines (i.e., #2 above), the piece of string that had been left in place following the removal of the rebar rod on the second day was used to agitate the hole, drawing it upstream and downstream like dental floss. (This took significant effort because the upstream end of the string became tightly embedded as the erosion channel gradually deviated away from the initial alignment of the string.) This would cause momentary increases in turbidity, but no sustained change in flow rate nor any significant change to the erosion visible through the acrylic sidewall of the model. Beginning around 8:35 a.m. the upstream portion of the pipe passing through the upstream gravel zone was agitated by repeatedly driving a ½ inch rebar into it and stirring the gravel to loosen the finer portions of the soil mix. However, each time the rebar was removed, the gravel zone would settle to fill the void left by the bar and the total flow rate remained unchanged.

At about 10:00 a.m. the downstream gravel zone was agitated along the alignment of the existing flow (#1 above). Although this was successful in moving the exit of the pressurized portion of the pipe upstream, it did not induce any accelerated erosion within the core zone and did not produce the anticipated headcutting process.

Through the middle of the day, the roof of the pipe channel within the core zone continued to collapse under gravitational forces (with no water actually touching the roof much of the time) as the cavity in the downstream side of the core grew wider. The cavity appeared to be about 4 inches wide and 2-3 inches tall at this point. The channel downstream from the core was about ¾-inch diameter, with its size primarily due to the size of the rod being using to agitate it.

At 3:05 p.m. an attempt was made to disturb the upstream zone to increase the flow and accelerate the failure progression. While rebar was inserted and being manipulated, the flow rate increased noticeably, but as soon as the rebar was withdrawn the upstream zone collapsed into the disturbed area and the flow rate returned to 34 GPM. The roof continued to collapse through the late afternoon. There was open channel flow in most of the pipe, at a flow rate that was too low to cause much active erosion of the pipe. The only significant enlargement of the pipe was taking place through gravitationally induced collapse of the roof, which was above the water surface.

On Friday morning very little had changed. At about 1:40 p.m. a shovel was used to dig out the majority of the upstream gravel zone at the entrance to the pipe. This applied nearly full reservoir head to the core zone and appeared to slightly enlarge the channel through the downstream gravel zone, with a small increase in total flow rate to about 39 gpm. However, we could also quickly see gravels being rearranged within the pipe as it stabilized again. No further erosion events or increases in flow rate took place. The test was stopped at about 2:52 p.m., with a total test period of about 48 hours since the restart after the reinsertion and second withdrawal of the rebar.

5.2   Discussion - Analyzing Internal Erosion Failure

After witnessing the complex erosion channel development process for this embankment, it was apparent that physically-based dam breach models such as WinDAM, EMBREA, DL BREACH, or others would be unable to simulate the event. All of these models presume the existence of a significant flaw that allows water to continuously flow under the driving reservoir head. In this test, the upstream and downstream gravel zones functioned first as filters, and then later as flow limiters, dissipating most of the hydraulic energy without incurring erosion in those zones. This

limited the hydraulic gradient that could be applied to the most erodible and water retaining portion of the embankment. Armoring of the interior surface of the erosion conduit also appeared to occur as fine particles in the soil matrix were removed, with coarser particles left behind that were resistant to continued erosion due to their size and their interlocking with surrounding similarly-sized particles.

The processes observed in the test seemed more amenable to analysis using the procedures described in the joint Bureau of Reclamation and U.S. Army Corps of Engineers document, "*Best Practices in Dam and Levee Safety Risk Analysis, Chapter IV-4, Internal Erosion Risks for Embankments and Foundations*" (USBR and USACE 2015). This publication describes a conceptual framework for internal erosion failure processes with four phases, illustrated in Figure 5-4 for the case of erosion through an embankment.

These four phases can be further subdivided to create a more detailed event tree describing each step required to progress from initiation to breach. A generic event tree describing the eight nodes of one possible failure mode is suggested by USBR and USACE (2015).

⇨Water level at or above threshold level
  ⇨Initiation – Erosion starts
    ⇨Continuation – Unfiltered or inadequately filtered exit exists
      ⇨**Progression – Continuous stable roof and/or sidewalls**
       ⇨**Progression – Constriction or upstream zone fails to limit flows**
       ⇨**Progression – No self-healing by upstream zone**
        ⇨Unsuccessful detection and intervention
         ⇨Breach (uncontrolled release of impounded water)

INITIATION	CONTINUATION	PROGRESSION	BREACH
Concentrated leak forms and erosion initiates along walls of crack	Erosion continues into the downstream shell (lack of a filter)	Enlargement of the concentrated leak	Breach mechanism forms
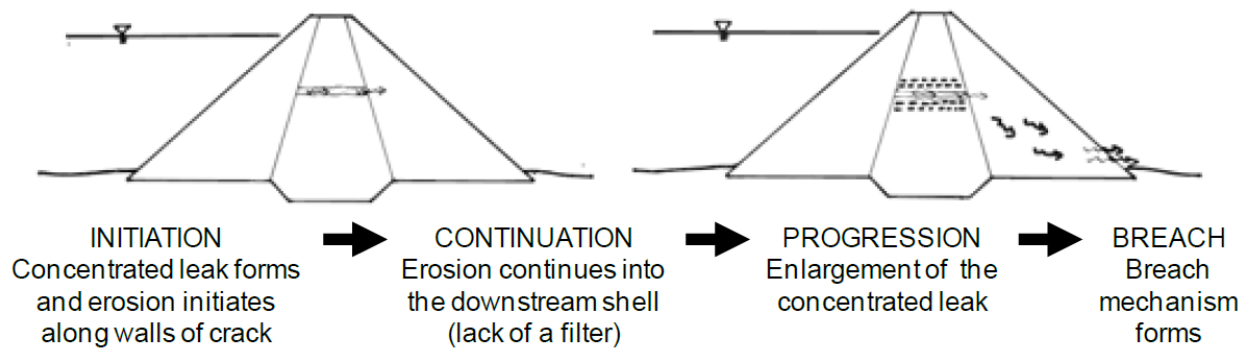
Figure 5-4 Internal erosion through an embankment, initiated by a concentrated leak (from USBR and USACE 2015, adapted from Fell et al. 2008).

The progression phase (emphasized in bold) in the event tree is subdivided into three sequential events. More detail can be added to other phases, and multiple failure modes should be considered. For example, the outcome of the first node in the progression phase could be a stable roof and/or sidewalls that would allow further growth of the concentrated leak and a breach by the mechanism of concentrated leak enlargement. Alternately, if the failure mode is stoping (vertical migration of the erosion channel), then a stable roof is not needed and that node is not included. A stope could eventually cause a sinkhole collapse of the crest that might allow breach by overtopping flow in the final phase. The USBR and USACE (2015) procedure provides the framework for analyzing these possibilities, and suggests a starting point for

evaluating the probabilities of completing each event needed to reach a breach. These suggested probabilities are based on the embankment design and configuration and engineering properties of the embankment materials. In typical risk analysis exercises, the probabilities are further modified through expert elicitation and consideration of factors that make each event more or less likely to occur. The final outcome of this evaluation process is a prediction of the probability of breach by various failure modes, and a prediction of the rate of breach development when it occurs. The breach rate is described with qualitative terms (slow, medium, rapid, very rapid) and associated numerical time ranges (weeks to years, days to weeks, hours to days, less than 3 hours).

In this embankment test the initiating event was forced (probability=1.0) when the rebar was removed from the embankment. During the first day, the failure mode was probably halted at the next node when the downstream gravel zone worked as a filter to heal the concentrated leak at the interface between the core and the downstream gravel. (The upstream gravel may have also contributed to the healing process at the third progression node, although healing occurred quickly before there was any visual evidence of completion of the first two progression nodes.)

On the second day of the test, greater damage was done to the embankment with the reinsertion and withdrawal of the rebar, and this allowed some degree of continuation to occur. With the lack of a stable roof, stoping was able to progress (first progression node not a factor for a stoping failure), but at the second and third progression nodes, some partial limiting of flows by the upstream zone and partial self-healing may have contributed to maintaining a slow failure progression. Within the time constraints of the test, progression into a breach phase did not occur, but if it had (and presuming no intervention), the breach phase could be evaluated qualitatively using tools provided in USBR and USACE (2015) (see Tables IV-4-24 through IV-4-27). Using these tables, a likely breach time range for this case is rapid to medium, about 1 to 7 days. The determination is quite subjective, but a primary factor is the presence of an upstream flow limiter. The influence of the downstream gravel zone is difficult to evaluate in this case, depending on whether the zone is considered to behave more like a coarse-grained rockfill, which would slow breach development, or a low plasticity, silty, sandy gravel, which would have rapid to very rapid breach development and would do little to slow the breach development process. The behavior exhibited during the test was more consistent with the rockfill behavior. Despite significant interventions to accelerate the failure process, failure did not occur within the 48 hours of testing that was performed.

6   COMPARISON TO PREVIOUS TESTS

6.1   Fuse Plug Embankments

Fuse plug embankments are designed to breach reliably at a controlled rate to serve as one-time-use controls for emergency spillway channels. When the embankment is overtopped by a rising reservoir, the embankment breaches at a pilot channel location and the breach widens until the full spillway width is opened for flow. Typical fuse plug embankments include both a core and rockfill zones, so in some ways they are similar to many rockfill dams. The two most notable studies of fuse plug embankments are the works of Tinney and Hsu (1961) and Pugh (1985). The tests performed in these two research programs provide an interesting comparison for the mechanisms and rates of erosion observed in the zoned embankment overtopping test conducted for this study. In general, much more rapid erosion of the gravel zones was observed in the fuse plug tests, with much less overtopping flow.

Tinney and Hsu (1961) conducted a multi-scale research investigation to support the design of a fuse plug embankment to control the Idaho spillway for the Oxbow Dam on the Snake River on the Oregon-Idaho border. Fuse plug embankments are designed to breach in a controlled manner when overtopped, in order to open a high-capacity spillway channel. They offer an affordable option to gated spillways by allowing flood surcharge to the stored and released when necessary without the need for mechanical gates. The study included small-scale three-dimensional laboratory models [0.67 ft (0.2 m) and 1.33 ft (0.4 m) embankment heights], larger two-dimensional sectional models [slices of the embankment along vertical planes, with 6 ft (1.8 m) embankment height] and a field test of a 12 ft (3.66 m) high embankment (half of prototype scale). All of these models utilized thin clay cores that were inclined downstream at a 45° angle above horizontal so that the cores were supported by a downstream rockfill zone that was intended to wash out quickly when subjected to overtopping flow. The rockfill materials in most of the fuse plug tests were quite clean, with 5% or less fines. Some of the rockfills were very uniformly graded and others were more broadly-graded, but none met the criteria for classification as well-graded soils. One sectional model test did utilize a processed, broadly-graded (but not well-graded) sand material (described as a *fine filter*) in the zone beneath the core. This material was unsatisfactory because it exhibited apparent cohesion that allowed it to stand nearly vertical, which did not fulfill the desired function of quickly removing support from the core. All of the embankments that were built from more uniform materials breached rapidly and reliably with small depths of overtopping flow:

- 0.4 inches (1 cm) in the small-scale laboratory models,
- 1 ft (0.3 m) in the large-scale field test (12 ft = 3.66 m tall embankment).

Pugh (1985) tested additional embankments with a similar design concept as those tested by Tinney and Hsu. Pugh's embankments had heights of 0.5, 1.0, and 1.25 ft (0.15, 0.30, and 0.38 m). The proposed prototype gradation for the rockfill zone in these tests was a well-graded gravel with no particles finer than medium sand. The materials actually used in Pugh's model-scale tests were broadly-graded sands, but with an insufficient range of sizes to qualify as well-graded. Again, these materials were clean, with negligible fines and in fact, no particles smaller than about 0.2 mm (fine sand). Although the results reported in Pugh (1985) focused mostly on the widening rate of the breach after breach initiation occurred, review of the video records of the tests showed that most of the eight tested embankments initiated the breach quickly, with structural failure of the core occurring within about 2-7 minutes under an applied overtopping flow depth of either 0.04 or 0.1 ft (12 or 30 mm), varying with the model scale. The clean

granular materials could be easily washed away and exhibited no ability to stand unsupported under their own weight or when subjected to even minimal shear stress from overflowing water.

The important factors accounting for the markedly greater erosion resistance of the class 6 road base material used in the NRC tests appear to be the well-graded nature of the coarse materials and the presence of significant quantities of fines (12%) with a substantial degree of plasticity (PI=6) and notable clay content (3%). Embankment zones with such properties are probably common—in some cases intentional and other times resulting from natural variability of available materials or segregation during handling and placement.

6.2   IMPACT Tests

The European IMPACT project took place over a period of three years from 2002-2004 and included a coordinated set of physical model tests, numerical modeling comparisons, and investigations of flood propagation, sediment movement, and uncertainty analysis related to embankment dam breaching. The physical modeling effort included 22 lab-scale models (2.0 to 2.6 ft high embankments [0.6 and 0.8 m]), and 5 large-scale field tests carried out in Norway. Four of the field tests involved either zoned embankments or embankments with broadly-graded gravel materials. These experiments provide interesting and valuable comparisons to our recently completed tests. Unfortunately, information about these tests is scattered across several different reports, with some discrepancies between them, probably due to differences between as-built and designed conditions for some of the tests. An attempt to resolve questions about some of the test data was provided by Hassan and Morris (2008).

6.2.1   Overtopping Tests

IMPACT test 2-2002 was an overtopping test of a 5-m high, homogeneous embankment constructed from a well-graded gravel. Although a gradation curve is provided, the origin of the material is not known. Later tests utilized both tunnel spoil and moraine materials in various embankment zones, so it seems likely that this gravel came from one of those sources. Tunnel spoil is likely to be angular, while moraine materials might range from subangular to rounded. In addition to gradation curves, the porosity, cohesion, and angle of internal friction were reported for most of the soils used in the IMPACT tests. Although this was a coarse-grained material (with less than 5% fines according to Figure 6-1), a non-zero cohesion of 0.9 kN/m^2 was reported. Curiously, the angle of internal friction (angle of repose) for all of the rockfill and moraine materials used in the IMPACT tests was the same at 42°.

The test of the homogeneous gravel dam took place in mid-October, with freezing temperatures the night before the test. Photos from the test in Figure 6-2 clearly show a headcut mode of erosion. It has been suggested that the embankment itself may have been partially frozen and that this may have been responsible for the headcutting behavior, but it seems doubtful that interior portions of the embankment would have been frozen. Instead, it seems more likely that the well-graded nature of the gravel, combined with the non-zero cohesion and some capillary tension created enough apparent cohesion to allow the soil to stand at a steep slope. Once established, this geometry prevented direct attack of the flow on the downstream slope, so a headcut mode of erosion occurred, with the crucial erosion taking place at the toe of the slope.
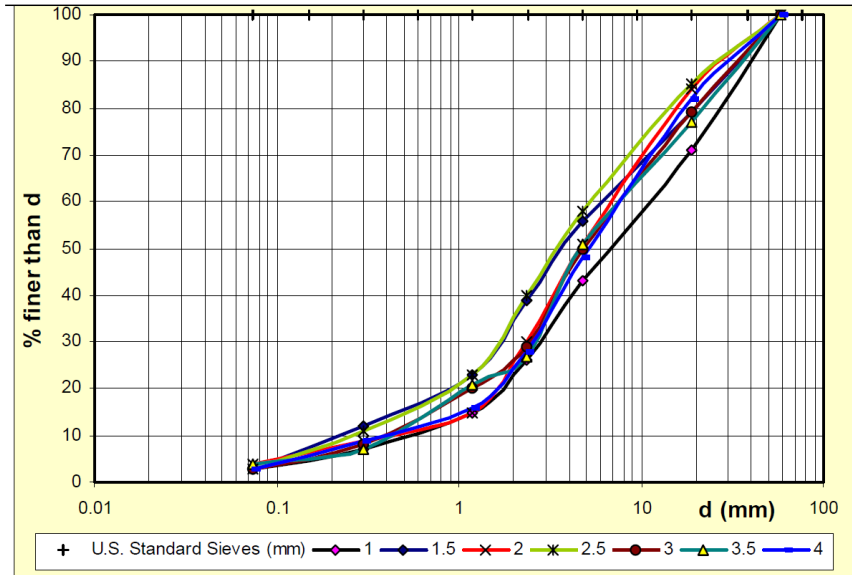
Figure 6-1 **Gradation curve for IMPACT Test 2-2002, homogeneous gravel dam (from IMPACT WP2 Technical Report: Section 4). This soil qualifies as well-graded (C_u=17.5, C_c=2.2) and has less than 5 percent fines. Legend labels indicate embankment layer height in meters.**

Figure 6-2   Headcut development during IMPACT test of homogeneous gravel dam, 2-2002 (from IMPACT WP2 Technical Report: Section 4).

IMPACT test 1-2003 was an overtopping test of a 5.9-m high, zoned embankment dam with a downstream rockfill zone of broadly-graded gravel (tunnel spoil), a central moraine core, and an upstream zone of uniformly graded gravel (Figure 6-3). Gradation curves for zones 1 and 2 are shown in Figure 6-4. Neither soil is well-graded, with the moraine material having a C_c value of about 0.53 and the rockfill zone having a C_c of 9.0. Although Figure 6-3 describes the pilot channel as 0.24 m deep and 6.5 m wide, it is also described as 0.2 m deep and 8 m wide in the IMPACT WP2 Technical Report, and 0.25 m deep and 8 m wide by Vaskinn et al. (undated). The latter report details the breaching process and reports that the core of the dam was overtopped for about 2 hours, then the notch was overtopped for 1.5 hrs, and finally the notch and full dam crest were overtopped for 1 hr before failure occurred. Estimated unit discharge through the notch was about 5.4 ft^3/s/ft (0.5 m^3/s/m) during the last hour, or about 1.5 ft (0.45 m) of overtopping head on the notch. In this test, erosion seemed to take a form that appears in Figure 6-5 to have both headcut and surface erosion characteristics, with a series of small headcuts, but not a tendency toward forming a single large headcut. Failure took place once the erosion broke through the upstream edge of the crest, and development of the full breach occurred quickly in about 10 minutes.
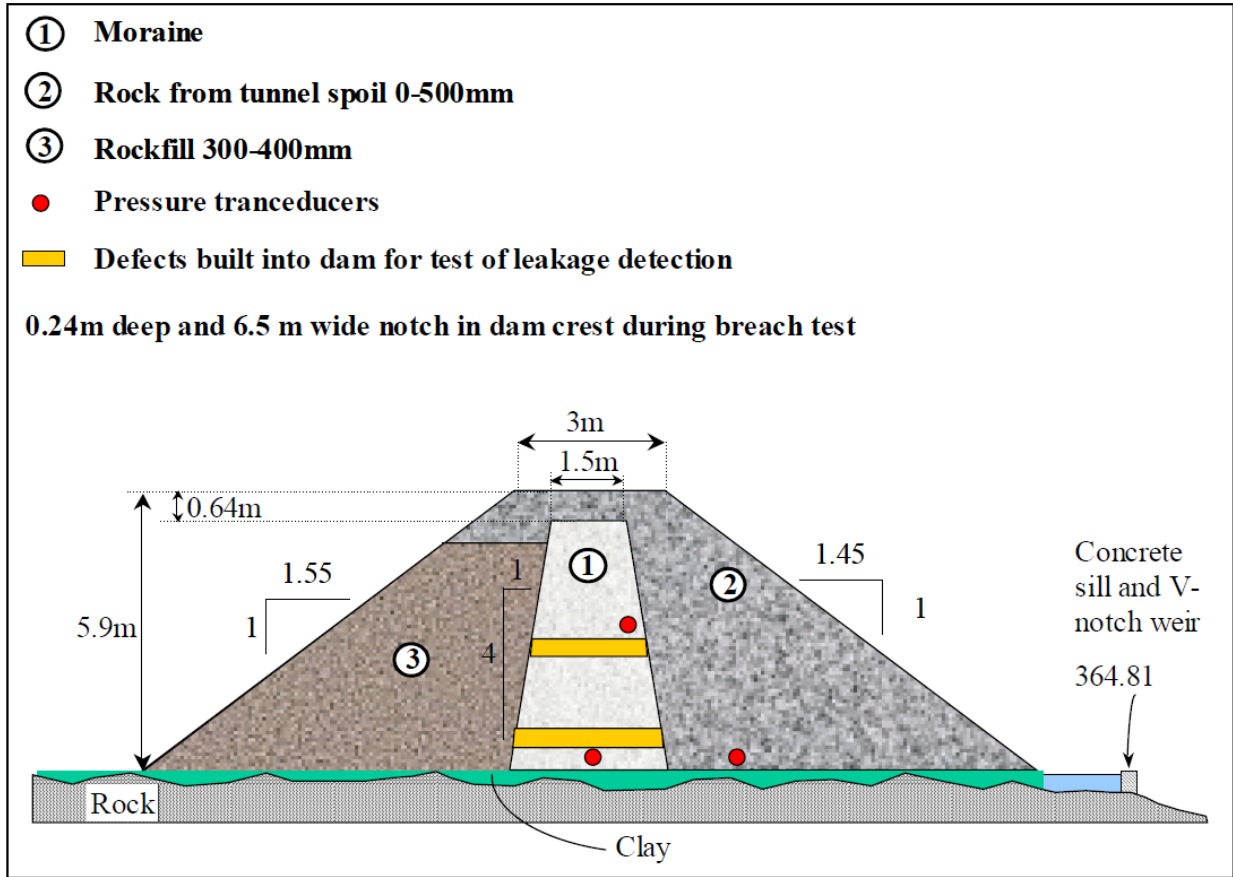
Figure 6-3 Embankment cross section from IMPACT test 1-2003, rockfill dam with central moraine core (from IMPACT WP2 Technical Report: Section 4).
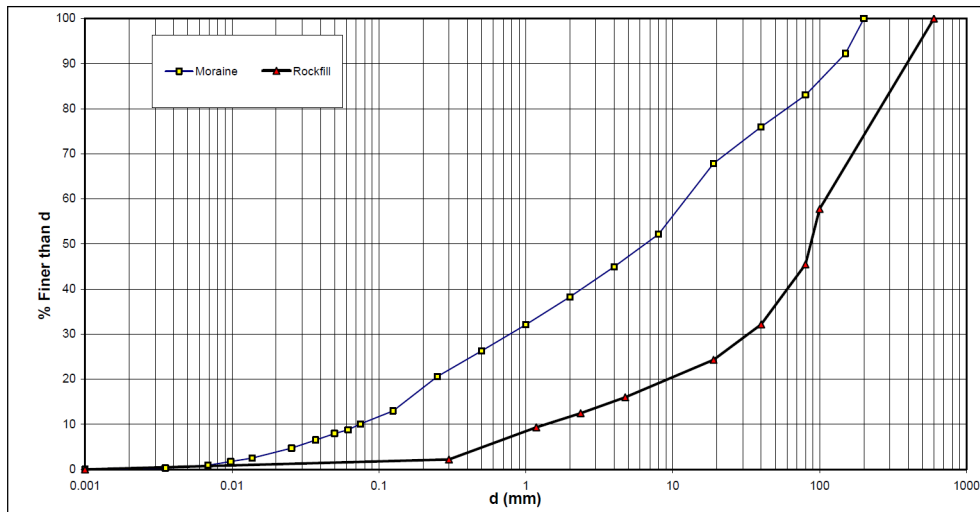
Figure 6-4 Gradation curves for IMPACT tests 1-2003 and 2-2003 (from IMPACT WP2 Technical Report: Section 4). The rockfill curve is zone 2 in Figure 6-3, and

the moraine curve is the zone 1 core. A complete gradation curve for the uniform gravel (300-400 mm) in zone 3 was not provided.

Figure 6-5   Headcut development during IMPACT test of zoned gravel dam, 1-2003 (from IMPACT WP2 Technical Report: Section 4).

Both of these tests demonstrated that broadly-graded rockfill materials can experience headcut erosion. The gravel zones of both embankments exhibited enough strength to stand at steep slopes and enough erosion resistance to avoid unraveling immediately under the initial surface flow. Although photos of the tests do not show a deep tailwater pool downstream of these embankments, it is likely that local tailwater developed quickly as materials eroded from the embankments were dropped a short distance downstream, creating a tailwater pool that could have enabled scour of the toe and creation of a vertical drop. In the test performed for the present study, the free overfall immediately downstream from the embankment did not support this kind of flow in the tailwater zone, which may partially explain why headcutting was not observed.

6.2.2   Internal Erosion Tests

Two internal erosion tests were conducted in the IMPACT project. The first test, 2-2003, utilized an embankment geometry and zoning that matched the zoned embankment overtopping test previously discussed, 1-2003. To create an internal erosion failure, two trigger mechanisms were built into the embankment, as shown in Figure 6-6. The triggers both utilized 200-mm

diameter pipes that were perforated on the top side within the moraine core. The first trigger pipe was surrounded by a 1-m square zone of uniform sand, and the second trigger pipe was embedded in a column of uniform sand extending to the top of the dam. Both pipes were controlled by valves that could be opened to flush the sand out and begin the failure process. The first trigger was opened to begin the test, but after 4 days a failure had not yet occurred. When the second trigger was opened, a sinkhole formed quickly at the crest of the dam and failure occurred from that point in a manner similar to the overtopping test.

The second internal erosion test utilized a homogeneous embankment composed of the broadly-graded moraine material shown in Figure 6-4. The trigger mechanism for this test was similar to the first trigger for test 2-2003, except that it extended to the upstream toe of the embankment (Figure 6-7). In contrast to the first test which did not experience failure after 4 days with the first trigger, this embankment failed quickly in less than 20 minutes when the trigger was activated. The principal difference was that the uniform sand extended into the reservoir, which allowed full reservoir head to be applied to the erosion channel as soon as the sand had eroded into the embedded pipe. In the first internal erosion test (2-2003) the upstream uniform rockfill zone protected the first trigger from ever being exposed to the undiminished head of the reservoir. When the second trigger was enabled, failure occurred quickly when the erodible material, was eroded all the way to the dam crest, leaving an open chimney that collapsed into a sinkhole. Apparently, head losses through the rockfill zone were sufficient in that test to prevent progressive erosion of the moraine material into the pipe after the trigger valve was opened.

There is a strong similarity in these two tests to what was observed in the NRC-funded internal erosion test described in section 5 of this report. The flow-limiting effect of the upstream rockfill zone prevented the erosion channel in the core from enlarging rapidly or extending itself through the upstream gravel zone to a degree that would allow full reservoir head to be applied to the erodible soil in the core. If the test had been continued long enough, a stoping failure process might have been completed, similar to the failure that took place in the first IMPACT test when the second trigger was activated.
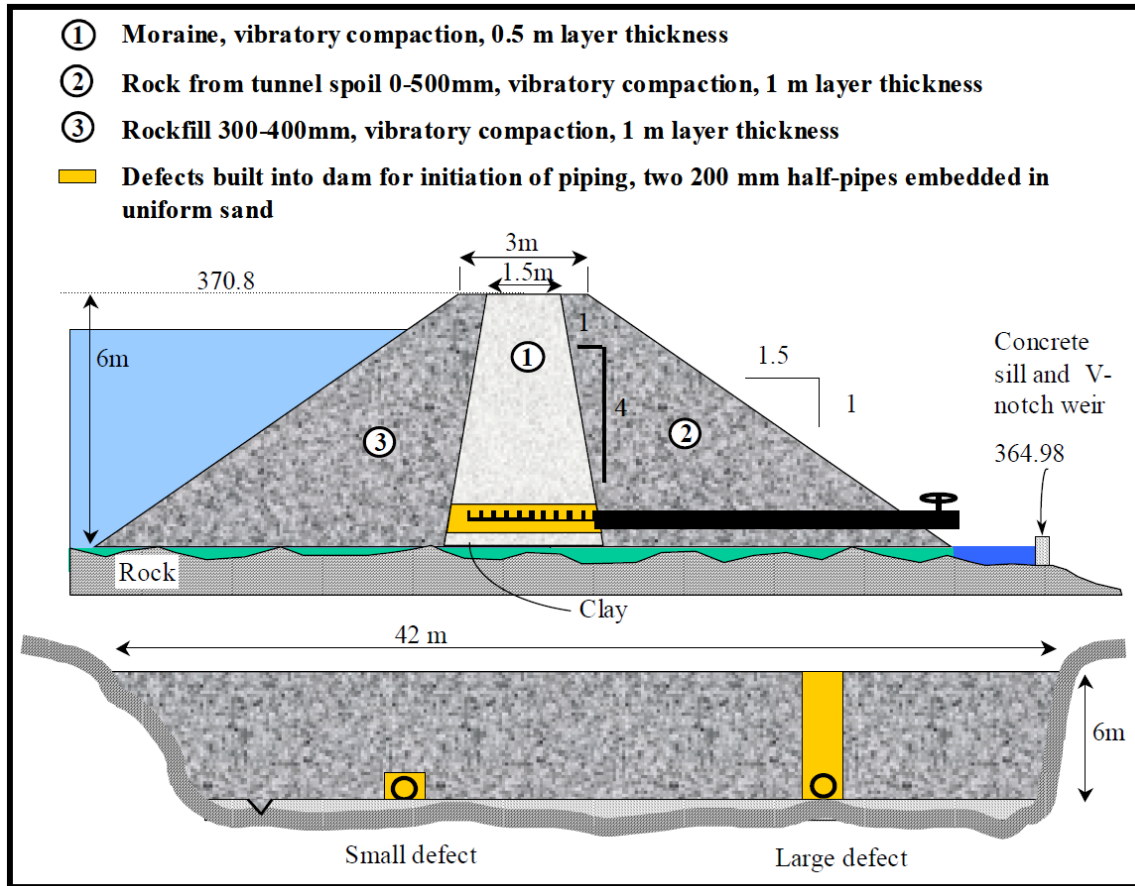
Figure 6-6   Embankment geometry for the first IMPACT internal erosion test (from Vaskinn et al. [undated] WP2.1 Breach Formation, Large Scale Embankment Failure Report).

Legend from figure:

① Moraine, vibratory compaction, 0.5 m layer thickness

② Rock from tunnel spoil 0-500mm, vibratory compaction, 1 m layer thickness

③ Rockfill 300-400mm, vibratory compaction, 1 m layer thickness

▬ Defects built into dam for initiation of piping, two 200 mm half-pipes embedded in uniform sand

Labels in figure: 3m, 1.5m, 370.8, 6m, 1, 4, 1.5, 1, Concrete sill and V-notch weir, 364.98, Rock, Clay, 42 m, 6m, Small defect, Large defect

Figure 6-7   Embankment cross section for the second internal erosion test in the IMPACT project, test 3-2003 (from IMPACT WP2 Technical Report: Section 4).

Labels in figure: 3m, 4.5m, Moraine, 1.3, 1, 5-6 m, 4.5m, Rock

7 SUMMARY OF FINDINGS AND FUTURE RESEARCH NEEDS

The laboratory testing performed in this study produced the following significant findings:

- The erosion rates of broadly-graded mixtures of granular and cohesive materials can be determined from embankment overtopping tests and there is potential to correlate erodibility parameters of these materials to laboratory jet tests of the cohesive fraction of such soils.
- Soils that exhibit cohesive behavior do not necessarily experience headcut development in all situations. Headcut development may depend upon other factors, such as the presence of tailwater and the development of recirculating flow against the downstream side of a potential headcut overfall.
- Physically-based erosion and breach simulation models need the ability to simulate surface erosion of the crest and downstream slope of an embankment during overtopping flow, and to predict when the dominant form of erosion will be headcutting or surface erosion.
- Internal erosion of zoned embankments containing broadly-graded mixed granular and cohesive soils (i.e., rockfills) is a complex physical process that cannot be effectively modeled at this time using existing physically-based erosion and breach models. Probabilistic risk techniques are the most effective current method for considering these cases.

Efforts to simulate the laboratory tests with the WinDAM C and DL Breach numerical models showed that the k_d value of the soil (the detachment rate coefficient) was the most important parameter affecting the model results. In the WinDAM C simulation of the internal erosion test of the homogeneous embankment, results were also sensitive to the initial diameter of the internal erosion conduit. WinDAM C was able to produce a realistic simulation of the growth of the internal erosion conduit in the homogeneous embankment test.

The laboratory tests performed in this study, the analysis of those tests with existing physically-based erosion simulation models, and the comparison with other laboratory tests of embankments with similar materials and zoning demonstrate that the understanding of erosion and breach processes for zoned embankments and rockfill-type soils is still filled with uncertainty. Significant research questions that need to be addressed include:

- How can we better predict rates of scour erosion for mixed materials? What are the dominant parameters and how can we relate prototype erosion rates to basic soil properties and/or laboratory erodibility tests?
- Can we develop methods to predict whether headcut or surface erosion will occur?
- Are we including all of the dominant erosion processes? Are there processes included in the numerical models that are not important in model tests or real events?
- Can we develop consistent methods for applying effective stress techniques to the analysis of surface erosion processes in laboratory tests <u>and</u> numerical models? Many laboratory tests have been analyzed using an effective stress approach that partitions the shear stress among components applied to bedforms, vegetation, and erodible soil grains. However, different models vary in how they apply this approach, which leads to a need for adjusting other model parameters to compensate. In particular, when surface erosion is the dominant process being modeled, guidance is needed for estimating the bedform resistance that is likely to develop in an eroding breach channel.

8   REFERENCES

ASTM Standard D698, 2007. Standard test methods for laboratory compaction characteristics of soil using standard effort. American Society for Testing and Materials.

ASTM Standard D4718, 2007. Standard practice for correction of unit weight and water content for soils containing oversize particles. American Society for Testing and Materials.

ASTM Standard D5852, 2007. Standard test method for erodibility determination of soil in the field or in the laboratory by the jet index method. American Society for Testing and Materials.

Chow, V.T., 1959. *Open-Channel Hydraulics*, McGraw-Hill Book Company, New York, pp. 108-123.

Courivaud, J.R., 2007. Analysis of the dam breaching database. CEA Technologies Inc., Dam Safety Interest Group, CEATI Report No. T032700-0207B, 79 pp.

Einstein, H.A., 1950. The bed load function for sediment transport in open channel flows. USDA Technical Bulletin 1026.

FEMA, 2011. *Filters for Embankment Dams: Best Practices for Design and Construction*, Federal Emergency Management Agency, Washington, DC.

Foster, M.A., and R. Fell, 2001. Assessing embankment dam filters that do not satisfy design criteria. *Journal of Geotechnical and Geoenvironmental Engineering*, 127(5):398-407.

Franca, M.J., and A.B. Almeida, 2002. Experimental tests on rockfill dam breaching process. IAHR – International Symposium on Hydraulic and Hydrological Aspects of Reliability and Safety Assessment of Hydraulic Structures, St. Petersburg, Russia.

Franca, M.J., and A.B. Almeida, 2004. A computational model of rockfill dam breaching caused by overtopping (RoDaB). *Journal of Hydraulic Research* (42):197-206.

Frenette, R., and I. Pestov, 2005. Flow and erosive stresses at the base of a headcut. *Journal of Hydraulic Engineering*, 131(2):139-141.

Hanson, G.J., 1989. Channel erosion study of two compacted soils. *Transactions of the ASAE*, 32(2):485-490.

Hanson, G.J., 1990a. Surface erodibility of earthen channels at high stresses, part I-open channel testing. *Transactions of the ASAE*, 33(1):127-131.

Hanson, G.J., 1990b. Surface erodibility of earthen channels at high stresses, part II-developing an in-situ testing device. *Transactions of the ASAE*, 33(1):132-137.

Hanson, G.J., K.M. Robinson, and K.R. Cook, 2001. Prediction of headcut migration using a deterministic approach. *Transactions of the ASAE*, 44(3):525-531.

Hanson, G.J., and K.R. Cook, 2004. Apparatus, test procedures, and analytical methods to measure soil erodibility in situ. *Applied Engineering in Agriculture*, 20(4):455-462.

Hanson, G.J., and S.L. Hunt, 2007. Lessons learned using laboratory jet method to measure soil erodibility of compacted soils. *Applied Engineering in Agriculture*, 23(3):305-312.

Hanson, G.J., and Simon, A., 2001. Erodibility of cohesive streambeds in the loess area of the midwestern USA. *Hydrological Processes*, Vol. 15, pp. 23-38.

Hanson, G.J., R.D. Tejral, S.L. Hunt, and D.M. Temple, 2010. Internal erosion and impact of erosion resistance. *Proceedings of the 30th Annual USSD Conference*, United States Society on Dams, Denver, CO.

Hanson, G.J., Temple, D.M., Hunt, S.L., and Tejral R.D., 2011. Development and characterization of soil material parameters for embankment breach. *Applied Engineering in Agriculture*, 27(4):587-595.

Hassan, M. and M.W. Morris, 2008. IMPACT Project Field Tests Data Analysis. FLOODSite Project Report No. T04-08-04.

Howard, A., and B. Howard, 2015. *Laboratory Soil Classification – Volume 1 of the Unified Soil Classification System*, Relativity Publishing, Lakewood, CO.

IMPACT Project, 2004. *Investigation of Extreme Flood Processes & Uncertainty*. Breach Formation (WP2) Technical Report. *http://www.impact-project.net/pub_wp2.htm*

Mohamed, M.A.A., 2002. Embankment breach formation and modelling methods. Ph.D. thesis, The Open University, England.

Morris, M.W., 2011. Breaching of Earth Embankments and Dams. Ph.D. thesis, The Open University, England.

Pugh, C.A., 1985. *Hydraulic model Studies of Fuse Plug Embankments*, Bureau of Reclamation Research Report REC-ERC-85-7, Denver, CO.

Reclamation, 1987. *Design of Small Dams, 3rd ed.* U.S. Dept. of the Interior, Bureau of Reclamation, Denver, CO.

Robinson, K.M., and G.J. Hanson, 1994. A deterministic headcut advance model. *Transactions of the ASAE,* 37(5):1437–1443.

Robinson, K.M. and G.J. Hanson, 1996. Influence of backwater on headcut advance. In *Proceedings of the ASCE North American Water and Environment Congress*, CD–ROM. C. T. Bathala, ed. Anaheim, Calif.: ASCE.

Simmler, H. and L. Sametz, 1982. Dam failure from overtopping studied on a hydraulic model. 14th ICOLD Congress, Rio de Janeiro.

Smith, R.E., D.L. Chery, Jr., K.G. Renard, and W.R. Gwinn, 1981. Supercritical flow flumes for measuring sediment-laden flow. U.S. Department of Agriculture Technical Bulletin No. 1655, 72 p.

State of Colorado, 2010. *Guidelines for Dam Breach Analysis*, Department of Natural Resources, Division of Water Resources, Office of the State Engineer, Dam Safety Branch, Denver, CO.

Temple, D.M., 1980. Tractive force design of vegetated channels. *Transactions of the ASAE*, 23(4):884-890.

Temple, D.M., K.M. Robinson, R.M. Ahring, and A.G. Davis. 1987. *Stability design of grass-lined open channels.* U.S. Department of Agriculture, Agriculture Handbook 667, 175 p.

Tinney E.R. and H.Y. Hsu, 1961. Mechanics of washout of an erodible fuse plug. *Journal of the Hydraulics Division*, Vol. HY3, May 1961.

USBR and USACE, 2015. Best Practices in Dam and Levee Safety Risk Analysis. Chapter IV-4. Internal Erosion Risks for Embankments and Foundations. U.S. Department of the Interior, Bureau of Reclamation, and U.S. Army Corps of Engineers. Version 4.0 *http://www.usbr.gov/ssle/damsafety/risk/methodology.html*

USDA, 2016. WinDAM C: Estimating Erosion of Earthen Embankments and Auxiliary Spillways of Dams, Natural Resources Conservation Service, http://go.usa.gov/8Oq.

USGS, 2012. Water Resources of Illinois: n-values Project – Equations. https://il.water.usgs.gov/proj/nvalues/equations.shtml?equation=05-strickler. Updated Dec. 19, 2012. Accessed April 2, 2018.

Vaskinn, K.A., A. Løvoll, and K. Höeg, undated. WP2.1 Breach Formation. Large Scale Embankment Failure. *http://www.impact-project.net/AnnexII_DetailedTechnicalReports/AnnexII_PartA_WP2/Impact_kav.pdf*

Wahl, T.L., 1998, *Prediction of Embankment Dam Breach Parameters: A Literature Review and Needs Assessment*, Dam Safety Research Report DSO-98-004, U.S. Dept. of the Interior, Bureau of Reclamation, Denver, Colorado, July 1998.

Wahl, T.L., 2007. Laboratory investigations of embankment dam erosion and breach processes", CEA Technologies Inc., Dam Safety Interest Group, CEATI Report No. T032700-0207A, 60 pp.

Wahl, T.L., 2014. *Measuring erodibility of gravelly fine-grained soils*. Hydraulic Laboratory Report HL-2014-05, U.S. Dept. of the Interior, Bureau of Reclamation, Denver, Colorado, September 2014.

Wahl, T.L., P.-L. Regazzoni, and Z. Erdogan, 2008. *Determining erosion indices of cohesive soils with the Hole Erosion Test and Jet Erosion Test*, Dam Safety Technology Development Report DSO-08-05, U.S. Dept. of the Interior, Bureau of Reclamation, Denver, Colorado, 45 pp.

Wahl, T.L., R. Rinehart, M. Klein and J. Rittgers, 2016. Visual and photogrammetric observations of an internal erosion failure. In B. Crookston & B. Tullis (Eds.), *Hydraulic Structures and Water System Management*. 6th IAHR International Symposium on Hydraulic Structures, Portland, OR, 27-30 June. doi:10.15142/T3370628160853 (ISBN 978-1-884575-75-4).

Washington State Department of Ecology, 2007. *Dam Break Inundation Analysis and Downstream Hazard Classification*, Dam Safety Guidelines, Technical Note 1. Olympia, WA.

Wu, W., 2013. Simplified physically based model of earthen embankment breaching. *Journal of Hydraulic Engineering*, 139(8):837-851.

Wu, W., 2016a. Introduction to DLBreach – A Simplified Physically-Based Dam/Levee Breach Model (Version 2016.4), Clarkson University, Potsdam NY.

Wu, W., 2016b. Inputs and Outputs of DLBreach – A Simplified Physically-Based Dam/Levee Breach Model (Version 2016.4), Clarkson University, Potsdam NY.

Yen, B.C., 1991. Hydraulic resistance in open channels. in *Channel Flow Resistance: Centennial of Manning's Formula*, B.C. Yen, ed., Water Resource Publications, Highlands Ranch, CO.

Yen, B.C., 2002. Open channel flow resistance. *Journal of Hydraulic Engineering*, 128(1):20-39.

APPENDIX A
SOILS LABORATORY REPORTS

Blue Rock Labs, Inc.

6435 S. Routt St.
Littleton, CO 80127
720-272-6282
Kendra@bluerocklabsinc.com

March 9, 2015

Mr. Robert Rinehart, P.E.
USBR-Materials Engineering & Research Lab
P.O. Box 25007
Denver, CO 80225

Dear Mr. Rinehart,

Blue Rock Labs, Inc. is pleased to present the laboratory testing for the Bonny Silt project. Included in this report are results of the five (5) Atterberg Limits tests, five (5) specific gravity tests, one (1) standard effort compaction test, and five (5) hydrometer/sieve analyses. We performed the tests in general accordance with ASTM standards.

The results contained herein are for the exclusive use of USBR-Materials Engineering & Research Lab and they do not constitute a warranty or guarantee of any type. Conditions observed in the test samples may not represent actual field conditions. We will not be responsible for any claims, damages, or liability associated with any other party's interpretations of this report without expressed written authorization. Blue Rock Labs, Inc. makes no expressed or implied warranty regarding the way in which the laboratory results are used.

We appreciate this opportunity to provide USBR-Materials Engineering & Research Lab with our laboratory services, and we look forward to working with you again in the future. If you have any questions, please contact me at 720-272-6282.

Sincerely,

Blue Rock Labs, Inc.

Kendra S. Adams, P.G., R.G.
President

Blue Rock Labs, Inc.
6435 S. Routt St.
Littleton, CO 80127
720-272-6282

TEST REPORT
Prepared For:
USBR-Materials Engineering & Research Lab
P.O. Box 25007
Denver, CO 80225
303-445-2395

Report No.:	**15121002**	**March 9, 2015**
Material:	**Soil Samples**	**Page 1 of 10**
Project:	**Bonny Silt**	
Sampled By:	**Client**	
Attention:	**Mr. Robert Rinehart, P.E.**	

ATTERBERG LIMITS & SPECIFIC GRAVITY (D4318 & D854: Method B)

Sample	S. G.	LL	PL	PI	USCS*
1	2.668	29	22	7	CL
2	2.675	26	21	5	CL-ML
3	2.675	26	22	4	ML
4	2.673	26	21	5	CL-ML
Composite of 1-4	2.675	27	21	6	CL-ML

*Classification based solely on Atterberg limit data.

STANDARD EFFORT COMPACTION (D698)

Data Attached.

PARTICLE-SIZE DISTRIBUTION (D422 & D6913)

Graphs & Tabulated Data Attached.
Rounding of values may cause slight differences in the sum of the percentages.

See the attached cover letter for disclaimer and warranty information.

Report No.:	15121002	March 9, 2015
Material:	Soil Samples	Page 2 of 10
Project:	Bonny Silt	
Sampled By:	Client	
Attention:	Mr. Robert Rinehart, P.E.	

Truck #1

U.S. Standard Sieve No.	Opening Size (mm)	Percent Passing
No. 4	4.75	100.0
No. 10	2.00	100.0
No. 20	0.840	99.9
No. 40	0.425	99.2
No. 60	0.250	97.7
No. 100	0.150	95.5
No. 140	0.106	93.2
No. 200	0.075	86.3
	Diameter	% Passing
	0.029	27.7
	0.021	19.3
	0.017	16.4
	0.013	13.3
	0.009	8.7
	0.007	7.7
	0.003	5.6
	0.001	4.0

Truck #2

U.S. Standard Sieve No.	Opening Size (mm)	Percent Passing
No. 4	4.75	100.0
No. 10	2.00	100.0
No. 20	0.840	99.9
No. 40	0.425	99.4
No. 60	0.250	97.9
No. 100	0.150	95.9
No. 140	0.106	94.0
No. 200	0.075	88.0
	Diameter	% Passing
	0.033	30.4
	0.022	16.9
	0.017	13.5
	0.013	8.9
	0.009	7.3
	0.007	4.4
	0.003	2.7
	0.001	2.0

Report No.:	15121002	March 9, 2015
Material:	Soil Samples	Page 3 of 10
Project:	Bonny Silt	
Sampled By:	Client	
Attention:	Mr. Robert Rinehart, P.E.	

Truck #3

U.S. Standard Sieve No.	Opening Size (mm)	Percent Passing
No. 4	4.75	100.0
No. 10	2.00	100.0
No. 20	0.840	99.9
No. 40	0.425	99.7
No. 60	0.250	99.1
No. 100	0.150	97.8
No. 140	0.106	96.2
No. 200	0.075	90.6
	Diameter	% Passing
	0.033	31.1
	0.022	17.8
	0.017	13.1
	0.013	9.8
	0.009	7.1
	0.007	4.6
	0.003	2.5
	0.001	1.6

Truck #4

U.S. Standard Sieve No.	Opening Size (mm)	Percent Passing
No. 4	4.75	100.0
No. 10	2.00	100.0
No. 20	0.840	99.9
No. 40	0.425	99.5
No. 60	0.250	98.6
No. 100	0.150	97.1
No. 140	0.106	95.5
No. 200	0.075	90.4
	Diameter	% Passing
	0.032	30.8
	0.021	19.5
	0.017	15.0
	0.010	10.7
	0.009	9.1
	0.006	7.3
	0.003	5.9
	0.001	3.7

Report No.:	15121002		**March 9, 2015**
Material:	Soil Samples		**Page 4 of 10**
Project:	Bonny Silt		
Sampled By:	Client		
Attention:	Mr. Robert Rinehart, P.E.		

Composite of 1-4

U.S. Standard Sieve No.	Opening Size (mm)	Percent Passing
No. 4	4.75	100.0
No. 10	2.00	100.0
No. 20	0.840	99.9
No. 40	0.425	99.5
No. 60	0.250	98.5
No. 100	0.150	96.9
No. 140	0.106	95.1
No. 200	0.075	89.2
	Diameter	% Passing
	0.033	41.1
	0.022	26.6
	0.018	21.3
	0.009	15.0
	0.007	12.8
	0.003	9.8
	0.001	6.6

6435 S. Routt St.
Littleton, CO 80127
Ph: 720-272-6282

Blue Rock Labs, Inc.

LABORATORY COMPACTION TEST
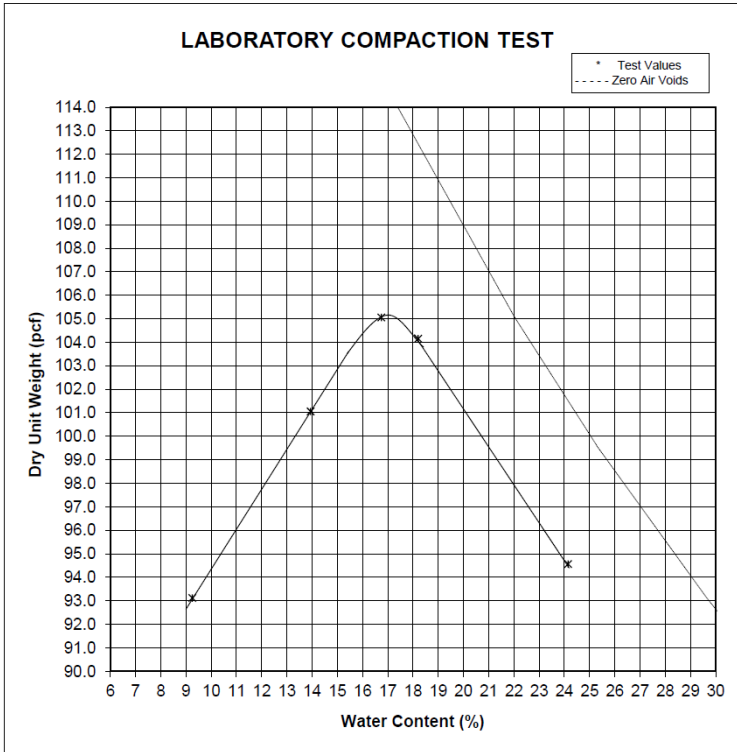
Test Information	
Project No.:	15121002
Test Date:	03/04/15
Proctor No.:	
Test Method:	ASTM D 698 Method A
Rammer Type:	Manual
Prep. Method:	Moist

Sample Description
Light brown, silt to silty clay with organics

Sample Properties	
Moisture Content	9.6
Liquid Limit	27
Plastic Limit	21
Plasticity Index	6
Specific Gravity:	2.675 Actual
Classification	CL-ML

Test Results:	
Maximum Dry Unit Weight (pcf):	105.2
Optimum Water Content (%):	17.0
Oversize Correction Values:	
Maximum Dry Unit Weight (pcf):	--
Optimum Water Content (%):	--

Tested By: KA   Input By: KA
Date: 03/04/15   Date: 03/06/15
Checked By: KA
Date: 03/07/15

A-7

PARTICLE SIZE DISTRIBUTION
ASTM D6913

Cobbles	Gravel		Sand			Fines	
	Coarse	Fine	Coarse	Medium	Fine	Silt	Clay

Cobbles (%)	Gravel (%)		Sand (%)			Fines (%)	
				13.7		86.3	
	Coarse	Fine	Coarse	Medium	Fine	Silt	Clay
				0.8	13.0	79.5	6.7

Project No.: 15121002

Boring: Bonny Silt

Sample: 1

A-8

PARTICLE SIZE DISTRIBUTION
ASTM D6913

Cobbles	Gravel		Sand			Fines	
	Coarse	Fine	Coarse	Medium	Fine	Silt	Clay

Cobbles (%)	Gravel (%)		Sand (%)			Fines (%)	
				12.0		88.0	
	Coarse	Fine	Coarse	Medium	Fine	Silt	Clay
				0.6	11.4	84.3	3.6

Project No.: 15121002

Boring: Bonny Silt

Sample: 2

PARTICLE SIZE DISTRIBUTION
ASTM D6913

Blue Rock Labs, Inc.

Cobbles	Gravel		Sand			Fines	
	Coarse	Fine	Coarse	Medium	Fine	Silt	Clay

Cobbles (%)	Gravel (%)		Sand (%)			Fines (%)	
			9.4			90.6	
	Coarse	Fine	Coarse	Medium	Fine	Silt	Clay
				0.3	9.1	87.0	3.6

Project No.: 15121002
Boring: Bonny Silt
Sample: 3

Blue Rock Labs, Inc.

PARTICLE SIZE DISTRIBUTION
ASTM D6913

Cobbles	Gravel		Sand			Fines	
	Coarse	Fine	Coarse	Medium	Fine	Silt	Clay

Cobbles (%)	Gravel (%)		Sand (%)			Fines (%)	
			9.6			90.4	
	Coarse	Fine	Coarse	Medium	Fine	Silt	Clay
				0.5	9.2	83.7	6.7

Project No.: 15121002
Boring: Bonny Silt
Sample: 4

PARTICLE SIZE DISTRIBUTION
ASTM D422 & D6913
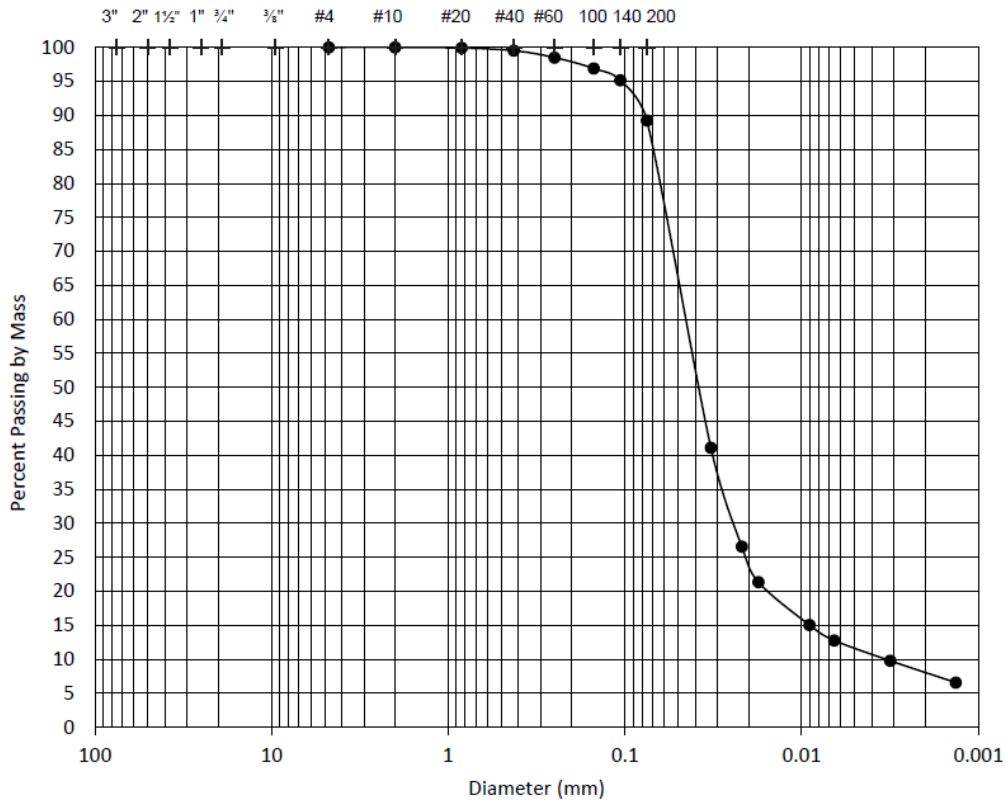
Cobbles	Gravel		Sand			Fines	
	Coarse	Fine	Coarse	Medium	Fine	Silt	Clay

Cobbles (%)	Gravel (%)		Sand (%)			Fines (%)	
				10.8		89.2	
	Coarse	Fine	Coarse	Medium	Fine	Silt	Clay
				0.5	10.3	77.8	11.4

Project No.: 15121002

Project Name: Bonny Silt

Sample: Composite 1-4

Blue Rock Labs, Inc.

6435 S. Routt St.
Littleton, CO 80127
720-272-6282
Kendra@bluerocklabs.com

May 3, 2017

Mr. Evan Lindenbach, P.E., P.G.
USBR Concrete, Geotechnical and Structural Laboratory
P.O. Box 25007
Denver, CO 80225

Dear Mr. Lindenbach,

    Blue Rock Labs, Inc. is pleased to present the laboratory testing for the Embankment Breach Model Type 6 Material project. Included in this report are results of the one (1) 1-point Atterberg Limits test, one (1) specific gravity test, one (1) coarse material specific gravity test, one (1) hydrometer-sieve analysis, and one (1) standard compaction test. We performed the tests in general accordance with ASTM standards.

    The results contained herein are for the exclusive use of USBR Concrete, Geotechnical & Structural Lab and they do not constitute a warranty or guarantee of any type. Conditions observed in the test samples may not represent actual field conditions. We will not be responsible for any claims, damages, or liability associated with any other party's interpretations of this report without expressed written authorization. Blue Rock Labs, Inc. makes no expressed or implied warranty regarding the way in which the laboratory results are used.

    We appreciate this opportunity to provide USBR Concrete, Geotechnical and Structural Lab with our laboratory services, and we look forward to working with you again in the future. If you have any questions, please contact me at 720-272-6282.

Sincerely,

Kendra S. Adams, R.G., P.G
President

Blue Rock Labs, Inc.
6435 S. Routt St.
Littleton, CO 80127
720-272-6282

TEST REPORT

Prepared For:
USBR Concrete, Geotechnical and Structural Laboratory
P.O. Box 25007
Denver, CO 80225
303-445-2336

Report No.:	17121002	May 3, 2017
Material	Road Base Sample	Page 1 of 4
Project:	Embankment Breach Model Type 6 Material	
Sampled By:	Client	
Attention:	Mr. Evan Lindenbach, P.E., P.G.	

ATTERBERG LIMITS (D4318, METHOD B) & SPECIFIC GRAVITY (D854, METHOD B)

LL	PL	PI	USCS[1]	Specific Gravity	Average Specific Gravity
25	19	6	CL-ML	2.812	2.774*

RELATIVE DENSITY (SPECIFIC GRAVITY) (C127)

	Relative Density (OD)	Relative Density (SSD)	Apparent Relative Density	Absorption (%)
+ ⅜ inch	2.63	2.71	2.85	2.9
+No. 4 to -⅜ inch	2.79	2.83	2.89	1.2

The material used in the C127 specific gravity test was obtained from the sieve specimen after sieving.

STANDARD COMPACTION TEST (D698, METHOD C)
Graphs and Tabulated Data Attached.

[1]Classification based solely on Atterberg Limits data.

*This value was calculated based on the average relative density SSD as determined in C127 and then following the equation given in D854.

See the attached cover letter for disclaimer and warranty information.

Report No.:	17121002	May 3, 2017
Material	Road Base Sample	Page 2 of 4
Project:	Embankment Breach Model Type 6 Material	
Sampled By:	Client	
Attention:	Mr. Evan Lindenbach, P.E., P.G.	

PARTICLE SIZE DISTRIBUTION (D6913 & D7928)
Graphs and Tabulated Data Attached.

Rounding of values may cause slight differences in the sum of the percentages.

U.S. Standard Sieve No.	Opening Size (mm)	Percent Passing
3/4"	9.5	100
3/8"	9.5	63
No. 4	4.75	46
No. 10	2.00	38
No. 20	0.84	31
No. 40	0.425	26
No. 60	0.250	21
No. 100	0.150	17
No. 140	0.106	14
No. 200	0.075	12
	0.045	10
	0.033	8
	0.021	7
	0.017	6
	0.012	5
	0.0088	5
	0.0063	4
	0.0035	3
	0.0013	3

PARTICLE SIZE DISTRIBUTION
ASTM D6913 & D7928
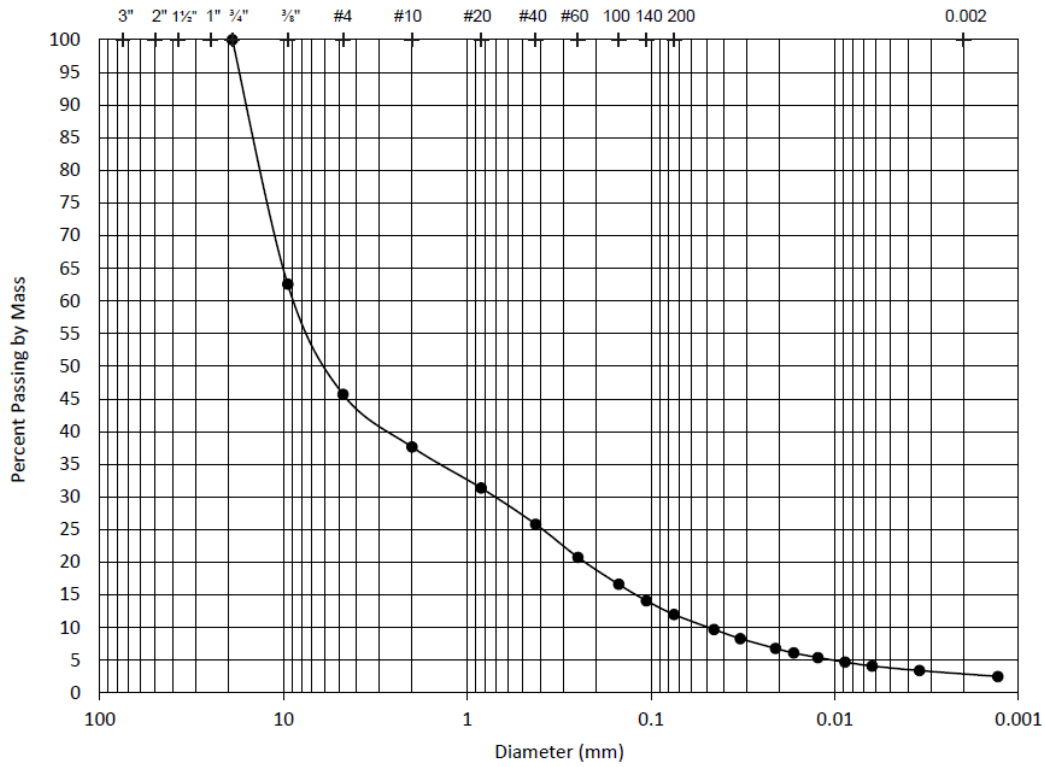
Cobbles (%)	Gravel (%)		Sand (%)			Fines (%)	
	54.3		33.7			12.0	
	Coarse	Fine	Coarse	Medium	Fine	Silt	Clay
		54.3	8.1	11.8	13.8	9.2	2.8

Project No.: 17121002
Project Name: Embankment Breach Model Type 6 Material

6435 S. Routt St.

Littleton, CO 80127

Ph: 720-272-6282

Blue Rock Labs, Inc.

Project: Embankment Breach Model Type 6 Material
Client: USBR
Sample Source: Road Base
Supplier: Martin Marietta

LABORATORY COMPACTION TEST

* Test Values
- - - - - Zero Air Voids
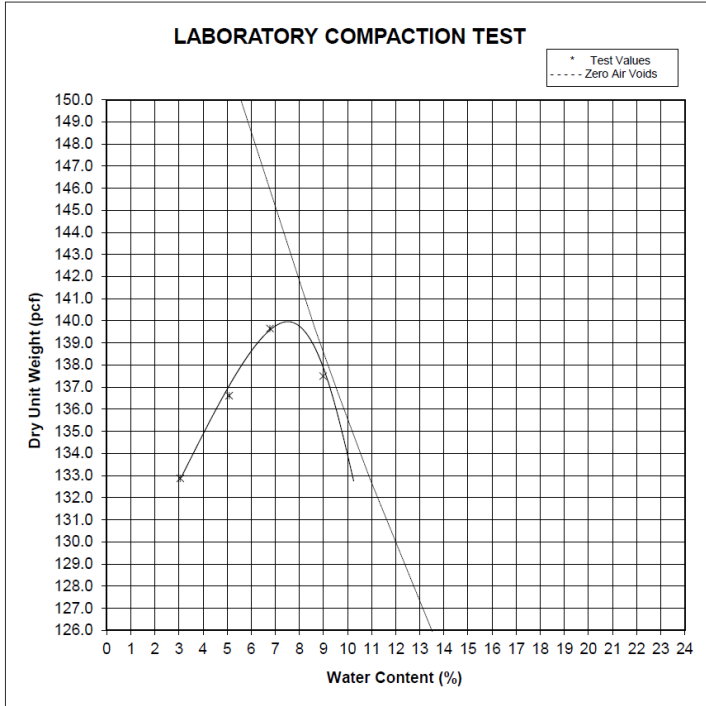
Test Information	
Project No.:	17121002
Test Date:	05/02/17
Proctor No.:	
Test Method:	ASTM D 698 Method C
Rammer Type:	Manual
Prep. Method:	Moist

Sample Description
3/4 inch minus

Sample Properties	
Moisture Content	--
Liquid Limit	25
Plastic Limit	19
Plasticity Index	6
Specific Gravity:	2.774 Actual
Classification	--

Test Results:	
Maximum Dry Unit Weight (pcf):	140.0
Optimum Water Content (%):	7.5

Oversize Correction Values:

Maximum Dry Unit Weight (pcf):	--
Optimum Water Content (%):	--

A-17

Results of In-Place Unit Weight and Water Content Testing of Compacted Earth Fill via
USBR 7205 - Determining Unit Weight of Soils Using the Sand Cone Method
Zoned Embankment Breach Model
United States Bureau of Reclamation
Hydraulic Laboratory, Technical Service Center, Denver CO

Date	Test Number	Test Depth from Crest (ft)	Test Location	Material Type	Index Properties		Water Content			Total Dry Unit Weight (lbf/ft^3)	Dry Unit Weight of - #4 (lbf/ft^3)
					Passing #4 (%)	Retained on #4 (%)	Minus #4 (%)	Plus #4 (%)	Total (%)		
6/5/17	1	2.0	3.5 ft South of Left abutment at center axis	Zone 1, Silt	100.0	0.0	17.5	---	17.5	105.4	---
6/5/17	2	2.0	6.5 ft south of Left abutment, 3.0 ft upstream of center axis	Zone 2, Base Course	36.6	63.4	11.0	2.5	5.6	127.3	---
8/28/17	3	2.0	1.5 ft south of Left abutment, at center axis	Zone 1, Silt	91.1	8.9	---	---	15.9	109.9	106.0
8/28/17	4	2.0	1.0 ft south of Left abutment, 2.0 ft upstream of center axis	Zone 2, Base Course	---	---	---	---	6.9	140.1	---

APPENDIX B
INTERNAL EROSION FAILURE MODE TABLES

From USBR and USACE (2015). "Best Practices in Dam and Levee Safety Risk Analysis. Chapter IV-4. Internal Erosion Risks for Embankments and Foundations."

**Table IV-4-24. Rate of Erosion of the Embankment Core or Foundation Soil
(adapted from Fell et al. 2001, 2003)**

Factors Influencing the Time for Progression and Breach				Approximate Likely Time (Qualitative)	Approximate Likely Time
Ability to Support a Roof	Rate of Erosion (Table IV-4-25)	Upstream Flow Limiter	Breach Time (Table IV-4-26)		
Yes	R or VR	No	VR or R–VR	Very Rapid	< 3 hours
Yes	R	No	R	Very Rapid to Rapid	3 to 12 hours
Yes	R–M	No	VR	Rapid	12 to 24 hours
Yes	R	No	R–M		
Yes	R	No	M or S	Rapid to Medium	1 to 2 days
Yes	R or R–M	No	M or M–S		
Yes	M or R–M	Yes	R or R–M		
Yes	M or R–M	No	S	Medium	2 to 7 days
Yes	R–M or M	Yes	S		
Yes	M	Yes or No	S	Slow	Weeks, even months to years

**Table IV-4-25. Rate of Erosion of the Embankment Core or Foundation Soil
(used in Table IV-4-24) (adapted from Fell et al. 2008)**

Soil Classification	(I_{HET})	Time for erosion in the core of the embankment or in the foundation	
		0.2-gradient along pipe	0.5-gradient along pipe
SM with < 30% fines	< 2	Very Rapid	Very Rapid
SM with > 30% fines	2 to 3	Very Rapid	Very Rapid
SC with < 30% fines	2 to 3	Very Rapid	Very Rapid
SC with > 40% fines	3	Rapid	Very Rapid
ML	2 to 3	Very Rapid to Rapid	Very Rapid
CL-ML	3	Rapid	Very Rapid
CL	3 to 4	Rapid	Very Rapid to Rapid
CL-CH	4	Rapid	Rapid
MH	3 to 4	Rapid	Very Rapid to Rapid
CH with LL < 65	4	Rapid to Medium	Rapid
CH with LL > 65	5	Medium to Slow	Medium

Note: I_{HET} is the index value from the Hole Erosion test (HET)

Table IV-4-26. Influence of the Material in the Downstream Zone of the Embankment on the Likely Time for Development of a Breach due to Gross enlargement of a Pipe (used in Table IV-4-24) (adapted from Fell et al. 2003)

Material Description	Likely Breach Time
Coarse-grained rockfill	Slow – Medium
Soil of high plasticity (PI > 50) and high clay-size content including clayey gravels	Medium – Rapid
Soil of low plasticity (PI < 35) and low clay-size content, all poorly compacted soils, silty sandy gravels	Rapid – Very Rapid
Sand, silty sand, silt	Very Rapid

Table IV-4-27. Qualitative Terms for Times of Development of Internal Erosion and Breach (adapted from Fell et al. 2003)

Qualitative Term	Equivalent Time
Slow (S)	Weeks or months, even years
Medium (M)	Days or weeks
Rapid (R)	Hours (> 12 hours) or days
Very Rapid (VR)	< 3 hours

APPENDIX C
UNIFIED SOIL CLASSIFICATION SYSTEM

USCS Soil Classification Summary

Dominant Coarse Fraction	% Fines	Grading	Fines	Group Symbol	Description
Gravel	0-4	Well Graded		GW	Well-Graded Gravel
Gravel	0-4	Poorly Graded		GP	Poorly-Graded Gravel
Gravel	5-12	Well Graded	Silt	GW-GM	Well-Graded Gravel with Silt
Gravel	5-12	Well Graded	Clay	GW-GC	Well-Graded Gravel with Clay
Gravel	5-12	Poorly Graded	Silt	GP-GM	Poorly-Graded Gravel with Silt
Gravel	5-12	Poorly Graded	Clay	GP-GC	Poorly-Graded Gravel with Clay
Gravel	13-49		Silt	GM	Silty Gravel
Gravel	13-49		Clay	GC	Clayey Gravel
Gravel	13-49		Silty Clay	GC-GM	Silty, Clayey Gravel
Sand	0-4	Well Graded		SW	Well-Graded Sand
Sand	0-4	Poorly Graded		SP	Poorly-Graded Sand
Sand	5-12	Well Graded	Silt	SW-SM	Well-Graded Sand with Silt
Sand	5-12	Well Graded	Clay	SW-SC	Well-Graded Sand with Clay
Sand	5-12	Poorly Graded	Silt	SP-SM	Poorly-Graded Sand with Silt
Sand	5-12	Poorly Graded	Clay	SP-SC	Poorly-Graded Sand with Clay
Sand	13-49		Silt	SM	Silty Sand
Sand	13-49		Clay	SC	Clayey Sand
Sand	13-49		Silty Clay	SC-SM	Silty, Clayey Sand
Gravel	50-70		Clay	CL	Gravelly Lean Clay
Sand	50-70		Clay	CL	Sandy Lean Clay
Gravel	50-70		Fat Clay	CH	Gravelly Fat Clay
Sand	50-70		Fat Clay	CH	Sandy Fat Clay
Gravel	50-70		Silty Clay	CL-ML	Gravelly Silty Clay
Sand	50-70		Silty Clay	CL-ML	Sandy Silty Clay
Gravel	50-70		Silt	ML	Gravelly Silt
Sand	50-70		Silt	ML	Sandy Silt
Gravel	50-70		Elastic Silt	MH	Gravelly Elastic Silt
Sand	50-70		Elastic Silt	MH	Sandy Elastic Silt
	71-100		Clay	CL	Clay
	71-100		Fat Clay	CH	Fat Clay
	71-100		Silt	ML	Silt
	71-100		Elastic Silt	MH	Elastic Silt
	71-100		Silty Clay	CL-ML	Silty Clay

Soil classifications are determined from the four basic properties shown in columns (1)-(4). Blank cells indicate properties that are not relevant for classification purposes within a specific range. Particles passing the U.S. No. 200 sieve are fines, and the percentage of fines is determined by weight. Particles passing the U.S. No. 4 sieve and retained on the No. 200 sieve are sand. Particles retained on the No. 4 sieve are gravel. The grading of soil (well-graded or poorly-graded) is determined by computing the coefficients of uniformity and curvature, C_u and C_c (see footnote on pg. 1-3). The nature of the fines (clay, silt, etc.) is determined from Atterberg limits tests (liquid limit LL, plastic limit PL, and plasticity index, PI=LL-PL) and the plasticity chart on the following page. This summary table does not address organic

soils or borderline soil classifications. Suffixes "with sand" or "with gravel" can be added to soil descriptions when such particles make up 15% or more of the gradation.

<u>Reference</u>
Earth Manual, 3rd ed. 1998. U.S. Dept. of the Interior, Bureau of Reclamation.

For classification of fine-grained soils
and fine-grained fraction of coarse-grained
soils.

Equation of "A"-line
Horizontal at PI=4 to LL=25.5,
then PI=0.73 (LL-20)

Equation of "U"-line
Vertical at LL=16 to PI=7,
then PI=0.9 (LL-8)

"U" LINE

"A" LINE

CH OR OH

CL OR OL

MH OR OH

ML OR OL

CL-ML

PLASTICITY INDEX (PI)

60

50

40

30

20

10
7
4
0

0   10   16 20   30   40   50   60   70   80   90   100   110

LIQUID LIMIT (LL)